O.K.

ISAS - INTERNATIONAL SCHOOL FOR ADVANCED STUDIES

Computational studies of the structure/function relation of proteins involved in neurotransmission and neurotransduction in excitable cells: nAChR and Ca^{2+}-ATPase.

Thesis submitted for the degree of
Doctor Philosophiæ

Candidate:
Valeria Costa

Supervisors:
Dr. Paolo Carloni
Prof. Andrea Nistri

October 2002

SISSA - SCUOLA INTERNAZIONALE SUPERIORE DI STUDI AVANZATI
TRIESTE
Via Beirut 2-4

TRIESTE

SUMMARY

The present theoretical work investigated the structural/functional properties of two transmembrane proteins involved in Ca^{2+} signalling of excitable cells.

The first class of proteins was that of nicotinic acetylcholine receptors (nAChRs). These are ligand-gated ion channels, permeable to Ca^{2+} and activated by nicotine agonists. Their role is to mediate intercellular communication converting the signal induced by the neurotransmitter released into the extracellular space to a transmembrane influx of Ca^{2+} (and Na^{+}) through the cell membrane. In this thesis, molecular dynamics (MD) simulations were initially used to investigate the structural properties of a novel class of peptides, whose binding to neuronal nicotinic receptors has been recently studied at SISSA. These peptides are related to the N-terminal region of Calcitonin Gene Related Peptide (CGRP). Using as a model system native nAChRs of rat chromaffin cells (Campos-Caro et al., 1997), whole cell patch clamp recordings (Di Angelantonio et al., 2002) have shown that $CGRP_{1-6}$, $CGRP_{1-5}$ or $CGRP_{1-4}$ act as selective, rapid and reversible modulators potentiating nAChRs, in sharp contrast with $CGRP_{1-7}$ that depresses nAChRs. Molecular dynamics (MD) simulations provided atomic structural models for these peptides. $CGRP_{1-7}$ exhibited a relatively rigid ring structure imparted by the disulphide bridge between Cys_2 and Cys_7 and the shorter peptides, missing such a bridge, exhibited propensity for α-helix configuration. Replacing Cys_7 with Ala yielded a fragment ($CGRP_{1-7A}$) with partial α-helix structure and ability to enhance nicotine currents. Circular dichroism measurements on $CGRP_{1-7}$ and $CGRP_{1-6}$ were compatible with these MD structural findings. To further understand the structural basis for such a diverse modulatory effect of the CGRP fragments, ligand-binding domain models of α3β4 and α4β2 cromaffin cell nAChRs were constructed and a set of ligands docked on their binding sites. The protein structural models were based on the acetylcholine binding protein (AChBP), which aligns the ligand binding domain of the nicotinic receptors and whose X-ray structure has been recently determined (Brejc et al., 2001). Full agonists (i.e. acetylcholine, nicotine and cytisine), muscarine (which is a well known selective agonist of muscarinic acetylcholine receptors), two CGRP N-terminal

fragments ($CGRP_{1-7}$ and $CGRP_{1-6}$) and an allosteric agonist (eserine) were docked to the binding pockets of the α3β4 and α4β2 nicotinic receptor models, as well as to the ones of the AChBP crystal structure. Our results show that the small agonists shared common properties on the docking mode; indeed, their ammonium group bound similarly the receptor binding sites. Furthermore, the calculated binding affinities were in agreement with the experimental data. Docking of muscarine, which is a well known selective agonist of muscarinic acetylcholine receptors, confirmed the selectivity of our nicotinic receptor binding site models. A possible mechanism of antagonist action for $CGRP_{1-7}$ and a possible site of binding for allosteric agonists, such as eserine, were also suggested.

The second protein investigated was the Ca^{2+} pump. This is involved in regulating muscle contraction and relaxation. After rapid increase in cytosolic Ca^{2+} concentration, these cations bind to the protein which pumps them into the sarcoplasmic reticulum restoring the cytosolic Ca^{2+} level. Molecular dynamics and electrostatic modelling were used in the attempt to investigate structural and dynamical features of key intermediates in the Ca^{2+} binding process of the protein. Structural models of the protein (containing either two, one or no calcium ions in the transmembrane domain) were constructed based on the X-ray structure (Toyoshima et al., 2000) The protein was embedded in a water/octane bilayer, which mimics the water/membrane environment. Our calculations provide information on the hydration of the two Ca^{2+} ions, not emerging from the X-ray structure. Furthermore, they indicate that uptake of the metal ions causes large structural rearrangements of the metal binding sites. In addition, they suggest that the two ions reach their binding sites via two specific pathways. Finally, they allow identification of residues in the outer mouth of the protein which might interact with the Ca^{2+} during the binding process.

INTRODUCTION

A large wealth of biological processes, like movement, heart beat and brain processing, are based on the action of uptake and release of Ca^{2+} ions, which act as intracellular messengers. In the cell, the concentration of Ca^{2+} ions rises and falls quickly as the homeostasis of internal Ca^{2+} levels must be kept tight. Ca^{2+} ions are uptaken either from extracellular sources by permeating through membrane channels or from internal Ca^{2+} stores (Figure 1), as the endoplasmic/sarcoplasmic reticulum (Berridge et al., 1998). External Ca^{2+} ions can enter into the cell through voltage-gated Ca^{2+} channels opened by membrane depolarisation, or through ligand-gated Ca^{2+} channels activated by neurotransmitters. Internal Ca^{2+} ions are released by channels activated through a series of chemical reactions (Berridge et al., 1998). Both plasma and (sarco)endoplasmic membranes contain also Ca^{2+} pumps which use ATP to restore Ca^{2+} concentration inside the cells after a signal (Clapham, 1995).

In the present thesis I investigated by theoretical methods the structural/functional properties of two transmembrane proteins involved in Ca^{2+} signalling. The first is the nicotinic acetylcholine receptors which are ligand-gated ions channels, permeable to Ca^{2+} and activated by nicotine agonists. Nicotinic receptor mediate intercellular communication converting the signal induced by the neurotransmitter released into the extracellular space to a transmembrane ion flux. These are key proteins for cholinergic transmission at the neuromuscular junction of striated muscle (muscle-type nicotinic receptors), the peripheral ganglion synapses of the autonomic nervous systems and several brain areas (neuronal nicotinic receptors).

The second system investigated here is the Ca^{2+} pump involved in Ca^{2+} translocation through the sarcoplasmic reticulum membrane in all cells. In particular, they are involved in regulating muscle contraction which requires rapid increase in cytosolic Ca^{2+} concentration. These cations bind to a protein which, once activated, pumps them insight the sarcoplasmic reticulum against their concentration gradient, restoring the cytosolic ambient Ca^{2+} level. Ultimately, this process causes muscle relaxation.

The focus of this thesis was to understand the structural properties of such proteins to gain information on their function and to ascertain the structural determinants responsible for Ca^{2+} passive and active transport.

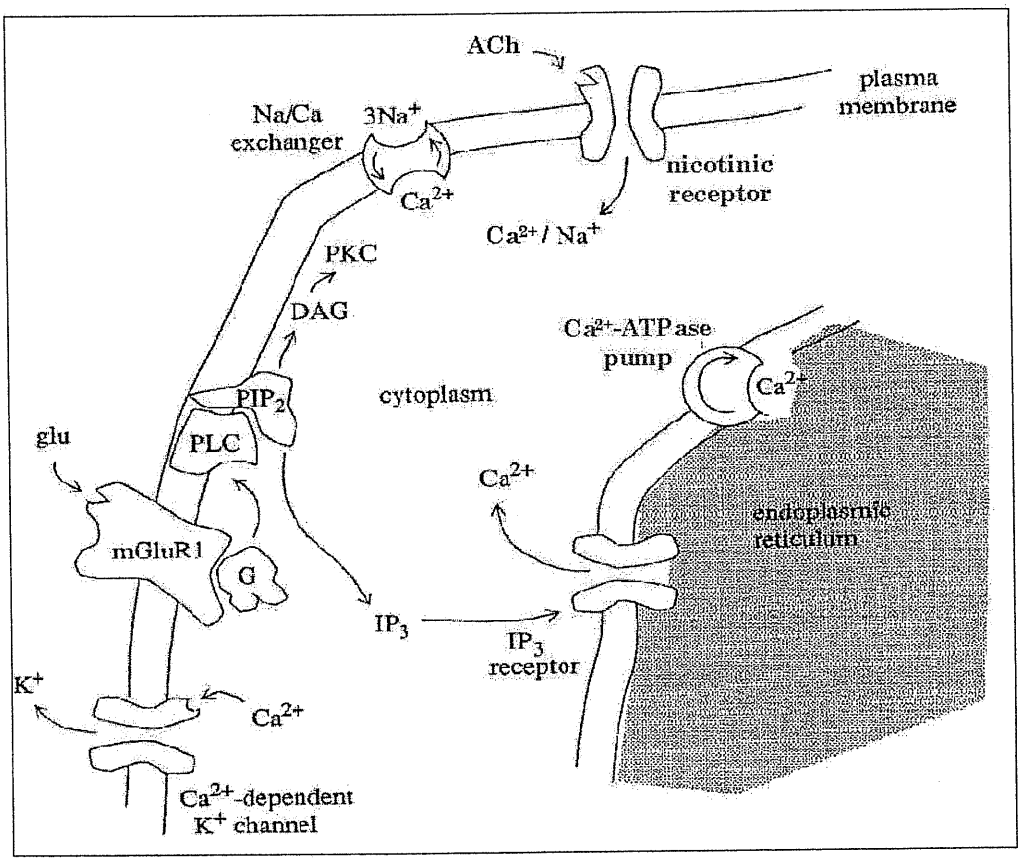

FIGURE1. Schematic representation of the intracellular and extracellular calcium translocation.

1. NEURONAL NICOTINIC RECEPTORS

1.1 A LIGAND-GATED ION CHANNEL

The nicotinic acetylcholine receptor (nAChR) belongs to a superfamily of ligand-gated ion channels. These channels mediate intercellular communication by converting the signal induced by a neurotransmitter released from the nerve ending into a transmembrane ion flux in the postsynaptic neuron or muscle fibre.

The superfamily includes muscle-type and neuronal-type nicotinic receptors, 5-hydroxytrtptamine type 3 (5-HT_3) receptors, γ-aminobutyric acid type A ($GABA_A$) and type C ($GABA_C$) receptors, glycine receptors, invertebrate glutamate (Cully et al., 1994) and histidine (Zheng et al., 2002) receptors. In the amino-terminal region, the all family of ligand-gated ion channels contains a disulphide-bonded cysteine pair, in which the Cys residues are separated by 13 residues (Kao and Karlin, 1986; Karlin and Akabas, 1995; Ortells and Lunt, 1995; Tsunoyama and Gojobori, 1998). For this reason, these receptors are also known as Cys-loop receptors.

Nicotinic receptors are gated by acetylcholine (ACh) and mediate transmission at the neuromuscular junction of striated muscles (muscle-type nicotinic receptors), at peripheral ganglion synapses of the autonomic nervous system and in several brain areas (neuronal nicotinic receptors; Gotti et al., 1997; Paterson and Nordberg, 2000). Muscarinic receptors are also activated by ACh, however, they belong to the super-family of G-protein coupled receptors, that is proteins interacting with heteromeric G-proteins.

1.2 STOICHIOMETRY

Nicotinic acetylcholine receptors (nAChRs) are composed of five membrane-spanning subunits arranged in such a way as to delimit an aqueous central channel (Itier and Bertrand, 2001). The sequences and hydropathy plots of the subunits are similar so, presumably, the threading of the subunits through the membrane is similar to the one determined in the *Torpedo Californica* ACh receptor (Kao and Karlin, 1986).

The combination of different subunits defines various nAChR subtypes and, depending on such combination, receptors reflect differences in pharmacological and electrophysiological properties. According to their increasing molecular weight, the protein subunits were classified in five groups named α (α1-α9), β (β1-β4), γ, ε and δ (Changeux, 1995). Given the vast number of combinations which could make up a pentameric structure, theoretically there is potential for a large number of distinct channel types; however, only a few of them have actually been found (McGehee and Role, 1995).

The nicotinic receptor family is divided in three classes: (1) muscle nAChRs, which are selectively labelled and blocked by the antagonist α-bungarotoxin (α-BTx); (2) heteromeric neuronal nAChRs, that do not bind α-BTx; (3) homomeric neuronal nAChRs, which do bind α-BTx.

Initial studies carried out on the neuromuscular junction have revealed that muscle-type receptors result from the assembly of five subunits in a pentamer with one β1, δ and γ subunits (replaced by ε subunit in adults) and two α1 (Changeux, 1990). This composition corresponds to the one found in the *Torpedo* electrical organ. Since this tissue allows extraction of enriched receptor fractions, it has been used as a model for nicotinic receptor investigations.

While subunit composition of the neuromuscular receptors was established rather early, less is known about neuronal receptor composition. The very limited amount of biological material makes biochemical experiments difficult and the putative stoichiometry must be derived from an ensemble of converging information. As neuronal nAChRs qualitatively share many of the physical and functional features of muscle nAChRs (Galzi and Changeux, 1995), they are expected to consist of five subunits assembly.

Neuronal clones have been isolated for genes of eight α subunit (α2-α9) and three β subunit (β2-β4), which show homology with the muscle α1 and β1 subunits, respectively (Colquhoun and Patrick, 1997). Insights into subunit arrangement have come from functional expression of the various subunits in isolation or in combination. These studies have suggested for neuronal receptors the following subdivision: (1)

homomeric α nAChRs, composed by five equal subunits (either α7, α8 or α9); (2) heterodimeric αβ nAChRs, formed by a combination of α (α2, α3 or α4) and β (either β2 or β4) subunits; and (3) complex receptors that include more than one type of α or β subunit (e.g. α3β2β4). This third group also comprises nAChRs containing subunits such as α5, α6 and β3 that do not form channels when expressed alone or in combination with any other single α or β subunit. There is some suggestion that also α7 may be involved in more complex combinations, but the evidence is as yet incomplete.

1.3 FUNCTION: ACTIVATION AND DESENSITISATION

ACh receptors are "allosteric" (in that they are oligomeric) since they contain multiple agonist-binding sites, non-competitive antagonist sites and gates that interact at distance through changes in the quaternary structure of the receptor. Indeed, the distance between ACh binding sites and the ion channel was estimated to be 20-40 Å from fluorescence transfer measurements (Herz et al., 1989).

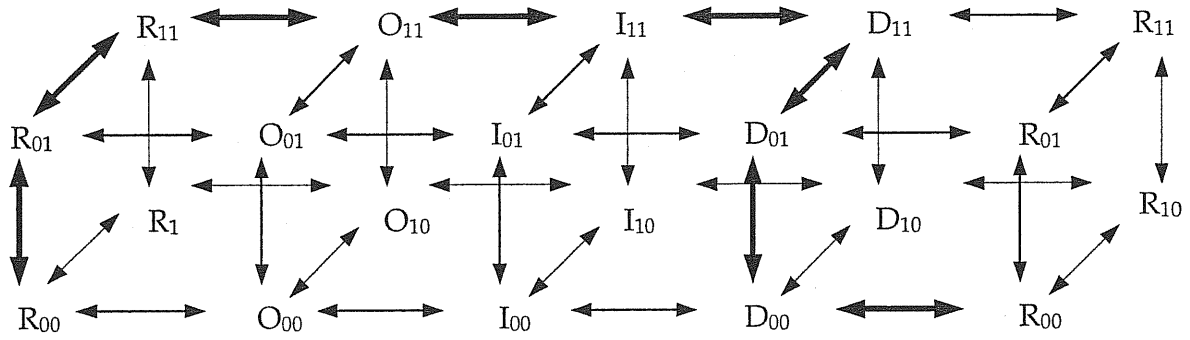

FIGURE 2. Transition between the four states of the ACh receptor. The states of the ACh receptors are resting (R), open (O), fast-onset desensitised (I) and slow-onset desensitised (D). It is assumed that the two agonist-binding sites are different. The subscripts indicate the state of occupation of the sites: 00 unoccupied, 01 or 10, single occupied; 11 double occupied. Resting state and desensitised states are directly connected by allowed transitions. Heavy arrows indicate the principal reaction pathway.

Four functional states have been described for ACh receptors (Figure 2): the resting (closed) state, the open state, the fast-onset desensitised (closed) state and the slow-onset desensitised (closed) state (for reviews see Reitstetter et al., 1999; Grosman and Auerbach, 2001). The resting state is the most stable in the absence of agonist, while the

slow-onset desensitised state is the most stable in the presence of agonist. The open state and the fast-onset desensitised state are metastable, in that their concentration rises transiently and reaches a low value at equilibrium. The role of desensitisation in cholinergic neurotransmission under normal physiological conditions is uncertain, but it is evident in some pathological conditions and is important for other neurotransmitters like GABA (Jones and Westbrook, 1996).

The nAChR behaviour can be described mainly by two different theoretical models. The first is the Monod-Wyman-Changeux (MWC) model of allosteric interactions (Karlin, 1967; Changeux and Rubin, 1968), which postulates that the protein spontaneously isomerises between discrete allosteric states characterised by "all or none" asymmetric changes, providing an adaptable rationalisation of most receptor phenomenology (Edelstein et al., 1996; Grosman and Auerbach, 2001). The second is the sequential model (Del Castillo and Katz, 1957) in which the conformational transitions occur only after agonist binding and lead to agonist-induced multiple intermediate states. This can be used to interpret other observed events not justified by the MWC theory (Kawai et al., 2000; Krauss et al., 2000).

1.4 CONDUCTANCE AND SELECTIVITY

All known ACh receptors, except for an anion selective invertebrate ACh receptor are cation selective (Takahama and Klee, 1990; Kehoe and McIntosh, 1998). This is in contrast with the anionic selectivity of all other Cys-loop receptors. Cation selective nAChRs are permeable to monovalent and divalent cations; permeability increases with monovalent ionic radius and decreases with divalent ionic radius, as a consequence of competitive influences of ionic size and charge (Adams et al., 1980; Lewis and Stevens, 1983).

Permeability ratios of calcium relative to sodium (P_{Ca}/P_{Na}) were estimated to be approximately 0.2 for the muscle nAChRs (Adams et al., 1980), 1–2 for a variety of standard neuronal nAChR subtypes and 6 for α-BTX-sensitive nAChRs that contain α7 or α9 subunits (Fieber and Adams, 1991; Vernino et al., 1992). Although monovalent cations (i.e. Na^+ and K^+) account for the great majority of nAChR current, the calcium

influx was also shown to be significant and biologically important (McGehee et al., 1995; Gray et al., 1996; Role and Berg, 1996; Wonnacott, 1997).

1.5 LOCALISATION AND ROLE OF nAChRS

These receptors are widely distributed on postsynaptic, presynaptic or even axon preterminal areas (Wonnacott et al., 1990; Lena and Changeux, 1993).

The cholinergic synapse between the motor neuron and skeletal muscle, called the neuromuscular junction, provides the best characterised example of fast nicotinic synaptic transmission. Upon arrival of an action potential, the presynaptic motor neuron releases ACh, which diffuses across the synaptic cleft and activates nAChRs on the postsynaptic muscle. The other well-characterised cases of fast nicotinic transmission are in the spinal cord and the autonomic ganglia (sympathetic and parasympathetic nervous system).

In contrast to the neuromuscular junction and autonomic ganglia, relatively rare cases of fast nicotinic synaptic transmission have been reported in the brain. The most widely observed synaptic role of nAChRs is to influence neurotransmitter release. Depending on the tissue and the stage of development, multiple subtypes of presynaptic and preterminal nAChRs have varying degrees of importance in regulating the release of many different neurotransmitters. Biochemical and electrophysiological experiments have shown that both presynaptic and preterminal nAChRs increase the release of neurotransmitters, such as dopamine, glutamate, serotonin and GABA, in tissue culture, brain slices and synaptosomes (McGehee et al., 1995; Role and Berg, 1996; Wonnacott, 1997; Albuquerque et al., 1997a).

Since neuronal nAChRs are highly Ca^{2+} permeable, it is widely documented that receptor activation can cause a significant calcium influx in presynaptic terminal and thus a modulation of the neurotransmitter release (Dani, 2001). Preterminal receptors, which are located before the presynaptic terminal, can indirectly affect release by activating voltage-gated channels.

1.6 STRUCTURE

The first image of the nicotinic receptor overall structure was obtained at low resolution by electron microscopy (Unwin et al., 1988). The *Torpedo* nAChR appears approximately 120 Å long of which 80 Å is the channel, 65 Å is the extracellular part and only about 15 Å extends to the cytoplasm. The external mouth of the channel is wide (about 25 Å) and is surrounded by polypeptide walls of comparable thickness.

Strong experimental evidence (Hucho et al., 1996) supports the widely accepted idea that all nAChR subunits share the following similar topology (Figure 3 A): an extended extracellular domain (N-terminal), four hydrophobic transmembrane regions (M1-M4), an intracellular domain which joins M3 and M4 (whose length varies with the subunit) and a second small extracellular domain (C- terminal). Each M2 segment is thought to form the main channel with some contribution from M1, so that the five subunits surrounding the water-filled pore form a cation selective channel, where Na^+, K^+ and Ca^{2+} can pass in accordance with their electrochemical gradients. The N-terminal domain is also called ACh binding domain since on the interface between α and neighbouring non-α subunits, an ACh-binding site is formed (Figure 3 B).

The recent report of the crystal structure of the acetylcholine binding protein isolated from snails further confirms the pentameric organisation of the N-terminal domain (Brejc et al., 2001).

1.6.1 EXTRACELLULAR DOMAIN: ACH-BINDING SITE

The reconstruction of functional receptors isolated by biochemical purification from the *Torpedo* electric organ constituted the first demonstration that these proteins can form both the ligand-binding site and the ionic pore. From investigations in the 1980s on the kinetic of the ionic current through a single channel, it has been accepted that two agonist-binding sites exist. The occupancy of these two sites, in a positive cooperative way, stabilises the receptor channel in an open state (Colquhoun and Sakmann, 1985; Hess et al., 1987). Later, ACh-binding sites were proposed to be located in two putative pockets of two receptor subunits, at approximately 30 Å above the membrane surface (Unwin, 1993; Unwin, 1995; Miyazawa et al., 1999; Tierney and Unwin, 2000).

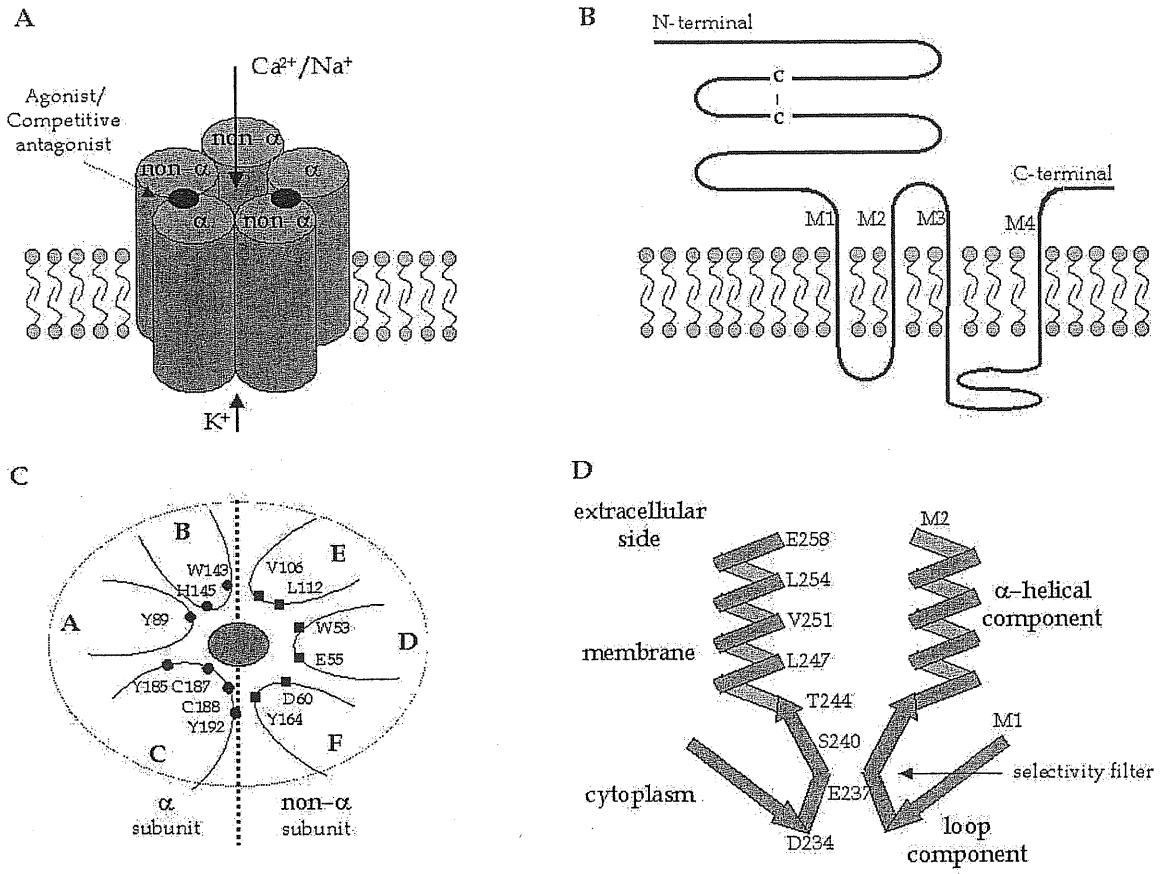

FIGURE 3. **Structure of nicotinic acetylcholine receptors.** **A**: Schematic representation of the quaternary structure, showing the arrangement of the subunits in a heterometric receptor, the location of the two ACh binding sites (between α and non-α subunit) and the axial cation-conducting channel. **B**: The threading pattern of receptor subunits throught the membrane consists of an extended extracellular domain (N-terminal), four hydrophobic transmembrane regions (M1-M4), an intracellular domain which joins M3 and M4 (whose length varies with the subunit) and a second small extracellular domain (C-terminal; Hucho et al., 1996). **C**: Agonist binding site loop model. **D**: Model for the structural and functional organisation of the ion channel. The residues with given numbers are believed to face the lumen of the ion channel. The data (Le Novere et al., 1999) suggest that the upper part of the channel, the α-helical component, forms a water pore, while the lower loop component contributes to the selectivity filter of the ion channel.

With the availability of specific chemical compounds and the amino sequences of different nAChR subunits, important advances concerning the knowledge of the ACh-binding sites have been made. For instance, photoaffinity experiments carried on the muscle-type receptors (Galzi et al., 1991a; Akabas and Karlin, 1995) and modelling studies (Ortells et al., 1997; Le Novere et al., 1999), have shown that the ligand-binding

site must be at the interface between the αs and their adjacent γ or δ subunits (Changeux et al., 1998; Taylor et al., 2000).

Six loops termed A-F have been identified for the ACh-binding sites. The α subunit, which contains the principal component of the binding site, comprises the A, B and C loops, while the complementary component of the adjacent subunit (γ, δ or ε for the muscle and β for the neuronal) comprises the D, E and F loops (Figure 3 C). Affinity-labelling of the ACh-binding site of the Torpedo $(\alpha 1)_2\beta 1\gamma\delta$ complex, led to the identification of the first residues, a pair of adjacent cysteines –αCys192 and αCys193 (loop C)– (Kao et al., 1984) which form a highly unusual disulphide bond (Kao and Karlin, 1986). Subsequently, four widely spaced aromatic residues -αThr93 (loop A), αThr149 (loop B), αThr190 and αThr198 (loop C)– were affinity labelled (Middleton and Cohen, 1991; Galzi et al., 1991b). These residues are conserved in all ACh receptor α-subunits except in neuronal α5 in which Asp190 replaces Tyr190. Also γ and δ, but not β, subunit contribution to the ACh-binding site was detected (Kurosaki et al., 1987; Blount and Merlie, 1989; Sine and Claudio, 1991; Sine, 1993). Specifically, competitive agonists and antagonists were observed to bind aromatic and charge residues on the γ subunit, namely γTrp53 (loop D), γTyr111 (loop E), γTyr117 (loop F) and γLeu109 (loop E) (Wang et al., 2000).

1.6.2 MEMBRANE DOMAIN: CHANNEL STRUCTURE, GAITING AND SELECTIVITY

The membrane channel has a key role in mediating receptor transmission. In fact, upon binding of a specific neurotransmitter, the channel (i) mitigates the energy barrier to ion translocation through the hydrophobic environment, (ii) selects ions and (iii) quickly opens and closes to permit their diffusion across the membrane according with their concentration gradient (Sakmann, 1992). Conductance and permeability properties of nAChRs could be understand on the basis of the ionic pore structure.

Cryo-electron microscopy of tubular arrays of *Torpedo* receptor in the membrane yielded a 9 Å resolution map that showed five bend rods around the central axis of the membrane domain; these were presumed to be α-helices lining the ion channel along the symmetry axis of the receptor (Unwin, 1993). Only later, several experiments –with

techniques such us infrared spectroscopy (Methot et al., 2001), computational methods (Le Novere et al., 1999) or chemical (Akabas et al., 1994; Zhang and Karlin, 1997) and mutational (Tamamizu et al., 2000) approaches– revealed that the membrane spanning segments were not completely α-helical, but a mixture of α-helix, β-strand and irregular secondary structures. Information about the tertiary structure of this region is limited to the approximate arrangement of the membrane spanning segments relative to the channel lumen and to the lipid bilayer: M2 and some M1 line the central lumen, and M3 and M4 are in contact with lipids.

By means of substituted-cysteine accessibility method (SCAM), it has been shown (Cohen et al., 1992; Wang and Imoto, 1992; Villarroel et al., 1992) that the ion channel was composted by two distinct structural components (Figure 3 D): an upper portion (the α-helical M2 segment), which delimits both an aqueous wide pore (~ 25 Å in diameter at the extracellular mouth) and the pharmacological site for non-competitive blockers, plus a lower short portion (the loop between M1 and M2 segments), which contributes to the narrowest portion of the channel (~ 6.5 Å in diameter and ~ 6 Å in length). Furthermore, the contribution of the M1 segment upper part to the channel, possibly by interaction with the M2 segment, was suggested by SCAM experiments (Akabas and Karlin, 1995; Zhang and Karlin, 1997).

With such a funnel shape of the ion channel (Miyazawa et al., 1999), the permeation mechanism could be interpreted as a two-step process (Figure 3 D). First, in the upper part of the channel, the energy barrier is lowered by allowing ions to be surrounded by water within the low-polarity interior of the channel and in the lipid bilayer. Then, in the lower section, the channel becomes narrow enough to force each hydrated cation to move in a single file (Dani, 1989). The energy barrier in this region can be lowered by interactions of the permeating ion with charged residues and with side-chain and backbone dipoles (Morais-Cabral et al., 2001; Zhou et al., 2001). This narrow section, which is at the cytoplasmic end of the channel, selects for ion charge and size and determines conductance (Cohen et al., 1992; Corringer et al., 1999). This region seems also to contain the resting gate (Wilson and Karlin, 1998; Wilson and Karlin, 2001).

1.7 AChBP: A NICOTINC BINDING DOMAIN STRUCTURAL MODEL

The knowledge of the extracellular domain structure of the all Cys-loop receptors, and particularly of the nicotinic receptors, took a giant step forward with the resolution of the acetylcholine binding protein (AChBP) structure from *Lymanaea stagnalis* (Brejc et al., 2001). The AChBP is a homopentameric soluble protein secreted by snail glial cells into cholinergic synapses, where it modulates synaptic transmission by binding ACh (Smit et al., 2001). AChBP binds agonists and competitive antagonists of the nAChR, including ACh, nicotine, epibatidine, (+)-tubocurarione and α-bungarotoxin, with an affinity spectrum similar to the α7 homomeric neuronal nicotinic receptor. Its similarity to the N-terminal domain of nicotinic receptors is such that the AChBP structure can reveal much about the nature of the nAChR ligand-binding domains.

The AChBP subunit, which was detected originally in a snail complementary-DNA library, contains 210 amino acids and is 20-24% identical to aligned sequences of the amino-terminal extracellular halves of nAChR subunits, and 15-18% identical to similarly sequences of 5-HT_3, $GABA_A$, $GABA_C$ and glycine receptor subunits (Figure 4). The eponymous disulphide-bond between cysteines is present also in the AChBP subunit, but it is only 12 intervening residues in place of 13 as in the Cys-loop receptor subunits.

1.7.1 OVERALL STRUCTURE

AChBP is a cylinder of 80 Å in diameter and 62 Å in height. Each of the five identical subunits occupies a sector of the cylinder in such a way to line an axial channel of 18 Å diameter (Figure 5 A-B). Each subunit starts at its amino termini with a three turn α-helix and thereafter forms ten β-stands with connecting loops, including two short 3_{10} helices. In three dimensions, each cysteine bridge is close to the subunit carboxyl terminus at the bottom of the cylindrical complex. In the aligned Cys-loop receptor subunits, the sequences continue immediately into the membrane-spanning domain M1 (Hucho et al., 1996); so, in the receptors the cysteine bridge is close to the extracellular surface of the membrane.

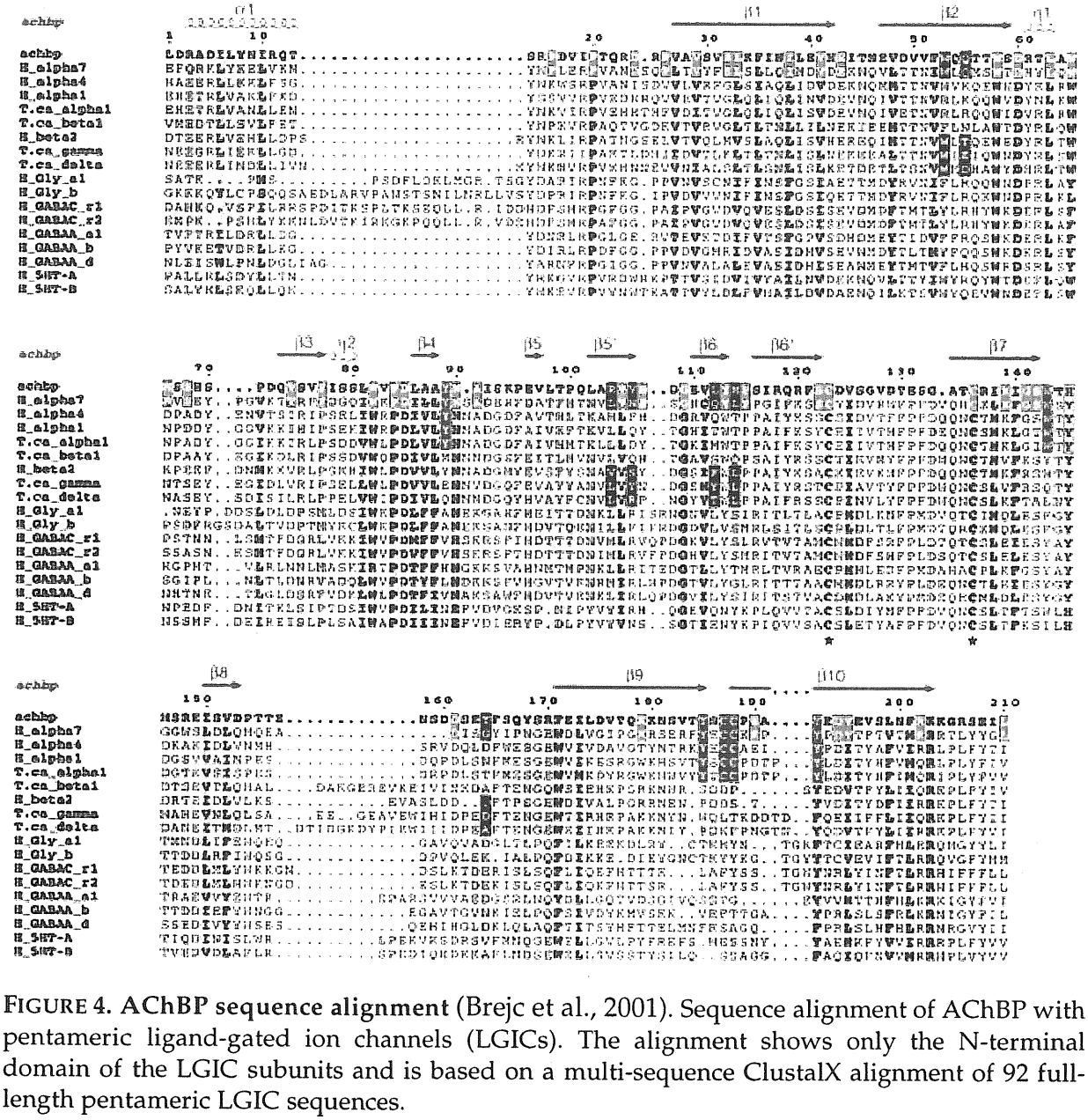

FIGURE 4. **AChBP sequence alignment** (Brejc et al., 2001). Sequence alignment of AChBP with pentameric ligand-gated ion channels (LGICs). The alignment shows only the N-terminal domain of the LGIC subunits and is based on a multi-sequence ClustalX alignment of 92 full-length pentameric LGIC sequences.

On the contrary, the amino terminus of the AChBP subunit is at the opposite end of the cylinder (the top), placing the amino termini of the Cys-loop receptor subunits farthest from the membrane.

The secondary structure of each AChBP subunit closely resembles that predicted for the extracellular domain of the nAChR subunits (Le Novere et al., 1999). It is similar in size and shape to the 3D view of the extracellular domain of *Torpedo* nAChR, obtained by cryo-electron microscopy, which also contains β-stands (Miyazawa et al., 1999). Brejc et al. (2001) mapped the contact residues in the subunit-subunit interfaces of the AChBP

and noted that they were poorly conserved among the Cys-loop receptor subunits. However, this lack of conservation among different subunits interfaces is to be expected because different contact residues would need to obtain specific arrangements of the subunits in heteropentameric Cys-loop (Karlin, 2002).

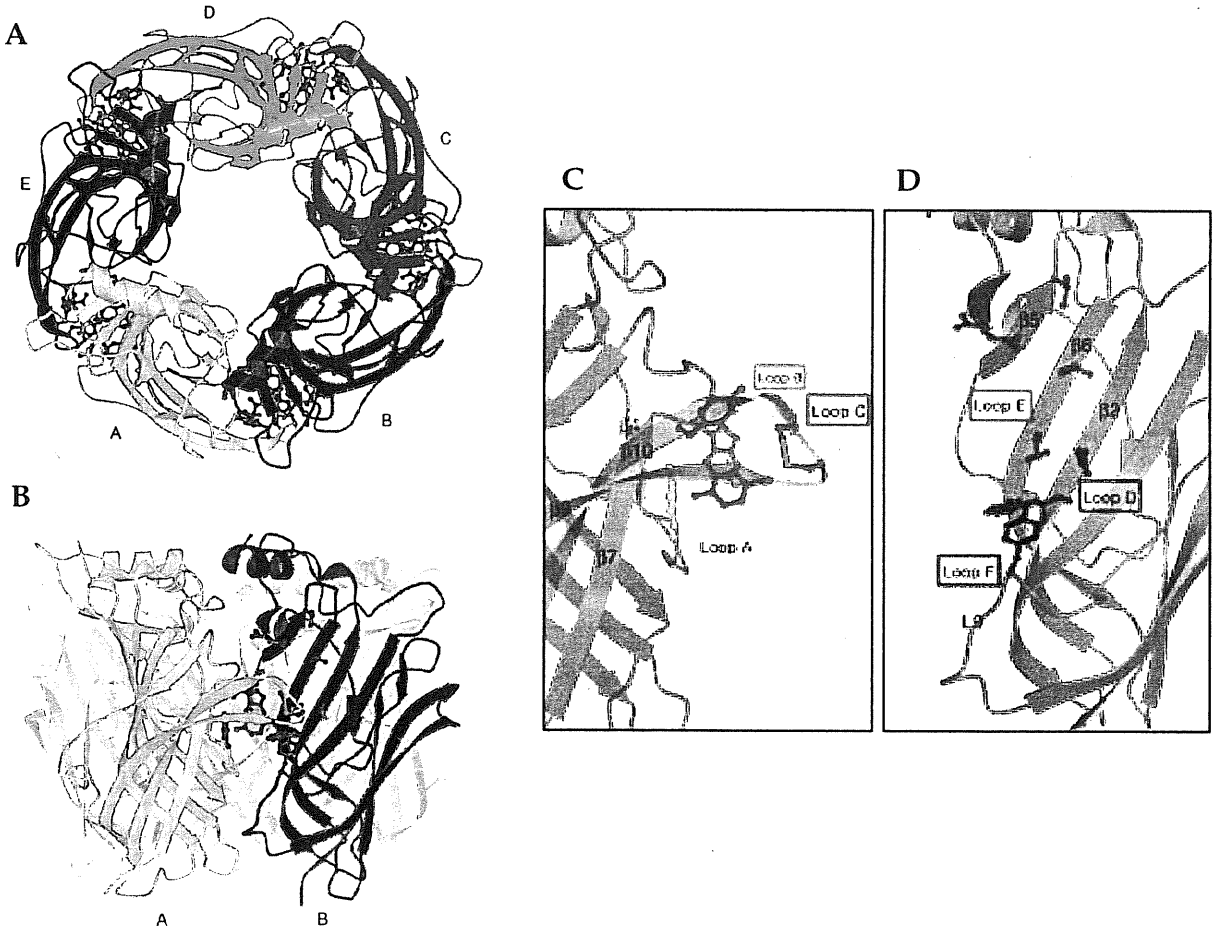

FIGURE 5. AChBP structure (Brejc et al., 2001). **A**: Each subunit of the pentamer has a different colour. Subunit are labelled anti-clockwise forming the (+) and (-) interface side of the ACh binding sites. **B**: View of the AChBP pentamer perpendicular to the five-fold axis. The equatorially located binding site is represented in ball and stick only in the A (yellow) and B (blue) interface. **C**: Location of the principal component (+) residues of the ligand-binding site on 'loops' A (yellow), B (dark yellow) and C (orange). **D**: Location of the ligand-binding residues on the complementary (-) 'loops' D (violet), E (light blue) and F (blue). Note that loops D, E and F are all on -strands.

1.7.2 ACH BINDING SITE

Although the AChBP was crystallised in the absence of a specific ligand, the ligand binding site was clearly identified as the cavity at the interface between pair of subunits. Indeed, the cavities are lined by the residues which were biochemically

shown to be involved in ligand-binding in nAChRs (Corringer et al., 2000). These binding pockets are mostly buried from the solvent and located close to the outside of the pentameric ring (Figure 5 A). When viewed perpendicular to the five-fold axis, they are roughly mid-way positioned, about 30 Å away from the C-termini (Figure 5 B), conforming to the expected location of the *Torpedo* receptor ligand-binding site, as determined by labelling (Fernando et al., 1994) and electron microscopy (Unwin, 1993) studies.

Each ligand-binding site is found in a cleft formed by a series of loops from the principal face of one subunit and a series of β-strands from the complementary face of an adjacent subunit (Figure 5 C-D). The principal component on the (+) side of the (+)/(–) interface consists of residues coming from loop A (+Tyr 89), loop B (+Trp143 and +Trp145) and loop C (+Tyr185, +Cys187, +Cys188 and +Tyr192). The complementary part of the binding side is, instead, formed by β-strands on the (–) protomer, contributing loop D (–Trp53, –Gln55), loop E (–Arg104, –Val106, –Leu112 and –Met114) and loop F (–Tyr164). While all residues of nAChR α subunits are conserved on the AChBP principal component, most of residues on the complementary side differ from the aligned one on the δ or γ subunits of *Torpedo* receptor (Figure 4). Four aromatic residues form the bottom half of the cavity (+Tyr89, +Tyr185, –Tyr164 and –Trp53), while the walls are formed by the rings of +Tyr192, +Trp143, the main chain of +Trp145, the side chains of –Met114 and –Gln55, and the disulphide bridge between +Cys187 and +Cys188. The hydrophobic parts of –Arg104, –Val106 and –Leu112 form the top of the binding site.

Quaternary ammonium binding by ACh receptors

Agonists and competitive antagonists of ACh receptors have at least one quaternary ammonium group or a protonated tertiary ammonium group. It seems likely that in the ACh receptor, the ammonium group binds in the cage of five aromatic side chains that are aligned with +Tyr89, +Trp143, +Tyr185 and +Tyr192 of the AChBP (+) side and –Typ53 of the opposite (–) side. A sixth aromatic side chain, –Tyr164, is not conserved in the nAChR γ or δ subunits. This aromatic ring arrangement is consistent with the important contribution of cation-π interactions in the binding of the ACh quaternary

ammonium group (Zhong et al., 1998a; Schmitt et al., 1999). Three negatively charged side chains at the aligned position (or close by) the *Torpedo* residues α_1D152, α_1D200 and γAsp174/δD180, which have been shown to affect the ACh binding affinity (O'Leary and White, 1992; Martin et al., 1996; Sugiyama et al., 1996), are also conserved in the AChBP. These negatively charged residues are probably the source of a negative electrostatic potential in the ACh binding site (Osaka et al., 1998; Akk and Auerbach, 1999), and their movements towards a bound quaternary ammonium group could be part of the activation mechanism (Sullivan and Cohen, 2000).

STRUCTURAL CHANGES OF THE BINDING SITE

In general, ACh receptor agonists are smaller than competitive antagonists. This is consistent with the idea that the ACh-binding site contracts around a bound agonist and less so around a bound antagonist (Karlin, 1969), similar to what occurs for AMPA-type glutamate receptors (Armstrong and Gouaux, 2000). From the AChBP structure, the most likely access routes to the ligand binding sites seems to be from above or below the double-cysteine-containing loop C, conforming with results obtained by biochemical experiments (Damle and Karlin, 1980). As Brejc et al. (2001) pointed out, the loop would have to move for a large antagonist to enter the site. It is possible that when the site is unoccupied, or occupied by an antagonist, the loop C is mobile and accessible. However, when an agonist occupies the site, the loop might be immobilised and the binding site capped. If the 'lid-shut' conformation corresponds to the active state of the binding site, which is coupled to the open state of the channel, the closed lid could explain the 2500-times slower dissociation of agonist from the receptor open state than from the resting state (Grosman and Auerbach, 2001; Karlin, 2002).

1.8 RECEPTOR MODULATION: ROLE OF AGONISTS AND ANTAGONISTS

The short- and long-term regulation of nAChR function is likely to be important for modulating synaptic efficacy. Nicotinic receptor function is short-term controlled by a number of factors which include peptide transmitters (e.g. substance P), various protein kinases, the cytoskeleton and Ca^{2+}. Long-term control of nAChRs can occur via

intracellular second messenger systems (e.g. cyclic adenosine monophosphate or protein kinase C).

Moreover, nAChRs are the molecular targets for the offensive or defensive mechanisms of a wide variety of plants and animals, hence Nature has provided an array of potent ligands. The nicotinic receptors can bind many natural substances such as (–)-nicotine, (–)-cytisine, (+)-anatoxin A, (+)-epibatidine or anabasine, which compete for the same extracellular binding site to initiate the conformational change that leads to the cationic pore opening. Since the ACh binding site is located at the interface between two subunits, each nAChR subtype binds agonists with different affinities.

Channel opening can be, also, inhibited by several ligands that compete for the neurotransmitter binding site. These molecules, named competitive antagonists, interact reversibly with the nAChR at, or close to, the agonist binding site, stabilizing the receptor in its closed pore conformation and preventing agonist access. The classic antagonist is *d*-tubocurarine (*d*-TC), however the most well-established subtype-selective ones are the α-bungarotoxin (α-BTx) and the α-conotoxins (α-CTx). These are peptides that bind some α subunits, probably between residues Phe187 and Asp200, partially overlapping loop C of the agonist binding site (Arias, 2000).

In addition to binding sites for agonists and competitive antagonists, all the ligand-gated ion channels possess sites for a heterogeneous class of compound named non-competitive (or allosteric) antagonists (NCA). These drugs inhibit agonist-evoked ion flux without inhibiting agonist binding. The NCAs are structurally and chemically very different from each other, nevertheless these molecules preserve certain common pharmacological properties such as apparent blockade of the ion pore by a steric mechanism, channel inactivation by allosteric process and enhancement of the desensitisation rate. A more complex picture has been observed for certain NCA that can also activate the nAChR by means of a weak agonist activity (Albuquerque et al., 1997b; Maelicke et al., 1995; Arias, 1997). For example, (–)-physostigmine (also called eserine) in addition to its non-competitive inhibitory property and anticholinesterase action (Canti et al., 1998), induces cation influx via muscle, neuronal and *Torpedo* receptors (Pascuzzo et al., 1984; Pereira et al., 1993; Sung et al., 1998; van, I et al., 1998).

Such effects were observed even in the presence of saturating concentration of ACh or competitive antagonists such as *d*-TC, α-BTx or α-CTx. The stoichiometry of the (–)-physostigmine binding site was found to be two for each receptor (Schrattenholz et al., 1993; Maelicke et al., 1995). Labelling results also suggest that these allosteric modulators interact with residue α1Arg125 (Schrattenholz et al., 1993), so that Arias (2000) proposed for the allosteric agonist binding site the gorge between the two hydrophobic segments 118-114 and 130-137.

All these compounds can discriminate among distinct nAChR subtypes and are thus useful to fingerprint nAChR subtypes in different cells and tissues.

1.9 THERAPEUTIC POTENTIAL OF NICOTINIC RECEPTOR ACTIVATION

Positive effects following administration of nicotine to humans have been observed for cognitive and attention deficits –Parkinson's disease (Lange et al., 1993)–, anxiety –Tourette's syndrome (Olale et al., 1997)–, ulcerative colitis and smoking cessation. Results of clinical studies have shown efficacy of nicotine for treatment of adult attention deficit hyperactivity disorder (Conners et al., 1996) and depression (Salin-Pascual et al., 1996). Nicotine also normalises an auditory gating deficit found in schizophrenic patients (Leonard et al., 1996; Freedman et al., 2000). Antinociceptive effects of nicotine has been known for some time, but the discover of epibatidine as a much more potent and broadly effective analgesic agent that acts via neuronal nAChRs (Qian et al., 1993), has stimulated renewed interest in targeting nAChRs for analgesia.

Furthermore, as nicotine and cytisine can attenuate the neurotoxin effect of β-amyloid (Kihara et al., 1998) and inhibit in vitro formation of amyloid from β(1-42) peptide (Salomon et al., 1996), they might have a role for potential attenuation of the process underlying Alzheimer's disease. An abnormal structural variant of nAChRs may account for some forms of epilepsy (Steinlein et al., 1995), suggesting the possibility of targeting this abnormal nAChR for a therapeutic treatment.

Despite evidence for the effectiveness of nicotine on numerous disorders, long-tem efficacy and minimising side effects remain to be resolved (Perry et al., 2000). Moreover, absorption of nicotine after oral ingestion is minimal. Potential side effects include those

on the cardiovascular and gastrointestinal systems, dependence, sleep disturbance and, at higher doses, neuromuscular effects. The possibility that these issues can be addressed with alternative agents that selectively and perhaps only partially activate specific subtypes of nAChRs, represents an opportunity for drug discovery. Most current efforts can be viewed as a search for agents that act via stimulation of nAChRs in the central nervous system (CNS), like nicotine and epibatidine do, but possess improved pharmacological and side effect profiles. Targeting nAChRs for therapy is not new; selective blockers of nAChRs at the neuromuscular junction or in ganglia (such as d-tubocurarine, trimethaphan, mecamylamine, hexamethonium and related compounds), have been used clinically as muscle relaxants during surgery or as antihypertensive agents (Holladay et al., 1997).

1.10 A MODEL CELL FOR STUDING NATIVE NACHRS: CROMAFFIN CELL

Many studies have been carried out on heterologous expression systems, consisting of cells lacking nicotinic receptors and made to express nAChRs with various subunit combination. Different biophysical and pharmacological properties of numerous subunit aggregates can then be investigated.

A suitable experimental model is represented by rat cromaffin cells which are found in the medullary portion of adrenal glands. The adrenal medulla is an endocrine gland of the sympathethic nervous system and regulates involuntary functions, such as heart rate, intestinal movements or pupil dilation, by discharging hormones into the bloodstream. Like neurones of the sympathetic system, the activity of adrenal medulla is controlled by nerves originating in the spinal cord, in particular the splanchinic nerve that releases ACh.

Cromaffin cells are used as a laboratory model of neurones since they directly derive from the neuronal crest, are electrically excitable so as to generate action potentials, and release catecholamine transmitters in a Ca^{2+} dependent fashion. These cells are activated by acetylcholine (released by the splanchnic nerve) and possess high nAChR density. Due to their properties, cromaffin cells have been widely used for pharmacological and physiological studies aiming at characterizing nAChRs (Khiroug et al., 1997; Khiroug et al., 1998; Giniatullin et al., 1999).

Subunit composition of nAChRs natively expressed in these cells has been recently characterized. α3, α5, α7 and β4 subunits are reported to be expressed in bovine chromaffin cells to form both homomeric α7 and heteromeric α3β4 (probably together with a α5 receptors; Campos-Caro et al., 1997). RT-PCR analysis of mRNA expression in cultured rat chromaffin cells indicates the presence of nearly every known nAChR subunit (α2, α3, α4, α5, α7, β2 and β4). However, combing data from various experimental approaches it seems that rat chromaffin cells more probably express α3β4, α3α5β4, α3β2 and α4β2 heteromeric receptors but not α7 homomeric receptors (Di Angelantonio, 2002). These results do not exclude the possibility of other subunit assemblies.

2. SARCOPLASMIC RETICULUM CALCIUM ATP-ASE

2.1 A P-TYPE ATPASE

P-type ATPases comprise an important family of homologous enzyme in eucaryotic and prokaryotic cells, which actively pump cations across cell membranes. Distinguishing features of P-type ATPases are the formation of a covalent aspartate phosphorylated intermediate and a dependence of ATPase activity on the specific binding of ions (Mintz and Guillain, 1997). P-type cation pumps, or also so-called ion motive pumps, constitute a diversified group of ATPases present in animal, plant and bacterial organisms (Mintz and Guillain, 1997).

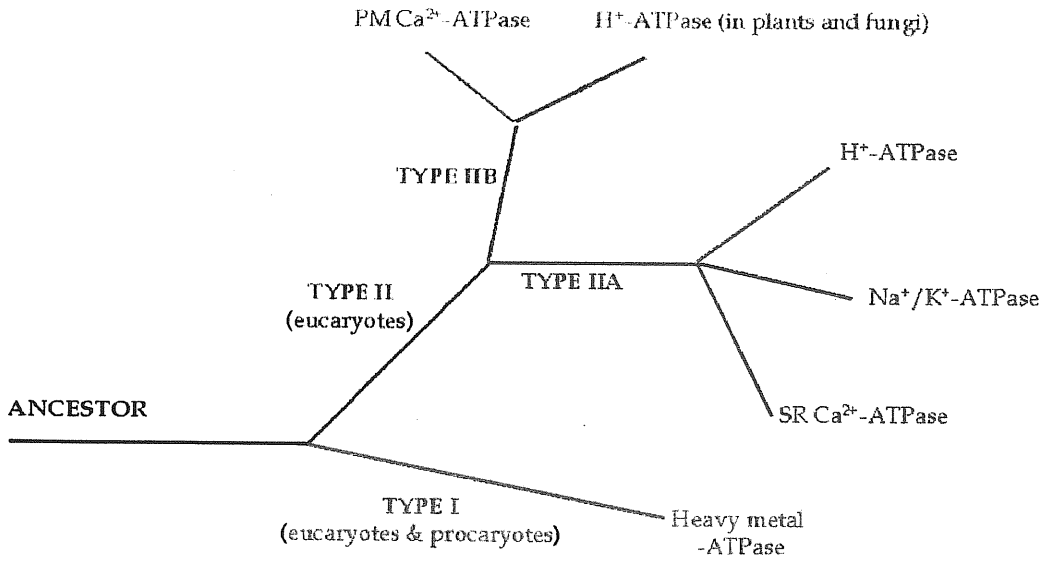

FIGURE 6. Phylogenetic tree of P-type ATPases. The figure suggests an ancestral prokaryotic division of cation transporting into Type I (heavy metal transporters) and Type II (calcium and magnesium transporters). During the course of evolution further diversification of Type II took place into Type IIA and IIB.

Figure 6 illustrates the probable phylogenetic tree of this family (Moller et al., 1996) which divides the proteins in three major groups. Type I is probably the family progenitor, meaning that P-type ATPases originally were involved in the transport of heavy metals like Cu^{2+}, Cd^{2+} and Hg^{2+}. Type II ATPases are instead characterised by the ability to transport cations of lower atomic masses like H^+ (type IIA) and Na^+, K^+ or

Ca^{2+} (type IIB). In eucariotyotic cells predominant members of the family include: Ca^{2+}-ATPases, involved in cell regulation of Ca^{2+} and present in both plasma and intracellular membranes; Na^+/K^+-ATPases, whose role is essential in cellular volume regulation, in membrane potential development or in transmembrane transport in intestine and other epithelial tissues; H^+-ATPases, important for many plants cellular function as nutrition; and finally vertebrate H^+/K^+-ATPases, involved in secretion of H^+ and K^+-equivalent in the stomach and distal colon, respectively.

Following initial discoveries of Na^+/K^+-ATPases (Skou, 1957) and sarcoplasmic reticulum Ca^{2+}-ATPases (Hasselbach and Mackinose, 1961), a large number of studies have been carried out on these two enzymes in order to characterise its translocation mechanism. Despite the attempt to unravel functional and structural properties of the enzyme family, in absence of structural information essential aspects of their mechanism cannot be resolved. To clarify these questions involves understanding the exact mechanism by which the cations are translocated across the membrane and the interaction between the cation binding sites and the catalytic sites (phosphorylation and ATP binding), leading to transport of the ions against their electrochemical gradient (energy transduction).

The resolution of a Ca^{2+}-ATPase crystal structure (Toyoshima et al., 2000) has provided the first structural basis to clarify some of these essential aspects. Ca^{2+}-ATPases of sarcoplasmic reticulum (SERCAs) are encoded by three genes: SERCA1, SERCA2 and SERCA3. The crystallised Ca^{2+}-ATPase belongs to SERCA1, which encodes the Ca^{2+}-ATPases of sarcoplasmic reticulum (SR) in fast-twitch skeletal muscles.

2.2 CA^{2+}-ATPASE REACTION MECHANISM

2.2.1 REACTION CYCLE

In the case of the Ca^{2+}-ATPase, the ATP chemical energy is used to pump Ca^{2+} from the cytoplasm of muscle cells to the sarcoplasmic reticulum (Ebashi and Lipman, 1962). Ca^{2+} transport is believed to occur in a multi-step reversible cycle (Figure 7), the so-called E_1-E_2 model (Makinose, 1973; de Meis and Vianna, 1979). The first step of the cycle is binding of two Ca^{2+} from the cytoplasmic region accompanied by a transition of

the complex between conformations E_2 and E_1. Then, in the second step, ATP binding activates the phosphorylation of Asp351, occluding Ca^{2+} within the protein to form a high-energy intermediate Ca_2E_1-P. Subsequently, the phosphorylated enzyme loses its high affinity for Ca^{2+} and opens the gate to the lumen space. Finally, hydrolysis of Asp351 regenerates the initial ATPase complex (E_2).

An important feature of this cycle is the total reversibility of the phosphorylation events (Makinose and Hasselbach, 1971), which has greatly facilitated the study of the transport cycle. In fact, not only the phosphorylated ATPase can react with ADP in presence of Ca^{2+} to regenerate ATP, but also the incubation of the ATPase with P_i in the absence of Ca^{2+} and in presence of Mg^{2+} (Masuda and de Meis, 1973) can lead to ATPase phosphorylation (Suko et al., 1981; Lacapere et al., 1981; Jencks et al., 1993).

The substrate for the ATPase reaction is MgATP: Mg^{2+} and ATP can bind and dissociate from the catalytic site independently or as the Mg^{2+} complex (Reinstein and Jencks, 1993). The enzyme can either first bind Ca^{2+} and then MgATP or first MgATP and then Ca^{2+}, even if in the first case the phosphorylation rate constant is higher (Petithory and Jencks, 1986).

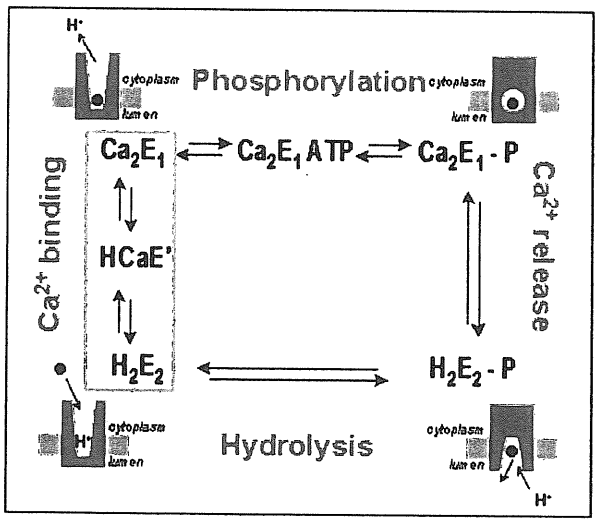

FIGURE 7. Sarcoplasmic reticulum Ca^{2+}-ATPase functional cycle. The reaction mechanism of the protein involves calcium-bound (E_1) and hydrogen-bound (E_2) conformations. Four steps characterise the cycle: (i) Ca_2E_1 contains two ions in the binding site and the Ca^{2+} ions can access the protein from the cytoplasmic site. (ii) Ca_2E_1-P is the same as Ca_2E_1 except that it is phosphorylated and the two Ca^{2+} are occluded in the protein. (iii) H_2E_2-P does not contain Ca^{2+} and the latter can access the protein from the lumen site. (iv) H_2E_2 is the same as H_2E_2-P except that the system is not phosphorylated and Ca^{2+} access the protein from the cytoplasmatic side. The protein is represented by a red box and the presence of a sphere, or an H^+ inside the cartoon, indicates presence of Ca^{2+} or protons.

COUNTER-TRANSPORT

Several millimolar Ca^{2+} accumulates in the SR lumen. This accumulation of four positive charges per turnover must be counter-balanced to allow several consecutive cycles to occur. It has been successively proposed first that Mg^{2+} and/or K^+ could be exchanged for Ca^{2+} (Kanazawa et al., 1971), then that the Ca^{2+} uptake was balanced by K^+ efflux through K^+ channel (Zimniak and Racker, 1978) and finally that H^+ was exchanged for Ca^{2+} (Chiesi and Inesi, 1980). The difficulty in these studies is to analyse whether the counter-balancing changes are transported by the Ca^{2+}-ATPase itself or by diffusion across the vesicle membrane which is permeable to H^+, or ever via another transporter. The assumption that H^+ is exchanged for Ca^{2+} was strongly sustained by the experimental observation that H^+ ejection during Ca^{2+} uptake was mediated by Ca^{2+}-ATPase itself (Yamaguchi and Kanazawa, 1984; Yamaguchi and Kanazawa, 1985). Nevertheless, because of membrane permeability, no electric potential difference or H^+ gradient can be accurately measured in native vesicles. Initially it is has been proposed an exchange of three H^+ for two Ca^{2+} (Levy et al., 1990), whereas later a proton counter-transport of one H^+ per each Ca^{2+} was sustained emphasising the similarity between Ca^{2+}/H^+, Na^+/K^+ and K^+/H^+-ATPases (Yu and Inesi, 1993).

The debate on proton counter-transport is still in course since an exhaustive demonstration has not been yet obtained. In the present work, a one per one H^+/Ca^{2+} exchange was supposed (Yu and Inesi, 1993).

CALCIUM BINDING MECHANISM

In 1980, Inesi et al. proposed that Ca^{2+} binding occurs as a cooperative two-step process, comprising fast binding of a first Ca^{2+} followed by a slow conformational change which allows binding of a second Ca^{2+}. Additional evidence of sequential character of calcium binding reaction was provided by studies of Sr^{2+} binding (Fujimori and Jencks, 1992). The existence of a fast phase was shown to be favoured in the presence of Mg^{2+}, at neural or alkaline pH and at low temperature (Dupont, 1982; Champeil et al., 1983; Guillain et al., 1984). It has also been shown that, in the absence of Ca^{2+}, the pump can be found in various forms depending on both H^+ and Mg^{2+} concentrations (Forge et al., 1993a). The existence of a fast phase was observed to be correlated with the existence of

a deprotonated form E_2 (Forge et al., 1993b). For instance, at pH 9, where all ATPases are deprotonated, Ca^{2+} binding process is fast. Conversely, at pH 6, where H_2E_2 is predominant, Ca^{2+} binding is slow because it first necessitates slow deprotonation.

As described by the E_1-E_2 model, Ca^{2+} binding process is accompanied by a protein conformàtional change (Dupont, 1977; Henderson et al., 1994a; Henderson et al., 1994a). In the hypothesis of 1:1 H^+/Ca^{2+} exchange, the cooperative mechanism of Ca^{2+} binding can be describe by the following scheme (Inesi et al., 1980):

$$H_2E_2 + Ca^{2+} \leftrightarrow HCaE' + Ca^{2+} \leftrightarrow Ca_2E_1$$

That is, Ca^{2+} binding to site I induces a conformational change of the protein (HCaE' state) which features high affinity for calcium in site II and then binding of the second Ca^{2+} causes the formation of the Ca_2E_1 state.

Finally, ATPase can bind other divalent cations such as Sr^{2+} and Ba^{2+} (Holguin, 1986), but transport has been characterised only for Sr^{2+} (Berman and King, 1990). On the contrary, Mn^{2+} was observed to have a weak inhibitory effect (Chiesi and Inesi, 1981).

MODELS FOR CALCIUM TRANSPORT

The original E_1-E_2 model proposed that, in E_1 conformation, the ATPase contained two high affinity binding sites for Ca^{2+} exposed to the cytoplasm, whereas in the E_2 conformation these two sites were transformed into low affinity sites exposed to the lumen of the SR; this is the alternating site model (Figure 8, for a recent review see Lee and East, 2001). More recently, it has become clear that the alternating-site model is not compatible with most kinetic and equilibrium data available for the Ca^{2+}-ATPase. Specifically, the alternating-site model predicts that binding of Ca^{2+} to the ATPase from the lumen side (to the E_2 conformation) will be competitive with binding of Ca^{2+} from the cytoplasmic side (to the E_1 conformation). In contrast, it has been shown that lumen Ca^{2+} ions do not compete with Ca^{2+} binding to the cytoplasmic pair of sites and can equally bind to both unphosphorylated (E_2) and phosphorylated (E_2P) conformations (Jencks et al., 1993; Khan et al., 1997).

The simplest explanation is that the Ca^{2+} can bind simultaneously at the two sides of the membrane (Jencks et al., 1993) as represented by the four-site model (Figure 8).

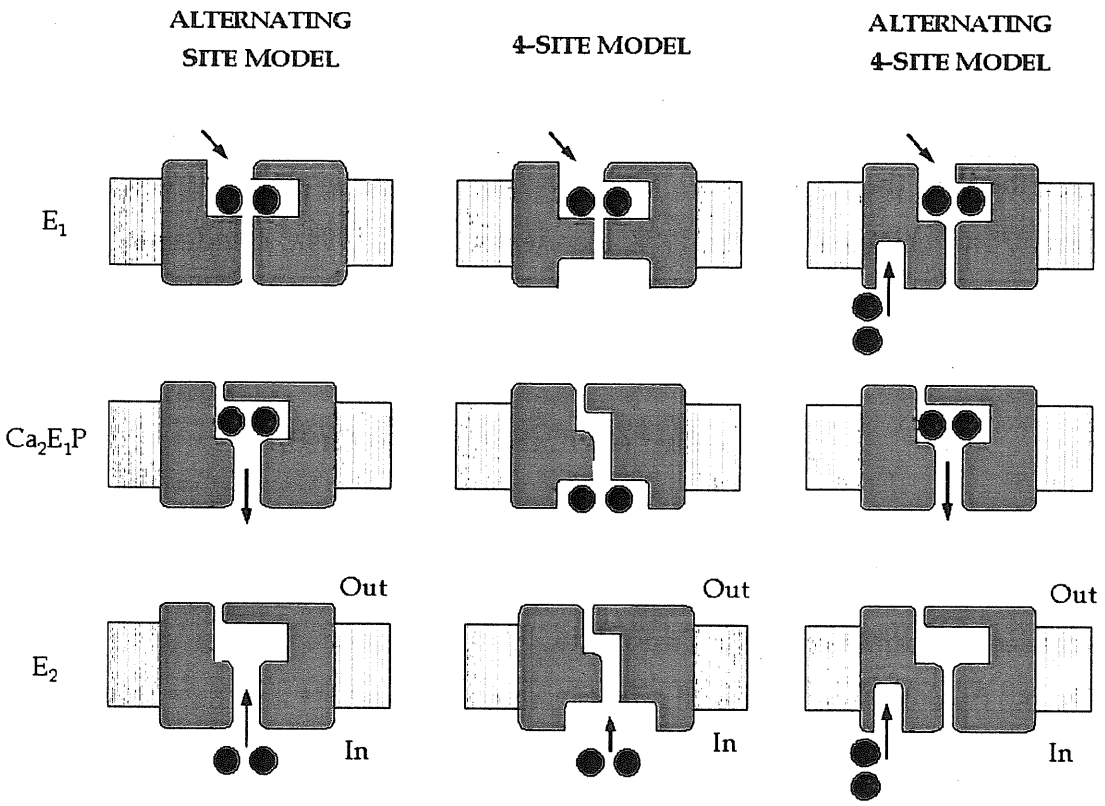

FIGURE 8. Three models of calcium transport by the Ca^{2+}-ATPase. The alternating-site model proposes the presence of one pair of sites which alternate from being exposed to the cytoplasm in E_1 conformation, to being exposed to the lumen in Ca_2E_1P and E_2 states. In the four-site model, upon phosphorylation of the Ca^{2+}-ATPase, two Ca^{2+} move from a pair of sites exposed to the cytoplasm in E_1 to a separate pair of sites exposed to the lumen in Ca_2E_1P and E_2. In the alternating four-site model, the pair of transport sites changes from being exposed to the cytoplasm in E_1 to being exposed to the lumen in Ca_2E_1P; in the E_2 conformation the transport sites are not accessible from either side of the membrane.

The major difference between the alternating- and four-site models is, therefore, that in the alternating-site model the two bound Ca^{2+} are released directly to the lumen from the pair of sites to which they first bind (the cytoplasmic pair of sites), whereas in the four-site model the two Ca^{2+} ions move from the cytoplasmic to the lumen sites and then are released. However, recent site-direct mutagenesis experiments (Clarke et al., 1989) support a model in which Ca^{2+} is released to the lumen directly form the cytoplasmic sites.

A third model, the so-called alternating four-site model (Figure 8), includes also this experimental evidence. This proposes the existence of two cytoplasmic transport sites

which, after ATPase phosphorylation, are exposed to lumen and characterised by low affinity for Ca^{2+}, as in the alternating-site model. Phosphorylation also results in closing of the pair of lumenal binding sites on the ATPase. Finally, the pair of transport sites in the E_2 state are unavailable for Ca^{2+} binding from either sides of the membrane (see Figure 8). The alternating four-site model ensures that (i) both E_2 and the phosphorylated ATPase (E_2P) can bind to Ca^{2+} ions only from the lumen space, as require by P_i phosphorylation experiments (Suko et al., 1981; Lacapere et al., 1981; Jencks et al., 1993) and (ii) cytoplasmic Ca^{2+} can be directly released to the lumen (Clarke et al., 1989).

2.3 WHAT NEWS FROM THE CRYSTAL STRUCTURE

The non-phosphorylated calcium-bound crystal structure of the Ca^{2+}-ATPase (Toyoshima et al., 2000) offers a very important structural basis to elucidate the reaction mechanism.

2.3.1 THREE-DIMENSIONAL STRUCTURE

The protein is composed by 994 amino acids (Brandl et al., 1987) and its structure comprises a cytoplasmic headpiece and a transmembrane (TM) domain (Figure 9 A). The cytoplasmic region consists of three distinct domains: phosphorylation (P), nucleotide-binding (N) and actuator (A) domains. The more remarkable feature of this X-ray structure is the position of the A and N domains which, in this configuration, are attached to the rest of the protein by only few interacting points.

The central part of the cytoplasmic region is occupied by domain P, composed by seven-stranded β-sheets and height short α-helices, and connected to TM and N domains by M4-M5 α-helices and two central loops, respectively. Its fold is homologous to the dehalogenase as expected from previous sequence alignments (Aravind et al., 1998; Stokes and Green, 2000). Domain P contains the residue of phosphorylation (Asp 351), which forms, together with other critical residues around it (Moller et al., 1996; McIntosh et al., 1999), a highly negatively charged surface accessible to solvent.

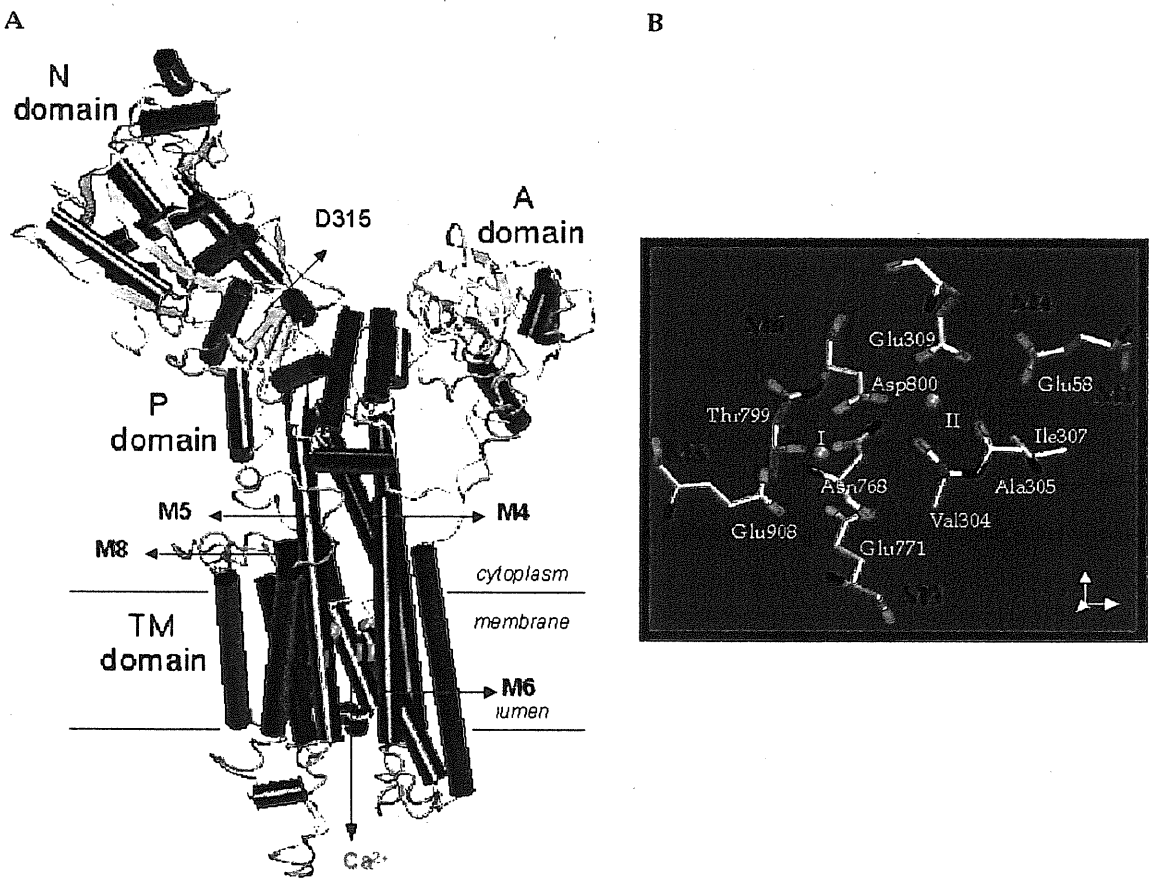

FIGURE 9. **Ca^{2+}-ATPase crystal structure**. A: The protein has been crystallised in the non-phosphorylated Ca^{2+}-bound configuration, which corresponds to the Ca_2E_1 state. The protein comprises a cytoplasmic headpiece, which consists of three domains, phosphorylation (P), nucleotide-binding (N) and actuator (A) domains, and a transmembrane (TM) domain. The essential residue of phosphorylation (D351), the two Ca^{2+} and the ϑ-helices (M4, M5, M6 and M8) forming the binding site are labelled accordingly. The putative cytoplasm/membrane and membrane/lumen interfaces are indicated. **B**: Structure of Ca^{2+} binding sites. Ca^{2+} ions lie side-by-side near the center of M4, M5, M6 and M8 α-helices. Glu908/Glu771 bind to $Ca(I)^{2+}$, Glu309 bind to $Ca(II)^{2+}$ and Asp800 bind to both ions.

Domain N is the largest of the three cytoplasmic domains, unexpectedly folded as anti-parallel seven-stranded β-sheets. It contains the critical residue Phe487 for ATP binding (McIntosh et al., 1996) and the well characterised residues Lys515 and Lys492 near it (Pick and Bassilian, 1981; McIntosh et al., 1992; Yamamoto et al., 1989). The overall ATP binding pocket is, as a consequence, a positively charged region, in marked contrast to the negatively charged zone around the phosphorylation site.

Domain A is the smallest of the three domains and is connected to the transmembrane region by long loops. Its function is unclear, although biochemical data (Andersen et al.,

1986; Juul et al., 1995) suggest that the domain moves substantially during active transport.

The TM region comprises ten α-helices (M1-M10), the length and inclination of which vary substantially. Most notable is M5 which is very long (~ 60 Å), lies at the centre of the molecule and extends from the lumenal side of the membrane to the centre of the P cytosolic domain. The TM region contains also the two binding sites for calcium.

2.3.2 Ca^{2+} BINDING SITES

The two sites are located near the centre of M4, M5, M6 and M8 transmembrane α-helices, as predicted from site-directed mutagenesis (Clarke et al., 1989; Andersen and Vilsen, 1994; Chen et al., 1996). Unexpectedly, two Ca^{2+} lie side-by-side at 5.7 Å far apart, approximately mid-way across the membrane. Following previous proposals (MacLennan et al., 1997a), the binding sites are termed as site I (involving α-helices M5, M6 and M8) and site II (most of the interaction coming from α-helix M4). Previous mutagenesis experiments anticipated the key residues involved in the binding of the two Ca^{2+} (Figure 9 B): Asn768 and Glu771 in M5, Thr799 and Asp800 in M6, Glu908 in M8 for site I and Glu309 in M4, Asn796 and Asp800 in M6 for site II (Andersen and Vilsen, 1995; Moller et al., 1996; MacLennan et al., 1997a.)

What mutagenesis could not revealed was the extensive contribution made to the coordination of Ca^{2+} by the main chain carbonyl group (particularly in site II) made possible by the unwinding of α-helices M4 and M6. However, this was anticipated from earlier spectroscopy (Troullier et al., 1996) and NMR (Soulie et al., 1999) studies and it indicates that local disruption of α-helices M4 and M6 at the level of the two metal sites may be the key for creating (or closing off) access to the Ca^{2+}-binding cavity.

Finally, mutagenesis experiments in which Glu309 was replaced by Asp suggests not only that the residue is particular important for binding Ca^{2+}, but also that plays a role in trapping Ca^{2+} to site II (Vilsen and Andersen, 1998).

2.3.3 PATHWAY FOR Ca^{2+} BINDING

The X-ray structure shows that the ATPase contains no immediately obvious channels leading from the cytoplasmic surface to the pair of high-affinity binding sites. In this respect the Ca^{2+}-ATPase is very unlike the porins (Cowan et al., 1995) and ion channels such as the potassium channel KcsA (Doyle et al., 1998), where the pathway across the membrane is obvious. Identification of the entry and exit pathways for Ca^{2+} in the Ca^{2+}-ATPase is made more difficult by the likelihood that the Ca^{2+}-binding site structure differs in the absence and presence of Ca^{2+} ions because of channel repulsion between the four carboxyl groups in the absence of the ions.

Running among the bottom of the P domain, close to the cytoplasmic membrane surface, there is the transmembrane loop L67, which contains four aspartic residues. Mutation of these acidic residues has been shown to result in reduced affinity for Ca^{2+} (Falson et al., 1997; Menguy et al., 1998), indicating that the loop could be a direct part of the initial Ca^{2+} binding sites. However, in the Ca^{2+}-bound configuration these residues are arranged in such a way that it is not clear how they could bind to the cytoplasmic calcium ions.

Toyoshima et al (2000) suggested a pathway for Ca^{2+} entry leading from the cytoplasmic surface to site II between α-helices M4 and M6, and involving backbone oxygens of the unwound region of α-helix M4, between residues Glu309 and Pro312.

An alternative pathway is suggested by the unexpected nature of the first transmembrane α-helix M1 (Lee and East, 2001). In fact, out of the four acidic residues in M1, all (except Glu51) are conserved in the family of SR/ER Ca^{2+}-ATPases, suggesting that they could be important for enzyme function. Specifically, location of Glu58 close to Ca^{2+} in site II means that this residue is likely to be able to 'sense' whether or not site II is occupied by Ca^{2+}. M1 could possibly provide the entry, since a short channel leads between Glu109 and Glu55 to site II. This channel is largely blocked by Glu309 in the two Ca^{2+}-bound configuration, but it is possible that in Ca^{2+}-free form, Glu309 is located to leave free access to site II.

Finally, activity measurements of Asn114Ala and Asn111Ala mutants (Clarke et al., 1989) suggested that also residues Asn111-Asn114 are important for the Ca^{2+} binding

process. These residues are located on α-helix M2, not far away from the channel proposed by Toyoshima et al. (2000); thus, residues Asn111 and Asn114 could also be involved in cytoplasmic Ca^{2+} binding.

As mentioned before, binding of Ca^{2+} to the cytoplasmic sites is ordered and cooperative. This means that binding of the first ion should induce a conformational change to increase the affinity for a second ion and formation of a second site. Moreover, binding of a second ion should prevent dissociation of the first (Girardet and Dupont, 1992; Inesi, 1987; Henderson et al., 1994b). In principle, two calcium binding mechanisms are possible (McIntosh, 2000): either the first ion binds directly to site I (as site II is not properly formed), or it binds to site II and it then moves to site I. Thereafter, in both cases, the second ion binds to site II blocking the exit of the first Ca^{2+}. However, an asymmetrical entrance, which corresponds to the first mechanism, could be a satisfying explanation for the cooperativity of Ca^{2+} binding to the ATPase.

2.3.4 E_1/E_2 CONFORMATIONAL CHANGES

A fascinating problem regarding the Ca^{2+}-ATPase and more generally all P-type pumps is to understand which conformational changes occur during the reaction cycle and how these are transmitted. The X-ray structure gives some information about the link between the membrane region and the cytoplasmic domains. In fact, it reveals a network of interactions involving domain TM, with the cytoplasmic top of α-helices M4/M5 and loop L67, and N and P domains, with the most conserved segments of the cytoplasmic region. To look for possible domain motion during the reaction cycle, Toyoshima et al. (2000) overlapped their Ca^{2+}-bound non-phosphorylated structure with a 8 Å structure of the same calcium pump in a Ca^{2+}-free decadanevate-containing configuration (Zhang et al., 1998). This comparison reveals that relatively large scale domain movements accompany the binding of calcium (Ogawa et al., 1998), which consists, initially, in a conformational change within the transmembrane domain, and then in reorganisation of the cytoplasmic headpiece (Figure 10). In order to fit the E_1 structure to the E_2 model, it is necessary to rotate the A domain of 90° parallel to the bilayer surface and to tilt the N domain towards the P domain by 22°.

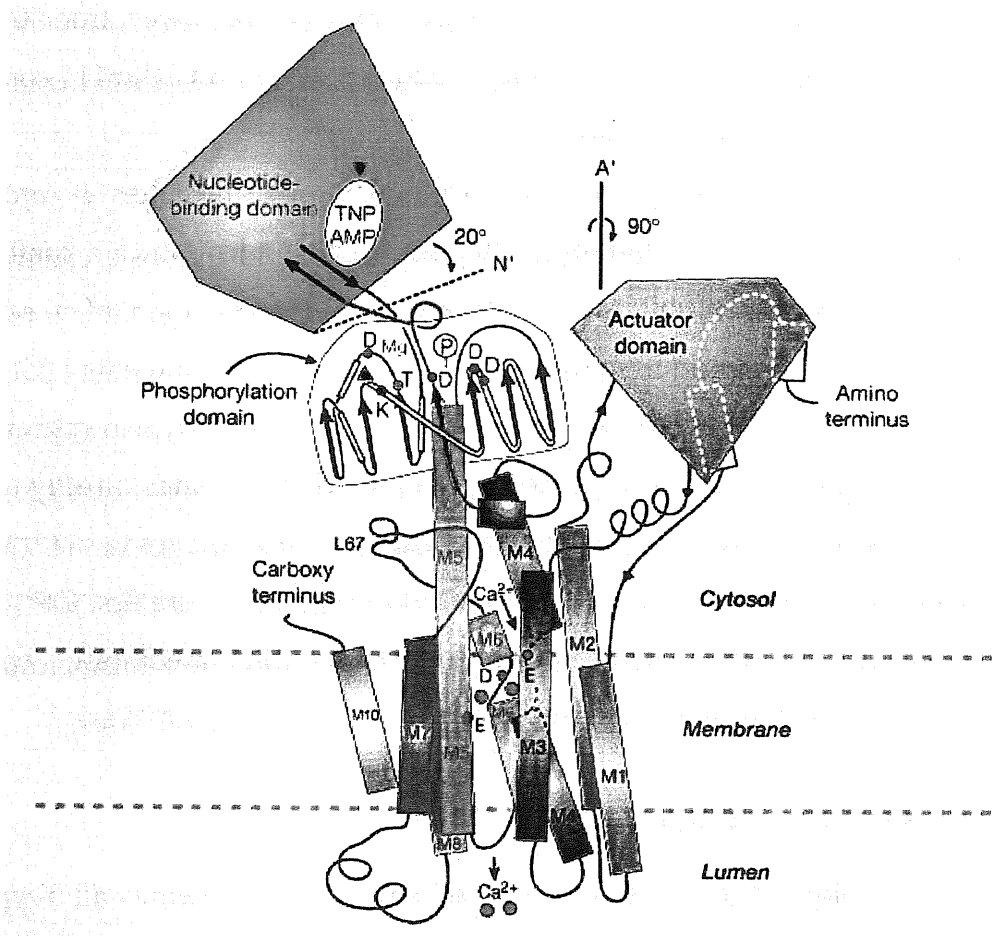

FIGURE 10. Overview of Ca^{2+}-ATPase conformational changes during Ca^{2+} binding process, as proposed by Toyoshima et al (2000) (MacLennan and Green, 2000). Small spheres and single letters mark the positions of residues involved in the Ca^{2+}-binding site or in catalysis (K, lysine (blue); T, threonine (violet); D, aspartate, and E, glutamate (red)). N' and A' indicate the rotation of the nucleotide-binding and actuator domains required to match the density of the Ca^{2+}-free conformation (Zhang et al., 1998). Cross-linked sites are shown as filled triangles and Ca^{2+} ions are shown as green spheres.

As a consequence, the gap between N and P domain was partially closed (from ~35 Å to ~15 Å). Such shifts in position are possible since the connecting strands between domains A and N to domain P have no regular secondary structure and are devoid of any major interactions. This A and N domain motion in has inevitable consequences for the TM helices organisation since, for example, moving domain A will require adjustments in the alignment of TM α-helices M1, M2 and M3 to which this domain is attached. Also the angular relations between α-helices M4 and M5 and P domain seems

to change, while the loop L67 fits well with both density maps indicating that it follows domain P.

Toyoshima et al. (2000) postulated that Ca^{2+} binding causes a reorganisation of M1-M3 helices in the E_2 conformation, releasing domain A; this release then facilitates the conformational change of the N-domain relative to the P domain. This results in the open E_1 structure which is accessible by ATP.

2.4 PROTEIN MODULATION: A TARGET FOR DRUGS AND DISEASES

Ca^{2+}-ATPases play a role in signaling in all (nucleated) cells but in particular they are involved in muscle contractions. In fact, muscle contraction is marked by a rapid increase in the cytosolic Ca^{2+} concentration. As a consequence, the ions inevitably bind to the membrane ATPases and, once the enzymes are activated, the pumps can restore the cytosol calcium levels to relax the muscles.

The activity of the Ca^{2+}-ATPase in cardiac muscle is controlled by interaction with phospholamban, a 52-residue protein found in the SR membrane (Simmerman and Jones, 1998). Co-expression studies have shown that the activity of skeletal muscle Ca^{2+}-ATPase is also modulated by the interaction with phospholamban (Sasaki et al., 1992; Hughes et al., 1996). This protein contains a hydrophilic N-terminal domain and a hydrophobic C-terminal domain, forming a transmembrane α-helix (Ahmed et al., 2000). The cytoplasmic domain of phospholamban has been shown to interact with residues K^{397}NDKPV^{402} of the skeletal muscle Ca^{2+}-ATPase (Toyofuku et al., 1994), located on the underside of the N domain. It has also been suggested that the transmembrane region of phospholamban interacts with residues at the top of α-helix M6 (Asahi et al., 1999). From the Ca^{2+}-ATPase X-ray structure (Toyoshima et al., 2000) only Leu802 and Thr805 appear to be on the outer face of M6 to interact with phospholamban. *In vivo* and *in vitro* studies (Cantilina et al., 1993; Hughes et al., 1996) suggest that binding of phospholamban to the Ca^{2+}-ATPase results in an apparent reduction of ATPase affinity for Ca^{2+}, changing the rates of one or more steps involved in Ca^{2+} binding. More controversial are, instead, the effects of phospholamban on the rate of ATP hydrolysis (Sasaki et al., 1992; Hughes et al., 1994; Kargacin et al., 1998).

The Ca^{2+}-ATPase is inhibited by a variety of hydrophobic molecules, including sesquiterpene lactores, such as thapsigargin (TG) or trilobolide, and simple hydroxy-containing molecules, such as dihydroxybenzene (for recent review see Lee and East, 2001). The presence of hydroxy groups has been shown to be important for both sets of inhibitor. TG is used by biologists to empty internal Ca^{2+} stores in eukaryotic cells, as a result of total inhibition of the SERCA pumps. TG inhibits Ca^{2+}-ATPase by binding to the E_2 conformation preventing further cycling of the enzyme (Sagara and Inesi, 1991; Sagara et al., 1992). TG interacts with E_2 with very high affinity (K_d < 1nM); full inhibition is obtained with 1:1 molar stochiometry in what has been termed a dead-end complex. Site-direct mutagenesis experiments (Yu et al., 1998) combined with the X-ray structure (Toyoshima et al., 2000) have permitted identification of the TG binding site between two lumenal loops connecting α-helices M3/M4 and M7/M8. Based on recent cryo-electromicroscopy studies (Young et al., 2001), a TG inhibition mechanism was also proposed, involving increase in transmembrane α-helices to prevent movements necessary for Ca^{2+} binding.

Given the important role played by calcium pumps in signaling, it is not surprising that defects associated with these pumps should cause disease. Two genetic diseases are known to result from mutations of SERCAs. Brody's disease is typified by impaired fast-twitch skeletal muscle relaxation after exercise and cramps (Brody et al., 1969). Although Brody's disease was the first one identified as SERCA related (Odermatt et al., 1996; MacLennan et al., 1997b), it is clear that it comprises a number of diseases resulting from different molecular defects. The second-related disorder to be identified was Darier's disease, which is autosomal dominant condition resulting from mutation of ATP2A2 gene. Interestingly, neuropsychiatry disorders including mental handicap are sometime associated with Darier's disease (Ruiz-Perez et al., 1999).

AIMS

I used Molecular Dynamics and electrostatics calculations as well as homology modelling and docking to investigate the structural/functional properties of two transmembrane proteins involved in Ca^{2+} signalling, namely neuronal nicotinic receptors and sarcoplasmic reticulum calcium pumps.

The ligand binding activation mechanism of neuronal nicotinic ACh receptors has been investigated by:

(a) analysis of the structural properties differentiating CGRP N-terminal fragments;

(b) ligand binding domain modelling of $\alpha3\beta4$ and $\alpha4\beta2$ nicotinic receptors present in rat cromaffin cells;

(c) obtaining binding characteristics of full agonists, CGRP N-terminal fragments and allosteric modulators.

The calcium binding process of the calcium pumps has been investigated by:

(d) studying the structural and dynamical features of the protein model (Ca_2E_1) when bound by two calcium ions;

(e) modelling of the H_2E_2 and HCaE′ structural complexes, which are two key intermediates in the Ca^{2+} binding process;

(f) inspection of the process through which Ca^{2+} reaches the two binding sites and analysis of the outer mouth of the cytoplasmic channel where Ca^{2+} binds.

METHODS

In this work I used tools from computational chemistry (such as Molecular Dynamics and electrostatics calculations) as well as modern structural bioinformatics techniques (such as homology modelling and docking). In this section, I will outline the principles of both.

1. MOLECULAR DYNAMICS SIMULATIONS

Classical molecular dynamics (MD) simulations provide detailed information on structure, dynamics and thermodynamics of biological molecules (such as proteins and nucleic acids), including, for example, protein stability, conformational changes, molecular recognition processes and ion transport. MD simulations are also routinely used for X-ray and NMR structure refinement and in computer-aided drug design.

The method is based on Newton's second law

$$\mathbf{F}_i = -\nabla_{\mathbf{r}_i} E = m_i \ddot{\mathbf{r}}_i \qquad (1)$$

where F_i is the force exerted on atom i, m_i the mass of the same atom and $\ddot{\mathbf{r}}_i$ its acceleration. In equation (1), the potential energy function (or force field) must be provided.

The integration of the second-order differential equation (1) provides the time-evolution of the system, known the initial positions and velocities. From the trajectory, which may be stored in the computer disk, the average values of some properties can be determined and compared with experimental results.

A general MD run can be schematised by the following few steps:

(i) reading of parameters that specify the conditions of the run (temperature and pressure, number of particles, time step, density);

(ii) reading of initial conditions (starting positions and velocities);

(iii) computation of the forces on all atoms;

(iv) integration of Newton equation of motion; this step and the previous one are repeated until the time evolution of the system for the desired length is computed.

(v) at the end of the run, calculation of properties averages.

For our MD calculations we used AMBER program (Case et al., 1997).

1.1 THE FORCE FIELD

As mentioned above, the forces are calculated as derivatives of a suitable potential energy function, which is defined by a set of parameters. For our MD calculations, we used the AMBER force field parameters (Cornell et al., 1995). A general form of the potential energy as developed for biomolecules reads:

$$E = E_{bonds} + E_{angles} + E_{dihedrals} + E_{van\ der\ Walls} + E_{electrostatic} =$$

$$\sum_{bonds} K_r (r - r_{eq})^2 + \sum_{angles} K_\vartheta (\vartheta - \vartheta_{eq})^2 + \sum_{dihedrals} V_n [1 + \cos(n\phi - \gamma)]/2$$

$$+ \sum_{i<j} \left[\frac{A_{ij}}{(r_i - r_j)^{12}} - \frac{B_{ij}}{(r_i - r_j)^6} + \frac{q_i q_j}{4\pi\varepsilon |r_i - r_j|} \right] \qquad (2)$$

where bonds, angles and dihedrals terms are the so-called bond interaction (that is, those involving covalently bond atoms) while the other sums represents the non-bond interactions.

$E_{bonds} + E_{angles}$ – The bond stretching and angle bending interactions are parameterised with a harmonic function in which the equilibrium bound and angle values (r_{eq} and θ_{eq}) as well as the force constants (K_r and K_θ) are adjusted to reproduce experimentally determined normal mode frequencies.

$E_{dihedrals}$ – The dihedral parameters are calibrated on small model compounds starting from *ab initio* quantum chemical calculations. Also the so-called "improper dihedral angles" are inserted between non linked bonds to preserve planarity in aromatic rings, restrict tetrahedral conformations, etc.

$E_{van\ der\ Waals}$ – van der Waals interactions are mimicked by a Lennard-Jones potential with parameters (A and B) assigned so as to reproduce chemical-physical properties in

simple organic liquids (densities, enthalpies of vaporisation, solvating free energies, etc).

$E_{electrostatic}$ – The electrostatic energy is evaluated as the interaction between atomic point charges. In AMBER, these charges are derived using quantum chemistry calculations so as to fit the quantum electrostatic potential calculated for a set of small representative molecules (Bayly et al., 1993). The dielectric constant (ε) is set to 1 when calculations are done in presence of an explicit solvent (e.g. water), whereas a distance dependent dielectric constant is used to mimic the presence of the solvent when the latter is not explicitly present.

The electrostatic and van der Waals interaction energies are calculated only between atoms of different molecules or for atoms in the same molecule separated by at least three bonds.

1.2 INTEGRATING THE EQUATION OF MOTION

The integration algorithms can be derived from the Taylor series expansion of the atoms coordinates around instant *t*

$$r(t+\delta t) = r(t) + v(t)\delta t + \frac{1}{2}a(t)\delta t^2 + \frac{1}{3}\dddot{r}\delta t^3 + O(\delta t^4) \quad (3)$$

where *r*, *v* and *a* are the position, velocity and acceleration vectors, respectively, and δt is the time step. The length of this time interval is chosen taking into account that no variation in the force field acting on the atoms should occur within each time step. Summing the expansions of $r(t+\delta t)$ and $r(t-\delta t)$, one obtains the Verlet algorithm (Verlet, 1967):

$$r(t+\delta t) = 2r(t) - r(t-\delta t) + \frac{1}{2}a(t)\delta t^2 + O(\delta t^4) \quad (4)$$

which uses only positions and accelerations at time t and t-δt to calculate new positions at time t+δt with an error of order $O(\delta t^4)$. From the knowledge of the trajectory one can derive the velocity as follow:

$$v(t) = \frac{r(t+\delta t) - r(t-\delta t)}{2\delta t} + O(\delta t^2) \quad (5)$$

with only $O(\delta t^2)$ order of accuracy. The advantages of the Verlet algorithm are its straightforwardness and modest storage requirements; the disadvantage is its moderate precision in the velocity calculation.

However, it is possible to obtain more accurate estimates of the velocity implementing other Verlet equivalent algorithms, differing for accuracy and computational speed (Allen and Tildesley, 1987). The simplest among these is the so-called leap-frog algorithm:

$$r(t+\delta t) \approx r(t) + v(t+\frac{1}{2}\delta t)\delta t$$

$$v(t+\frac{1}{2}\delta t) \approx v(t-\frac{1}{2}\delta t) + a(t)\delta t \qquad (6)$$

which is currently used in the AMBER program. In this algorithm, first the velocities are calculated at half integer time steps $t+1/2\delta t$, then these are used to calculate the positions, at time $t+\delta t$. In this way, the velocities *leap* over the positions and the positions *leap* over the velocities. The advantage of this algorithm is that the velocities are explicitly calculated, the disadvantage is that they are not calculated at the same time as the positions. As a consequence, kinetic and potential energy cannot directly compute the total energy at time t, but energy evaluation is possible using the following approximate value of velocities at time t :

$$v(t) \approx \frac{1}{2}\left[v(t+\frac{1}{2}\delta t) + v(t-\frac{1}{2}\delta t) \right] \qquad (7)$$

1.3 ENERGY CALCULATION: EWALD SUMS METHOD

In order to mimic the presence of the bulk, periodic boundary conditions can be used. In this approach, the volume containing the N atoms is treated as an infinite periodic lattice of identical cells and each atom interacts with all the other in this infinite periodic system, that is all other atoms in the same periodic cell and all atoms (including its image) in all other cells. For instance, since in biological systems all intermolecular interactions are pairwise additive, the total potential energy in a infinite periodic system can be written as:

$$E = \frac{1}{2}\sum_{i=1}^{N}\sum_{j=1}^{N}\sum_{n=0}^{\infty}{}'E(r_{ij} + nL) \tag{8}$$

where L is the diameter of the periodic box, n is an arbitrary vector of three integer numbers and the prime over the sum indicates that the term $i=j$ is to be excluded when $n=0$. To simplify the calculations is useful to split the energy function in two parts: a short-range term (involving atoms within a sphere with $r < r_c < L/2$, that is within the main cell) and a long-range term (for atoms that are more distant than r_c):

$$E = \frac{1}{2}\left[\sum_{r_{ij}<r_c}{}'E(r_{ij}) + \sum_{r_{ij}>r_c}E(r_{ij})\right] \tag{9}$$

The intramolecular and Lennard-Jones interactions can be treated as short-range interactions, since its energy functions decay rapidly. Even if these potential functions are not rigorously zero for $r \geq r_c$, truncation in the calculation at r_c will result in a systematic error which may be correct adding a tail contribution. For Coulomb interactions, instead, the tail correction diverges since the electrostatic energy function goes to zero only for r->∞. In such case the nearest-image convention cannot be used and interactions with all periodic images must be taken explicitly.

The more rigorous way to treat these interactions is the so-called Ewald method. In this method, the electrostatic potential energy ($E_{electrostatic}$ in eq. 2) of an electrically neutral ($\Sigma_i\, q_i = 0$) N atoms system in a cubic box with length L, assuming periodic boundary conditions, can be rewritten as:

$$E_{electrostatic} = \frac{1}{2}\sum_{i=1}^{N} q_i \phi(r_i) = \frac{1}{2}\sum_{i=1}^{N} q_i \sum_{j,n}{}' \frac{q_j}{|r_{ij} + nL|} \tag{10}$$

In the equation, $\phi(r_i)$ is the electrostatic potential of ion i and the prime on the summation indicates that the sum in the main cell ($n=0$) is over all atom $j \neq i$.

The idea of the Ewald method is to screen each charge q_i with a diffuse charge distribution of the opposite sign, such that the total charge of this cloud exactly cancels q_i.

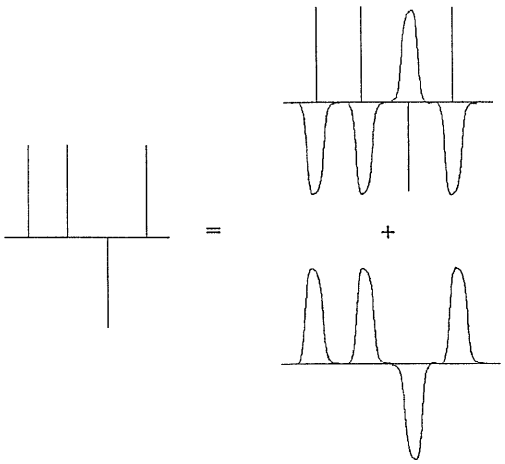

Figure 11. A set of point charges may be considered a set of screened charges minus the smoothly varying screening background.

The contribution to the electrostatic potential at a point r_i due to a set of screened charges can be easily computed by direct summation, because the generated electrostatic potential is a rapidly decaying function of r.

To restore the initial system, one adds the energy contribution of a screening charge around atom *i* with the same charge q_i. This screening charge distribution is assumed to be a Gaussian of width $\sqrt{2}/\alpha$ (Figure 11). As a result the all system charge density can be rewritten as follow:

$$\rho(r) = \rho(r) + \rho_g(r) - \rho_g(r)$$

$$= \sum_{i=1}^{N} q_i \delta(r - r_i) + \sum_{i=1}^{N} q_i (\alpha^2/\pi)^{3/2} \exp\left[-\alpha^2 (r - r_i)^2\right] - \sum_{i=1}^{N} q_i (\alpha^2/\pi)^{3/2} \exp\left[-\alpha^2 (r - r_i)^2\right] \quad (11)$$

Introducing this expression in the potential energy function and making some calculations, the energy reads:

$$E_{electrostatic} = E_{short-range} + E_{long-range} + E_{self}$$

$$= \frac{1}{2} \sum_{i \neq j}^{N} q_i q_j \operatorname{erfc}(\alpha r_{ij})/r_{ij} + \frac{1}{2} \sum_{k \neq 0} \frac{4\pi L^3}{k^2} |\rho(k)|^2 \exp(-k^2/4\alpha^2) - \alpha/\pi^{1/2} \sum_{i=1}^{N} q_i^2 \quad (12)$$

where: (i) $E_{short-range}$ is the electrostatic energy of screened charges, that can be calculated as direct sum of a rapidly converging series in the real space; (ii) $E_{long-range}$ is the long-

range contribution of the gaussian charge distributions, which is represented by a rapidly converging Fourier series in the reciprocal space defined by vectors k; (iii) E_{self} is the correction for the spurious self-interaction between the continuous Gaussian charge cloud of total value q_i and the point charge q_i located at the center of the Gaussian.

The rate of convergence of $E_{short\text{-}range}$ and $E_{long\text{-}range}$ increases and decreases, respectively, by increasing α. A compromise for assigning this value should be reached to obtain the both terms convergence and in particular the convergence for the short term within the cut-off radius r_c.

The AMBER program uses an efficient algorithm for calculating the Ewald sums, the Particle Mesh Ewald Method, which interpolate the electrostatic potential on a grid using smooth functions (Darden and York, 1993; Essman et al., 1995).

1.4 TEMPERATURE AND PRESSURE CONTROL

In conventional Molecular Dynamic simulations, the total energy E is the constant of motion and the calculated time averages are equivalent to the averages done on a microcanonical ensemble (constant-NVE). However, it is often more convenient to perform simulations in other ensemble, at constant temperature and volume or temperature and pressure (i.e. NVT and NPT). Several algorithms, all based on the reformulation of the Lagrangian equation of motion, have been implemented to this issue. Here I describe the one currently used by AMBER (Case et al., 1997).

Temperature is kept close to the desired target value T_0 using the weak coupling method originally proposed by Berendsen et al. (1984). This method virtually couple the system to a thermal bath at a target temperature T_0, by the equation:

$$\frac{dT}{dt} = \frac{1}{\tau_T}[T_0 - T] \tag{13}$$

where T is the instantaneous value of temperature and τ_T is the temperature coupling time. The idea is to modify atomic equation of motions step by step so that the system moves towards a reference temperature T_0.

The instantaneous temperature T of a system with N_{df} degree of freedom is defined in terms of the kinetic energy $E_k(t)$ by the relation:

$$E_{kin}(t) = \sum_{i=1}^{N} \frac{1}{2} m_i v_i^2(t) = \frac{1}{2} N_{df} k_b T(t) \tag{14}$$

where the summation over the atoms is restricted to the set of N_{df} degree of freedom. A change in temperature δT will relate with a change in kinetic δE_k through the heat capacity per degree of freedom (c_v):

$$\delta E_{kin}(t) = N_{df} c_v \delta T \tag{15}$$

Scaling the atomic velocities by a factor λ, one obtain the following change in kinetic energy:

$$\delta E_{kin}(t) = [\lambda(t)^2 - 1] \frac{1}{2} N_{df} k_b T(t) \tag{16}$$

Rewriting the equation (13) in discrete approximation and substituting δt with the MD time step, for the temperature scaling factor $\lambda(t)$ one obtains the following expression:

$$\lambda(t) = \left[1 + \frac{2 c_v \delta t}{k_b \tau_T} \left(\frac{T_0}{T} - 1 \right) \right]^{1/2} \tag{17}$$

The factor $\lambda(t)$ is used to scale velocities v_i at each step t, in order to relax the temperature towards the target value T_0. The relaxation rate is controlled by the ratio of heat capacity per degree of freedom c_v and by the time coupling constant τ_T.

Analogously to the temperature control, for the purpose of constant pressure simulations of isotropic systems, a simple scaling of atom position as well as volume could be implemented (Berendsen et al., 1984). A change of volume V per time unite is linked to the pressure as follows:

$$\frac{1}{V} \frac{dV}{dt} = \frac{\beta}{\tau_P} [P_0 - P(t)] \tag{18}$$

where β is the isothermal compressibility, P is the instantaneous (or internal) pressure, P_0 is the target pressure (or external pressure) and τ_P the pressure coupling time. Solving eq. (18) in a discrete time approximation as in the temperature case, one obtain for atoms position the following scaling factor:

$$\mu = \left[1 + \beta \frac{\delta t}{\tau_p}(P_0 - P(t)\right]^{1/3} \tag{19}$$

Temperature and pressure coupling constants are parameters to be set sufficiently small to achieve the required average T and P, but also sufficiently large to avoid disturbance of the system physical properties by coupling to the baths.

1.5 CALCULATED PROPERTIES

Once the trajectory and the velocities produced in a MD run have been stored onto disk, numerous properties can be calculated and eventually compared with experiments. My work has focused essentially only on the structural properties.

1.5.1 ROOT MEAN SQUARE DISPLACEMENT

The root mean square displacement (rmsd) of the backbone atoms at time *t* with respect to the initial minimised structure, reads

$$\text{rmsd}(t) = \Delta r(t) = \sqrt{\frac{1}{N}\sum_{i=1}^{N} \Delta r_i(t)^2} \tag{20}$$

where $\Delta r_i(t) = r_i(t) - r_i(t_0)$ is the displacement of atom *i* during time *t* and *N* is the number of backbone atoms over which the average is done. For the time averaged rmsd calculation, the rmsd values must be also mediated over the simulation time: $\text{rmsd} = \langle \text{rmsd}(t) \rangle$, where the brackets $\langle\rangle$ indicate temporal average. The rmsd per residue, instead, is the rms displacement of each residue mediated over the atoms residue and the simulation time. The rms fluctuation, which is the rms displacement calculated with respect to the main position of each atom *i*:

$$\text{rmsf}_{res}^2 = \left\langle \Delta r_{res}^{\ 2} \right\rangle = \left\langle (r - \langle r \rangle)_{res}^2 \right\rangle \tag{21}$$

can be compared with the crystallographic B-factor by the Debye-Waller relation:

$$B_{res} = \frac{8\pi^2}{3} \text{rmsf}_{res}^2 \tag{22}$$

1.5.2 GYRATION RADIUS

The radius of gyration (G_R) of the backbone atoms is calculated as:

$$G_R = \frac{1}{N_R}\sqrt{\frac{1}{M}\sum_{1=1}^{M}(r_i - r_G)^2} \tag{23}$$

where N_R is the number of residues, M is the number of steps for which averages are calculated, r_i is the position vector of all backbone atoms at step i, and r_G is the position vector of the mass center.

1.5.3 LARGE- SCALE MOTIONS

Large-scale or essential motions (Garcia, 1992; Amadei et al., 1993) can be calculated on the basis of the covariant matrix of the C_α atoms:

$$C_{ij} = \left\langle (r_i - \langle r_i \rangle)(r_j - \langle r_j \rangle)^T \right\rangle \tag{24}$$

where r_i and r_j indicate the instantaneous positions of the C_α atoms i and j, and the brackets $\langle\rangle$ indicate temporal average. The symmetric matrix C can always be diagonalized by an orthogonal coordinate transformation B:

$$r - \langle r \rangle = Bq \quad \text{or} \quad q = B^T(r - \langle r \rangle) \tag{25}$$

which transforms C into a diagonal matrix $\Lambda = \left\langle qq^T \right\rangle$ of eigenvalues λ_i. When a sufficient number of independent configurations (at least 3N+1) are available to evaluate C, there will be 3N eigenvalues of which at least 6, representing the overall translational and rotational motion, are nearly zero. These two motions can be eliminated by performing a rmsd fit between the MD snapshots and the first conformer (Amadei et al., 1993).

Generally, in order to describe the long-range motions of a protein it is sufficient to consider only few $M < 3N+1$ independent configurations corresponding to the eigenvectors with higher values. Indeed, it turns out that most of the total motion is spanned by the first eigenvectors. The amount of motion covered by this subset of M essential eigenvectors is the summation over the first M essential eigenvalues

$$\sum_{1}^{M}\left\langle (r_i - \langle r_i \rangle)^2 \right\rangle = \sum_{1}^{M}\lambda_i \qquad (26)$$

sorted in decreasing order.

To figure out the contribution of different protein domains to an essential eigenvector, one calculates the scalar product between the eigenvector q_j and the displacement $R_i=[r_i(t_{initial}) - r_i(t_{final})]$ of the C_α atoms belonging to a certain domain:

$$\frac{1}{N_D}\sum_{1}^{N_D} R_i \cdot q_j \qquad (27)$$

where N_D is the number of domain C_α atoms.

2. ELECTROSTATIC CALCULATIONS

Electrostatic interactions play an important role in many biological processes (Honig and Nicholls, 1995). In a continuum approximation of the solute/solvent system the electrostatic potential can be determined by solving the Poisson-Bolzmann (PB) equation:

$$\nabla \cdot [\varepsilon(r)\nabla\Phi(r)] - \varepsilon(r)\kappa(r)^2 \sinh[\Phi(r)] + 4\pi\rho^f(r)/KT = 0 \qquad (28)$$

where $\rho^f(r)$ is the fix charge density of the molecule, $\varepsilon(r)$ the distance dependent dielectric constant and $\kappa(r) = 1/\lambda^2$ with $\lambda = \sqrt{ekT/8\pi q^2}$ the Debye length.

An analytical solution of the equation ($\Phi(r) = \Phi(r;\varepsilon,\rho,\kappa^2)$) can be obtained only for very simple geometries and charge distributions, e.g. spheres. For proteins, the equation can be solved numerically by the finite difference methods on a grid (Gilson and Honig, 1988). As a first step, the molecular surface is generated using a spherical probe of 1.4 Å (the water van der Waals radius). A grid is, therefore, generated (typical mesh ~ 1 Å) and a charge is assigned to each point mesh if within an atom sphere. According to the surface, a high dielectric constant value is then assigned to the grid points that lie on the external part of the macromolecule, which are supposed belonging to the solvent (ε = 80), and a low dielectric constant value is assigned to the remaining grid points. The meaning of the latter is to mimic the thermal charge shielded of the protein, and usually

is chosen in the range between 2 and 8. Smoothing algorithms are used in order to obtain the good results using a large spaced grid (Gilson and Honig, 1988).

3. COMPARATIVE PROTEIN STRUCTURE MODELING

A three-dimensional model for a protein of unknown structure (the target) can be built on the basis of one or more detailed proteins of known structure (the templates; Sanchez and Sali, 1997). The necessary conditions for a comparative (or homology) protein structure modelling are that the similarity between target sequence and template structure is detectable and that the correct alignment between them can be constructed.

Comparative modelling usually consists of the following four steps:

(i) search for templates and selection of one or more of them;

(ii) target–template alignment;

(iii) model building;

(iv) model evaluation.

3.1 SEARCH AND SELECTION OF TEMPLATES

The sequences of known protein structures (Protein Data Bank, PDB, Berman et al., 2002) are compared with the sequence of the target. The one(s) with the highest sequence similarity (i.e. higher percentage of identical residues, lower number and shorter length of gaps in the alignment) is (are) chosen. The criteria for defining similarity include: (a) the number of identical residues; (b) the number and length of gaps in the alignment; (c) the presence of an identical or similar ligand in the active site; (d) the resolution of the template X-ray structure.

3.2 ALIGNMENT

The sequences of templates and target can be aligned automatically when the sequence identity is above 40%. Below this threshold, manual intervention is required. Alignments can be improved manually by including structural information from the template; gaps, for example, should be avoided in secondary structure elements of α-

helices and β-strands and inserted in loops and core regions. In case of low sequence identity, the accuracy of the alignment is the key factor for the quality of the resulting model.

For our models we used CLUSTAL, a family of programs that have been produced to carry out multiple alignments since 1988 (Higgins and Sharp, 1988; Thompson et al., 1994). CLUSTAL consists of three steps: (i) it aligns each pair of sequences and it records the similarity of the sequences as the percent identity between them, ignoring any positions with gaps; (ii) these scores are used to build an approximate phylogenetic tree between the sequences using the Neighbour-Joining method (Saitou and Nei, 1987); (iii) finally, the multiple alignment is built up gradually by aligning together larger and larger groups of sequences, following the branching order of the previous approximate phylogenetic tree.

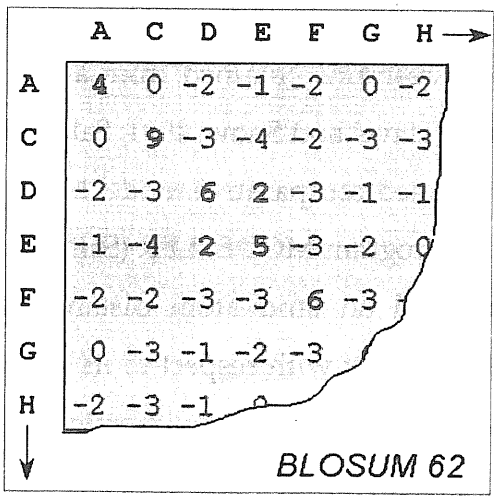

FIGURE 12. BLOSUM62 Substitution Scoring Matrix. A 20 x 20 section of the matrix is shown here. Every possible identity and substitution is assigned a score based on the observed frequencies of such occurrences in alignments of related proteins. Identities are assigned the most positive scores. Frequently observed substitutions receive positive scores; seldom observed substitutions are given negative scores.

Many parameters can be used to control the alignments either for the initial pairwise alignments or for the final multiple alignments. The result normally do not significantly vary changing the pairwise parameters, whereas they are rather sensitive to the multiple alignment parameters. The latter are: (a) the gap-opening penalty, which gives the cost of opening a new gap; (b) the gap-extension penalty, which gives the cost of extending a gap; and (c) the amino acid weight matrix, which compare two aligned

sequences yielding a table of scores for each pair of residues. The scoring matrix used here is BLOSUM 62 (Block Substitution Matrix; Henikoff and Henikoff, 1992) (Figure 12).

3.3 MODEL BUILDING

The original and still most widely used method to construct a 3D structural model for the target protein is modelling by rigid-body assembly (Blundell et al., 1987). This consists in constructing the model starting from few core regions and/or from loops and side chains that are obtained from dissecting related structures. Another group of methods, modelling by sequence matching, relies on the approximate positions of the conserved amino acids from the template to calculate the coordinates of the others residues (Jones and Thirup, 1986). The third family of methods, modelling by satisfaction of spatial restrains, uses either distance geometry or optimisation techniques to satisfy spatial restrains obtained from alignment of the target sequence with the template structures (Havel and Snow, 1991; Sali and Blundell, 1993).

In this work, we used automated comparative model building by satisfaction of spatial restrains as implemented in program MODELLER (Sali and Blundell, 1993). The spatial restrains are the one imposed on atom-atom distances or on differences between dihedral angles values of the target with respect to its template. These are obtained on the basis of the sequences alignment. The stereochemical restraints (i.e. bond distances, bond angles, planarity of peptide groups and side-chain rings, chiralities of C_α atoms and side chains, van der Waals contact distances and bond lengths, bond angles and dihedral angles of cysteine disulphide bridges) are, instead, intrinsic properties of each amino acid or of a couple of them. These restrains can be easily obtained from the amino acid sequence of a protein.

A restrain for a certain feature x is defined in terms of the probability density functions (pdf) as

$$p(x_1 < x < x_2) = \int_{x_1}^{x_2} p(x)dx \qquad (29)$$

The probability density functions can be calculated either analytically using statistical and classical mechanics, or empirically using databases of known protein structures. In

both cases, the pdfs suitable for restraining a certain feature x can be rewritten as a conditional probability function p(x/a, b,..) of several parameters (a, b, ..), such as bond lengths and dihedral angles.

A bond length restrain, for example, can be obtained using the harmonic model for chemical bonds and classical statistical mechanics. As a result, the probability density function for the bond length is the following Gaussian probability density function (Hill, 1960)

$$p(r) = \frac{1}{\sqrt{2\pi}\sigma_r} \exp\left[-\frac{1}{2}\left(\frac{r - r_{eq}}{\sigma_r} \right)^2 \right] \qquad (30)$$

where $\sigma_r = \sqrt{k_B T / K_r}$.

Finally, the best model is obtained by an optimisation procedure of this function (using methods such as conjugate gradients minimisation and simulated annealing molecular dynamics) that minimises violations of the spatial restrains. This procedure is conceptually similar to the one used in the structure determination from NMR data.

3.4 MODEL EVALUATION

Two types of evaluation should be carried out in order to check for possible errors in steps (i)-(iv): (a) an "internal" evaluation, that is a check whether the obtained model satisfies the used restrains. This test should always be done if the sequence identity is 30% or lower. (b) An "external" evaluation that relies on information that is not used in calculating the model (Luthy et al., 1992). This is done to recognise unreliable regions in the model. One way to approach this problem is to calculate an energy profile for each atom, as in PROSAII program (Sippl, 1993). Errors in the model may appear as peaks of positive energy in the profile. Another way is to evaluate the stereochemistry (bond length and angles, dihedral angles, atom-atom overlaps, etc ..) with programs such as PROCHECK (Laskowski et al., 1996). Finally, an important evaluation tool is the experimental knowledge about structure and function of the protein. A model should be consistent with all experimental observations such as site-directed mutagenesis, cross-linking data, ligand-binding, and so on.

3.5 REEVALUATION OF MODEL

The reliability of the model can be improved by changing the alignment and/or the template selection and recalculate the model iteratively until no improvement is detected. The more exhaustive is the exploration of the templates and the alignments, the more likely it is that the accuracy of the final model will improve.

4. FLEXIBLE DOCKING OF LIGANDS TO PROTEINS

A docking calculation attempts to find the most probable conformer(s) of a ligand/receptor complex, given the structure of both isolated components. The ligand structure may be taken from the crystal structure of the protein/ligand complex or from a database of compounds, such as the Cambrige Crystallographic Database (CCD) (Allen et al., 1979) or the Concord-generated (Rusinko et al., 1989) set of coordinates from Available Chemicals Directory (ACD).

4.1 DOCKING CALCULATIONS

The large number of the conformational degrees of freedom for both ligand and binding site hampers the use of a physical interaction potential energy between receptor and ligand. One has in general to resort to approximate and empirically derived scoring functions. In this work, ligands has been docked into receptor binding sites using the DOCK suite of programs (Ewing and Kuntz, 1997). If both ligand and potential site of interest of the receptor are known, as in the case of the work presented here, the following protocol can be used: (i) the molecular surface of the receptor active site is built using Connolly's MS algorithm (Connolly, 1983). (ii) The program SPHGEN (Kuntz et al., 1982) is used to fill up the binding cavity with spheres having variable radii (from 1.0 to 1.4 Å) so that the possible location for the ligand atoms within the active site is calculated as the center of overlapping spheres. Several sets of these atom-sphere pairs are generated, which identify a specific orientation of the ligand relative to the receptor. (iii) Then, using the program GRID (Meng et al., 1992) an energy potential grid is computed within the volume defined above. This is done taking into account the partial charges of the protein atoms located within a certain cut-off distance from the

active site. (iv) Finally, the DOCK program evaluates the interaction energies of all possible ligand conformations. An empirical scoring function approximates the binding energy in terms of van der Waals and electrostatic interactions between the ligand and the receptor:

$$E = \sum_{i}^{lig} \sum_{j}^{rec} \left[\frac{A_{ij}}{r_{ij}^{12}} - \frac{B_{ij}}{r_{ij}^{6}} + \frac{q_i q_j}{4\pi\varepsilon r_{ij}} \right] \tag{31}$$

In this equation, *i* and *j* are the atoms of the ligand and the receptor, respectively, ε is the dielectric constant (assumed to vary linearly with r) and A_{ij} and B_{ij} are the van der Waals repulsive and attractive parameters, respectively, which can be calculated as

$$A_{ij} = \sqrt{A_{ii}} \cdot \sqrt{A_{jj}} \quad \text{and} \quad B_{ij} = \sqrt{B_{ii}} \cdot \sqrt{B_{jj}} \,. \tag{32}$$

The single atom type parameters (A_{ii}, A_{jj}, B_{ii} and B_{jj}) are calculated as a function of the atomic van der Waals radius R and a well depth μ

$$A = \mu(2R)^{12} \quad \text{and} \quad B = \mu(2R)^{6} . \tag{33}$$

Using this approximation, the overall ligand receptor interaction energy can be written as follow:

$$E = \sum_{i}^{lig} \left[\sqrt{A_{ii}} \sum_{j}^{rec} \frac{\sqrt{A_{jj}}}{r_{ij}^{12}} - \sqrt{B_{ii}} \sum_{j}^{rec} \frac{\sqrt{B_{jj}}}{r_{ij}^{6}} + \frac{q_i}{4\pi} \sum_{j}^{rec} \frac{q_j}{\varepsilon r_{ij}} \right] \tag{34}$$

To evaluate the ligand/receptor interaction, the potential energy of the receptor is first computed on a grid of points and then the ligand/grid interactions energy are calculated. Each grid point *k* is defined by three parameters

$$A_k = \sum_{j}^{rec} \frac{\sqrt{A_{jj}}}{r_{kj}^{12}} \qquad B_k = \sum_{j}^{rec} \frac{\sqrt{B_{jj}}}{r_{kj}^{12}} \qquad Q_k = \sum_{j}^{rec} \frac{q_j}{4\pi\varepsilon r_{kj}} \tag{35}$$

where the sum over receptor atoms are done within a certain cut-off distance. The ligand/grid interaction is finally approximated by the sum

$$E = \sum_{k}^{grid} \sum_{i}^{lig} \left[A_k \sqrt{A_{ii}} - B_k \sqrt{B_{ii}} + q_i Q_k \right]. \quad (36)$$

In our calculations the receptor parameters (atomic van der Waals radii, well depth and partial charges) were taken from AMBER force field (Cornell et al., 1995).

4.2 LIGAND/RECEPTOR BINDING EVALUATION

A critical point of the docking study is the evaluation of the obtained structures for the ligand/receptor complexes. The evaluation process is important since it is meant to serve as a discriminator between "correct" and "incorrect" binding modes, and, for multiple ligand docking, between binding and non-binding molecules. Because the ligand binding affinity is directly related to the binding free energy, it is clear that an evaluation function that approaches best the experimental free energy is likely to yield the best result. In this work, the free energy of binding was calculated with the DOCK's program scoring function.

Under the assumption of an accurate free energy calculation, the first evaluation of the structures obtained from docking runs, could be done on the basis of their scores. However, several complexes could have similar free energy values but differ in their configurations. As a consequence, one need a second evaluation factor. On this attempt, I assembled the obtained ligand/receptor structures in classes, using a custom-made clustering program. Each class contained all the ligand structures which differ in less than a certain rmsd value from at least one of the other structures contained in the same class. The sampling was done by a 0 K temperature Monte Carlo simulation.

5. PROGRAMS

The programs used in this thesis are:

AMBER (Case et al., 1997) – http://www.amber.ucsf.edu/amber/amber.html

DELPHI (Gilson and Honig, 1988) – http://trantor.bioc.columbia.edu/delphi/

CLUSTALW (Thompson et al., 1994) –
http://www.ch.embnet.org/software/ClustalW.html

MODELLER (Sali and Blundell, 1993) –
http://guitar.rockefeller.edu/modeller/modeller.html

PROCHECK (Laskowski et al., 1996) –
http://www.biochem.ucl.ac.uk/~roman/prochek/reference.html

DOCK (Ewing and Kuntz, 1997) - http://www.cmpharm.ucsf.edu/kuntz/

STRUCTURE AND DYNAMICS OF THE CGRP N-TERMINAL FRAGMENTS

Several neuropeptides can act as neurotransmitters per se as well as neuromodulators of receptors of other transmitters (Otsuka and Yoshioka, 1993). Important insights into the phenomenon of peptide-induced receptor modulation have been provided by studies on muscle-type nicotinic acetylcholine receptors. In particular, it has been shown that the endogenously occurring calcitonin gene-related peptide (CGRP) facilitates nAChR desensitisation via intracellular second messenger mediated phosphorylation (Mulle et al., 1988; Miles et al., 1989; Lu et al., 1993) and increases nAChR biosynthesis (Changeux et al., 1992).

More recently, the CGRP modulation of neuronal-type nicotinic receptors was also studied on rat chromaffin cells (Giniatullin et al., 1999). The main novel observation was that CGRP selectively and rapidly blocked neuronal nAChRs (a phenomenon unlikely caused by intracellular massagers in view of its speed) and its inhibitory effect was independent of $[Ca^{2+}]_i$ or membrane potential. The block by CGRP was insensitive to the receptor antagonist $hCGRP_{8-37}$, but mimicked by $CGRP_{1-7}$. Giniatullin et al (1999) proposed that the 1-7 amino acid sequence of CGRP was responsible for the direct, rapid block of nAChRs, whereas the full-length peptide molecule was necessary for the delayed rise in internal Ca^{2+} potentially able to trigger phosphorylation-dependent modulation of nicotinic receptor function.

With the attempt to identify the minimal amino acids sequence retaining this antagonist action, the effects of a shorter fragment of this peptide, namely $CGRP_{1-6}$, was investigated (Di Angelantonio et al., 2002). As a result, it was interestingly observed that this compound exhibited a powerful potentiating action on nAChRs. $CGRP_{1-6}$ manifested a rapid onset and agonist-surmountable potentiation of inward currents evoked by pulse applications of nicotine.

To verify if conservation of $CGRP_{1-6}$ was essential for the enhancing action, the effects of shorter fragments, namely $CGRP_{1-5}$, $CGRP_{1-4}$ or $CGRP_{1-3}$ were then investigated.

Deleting one amino acid from the $CGRP_{1-6}$ C-terminal clearly yielded a compound ($CGRP_{1-5}$) still endowed with potentiating activity on nAChRs (although with reduced potency). Even the $CGRP_{1-4}$ fragment retained a slight, yet significant potentiation which was lost with $CGRP_{1-3}$.

The potentiation induced by $CGRP_{1-6}$ and its derivatives is in sharp contrast with the depression of nicotine evoked currents induced by $CGRP_{1-7}$ (Giniatullin et al., 1999). In order to understand why deletion of a single amino acid from $CGRP_{1-7}$ transforms the biological activity of the peptide fragments from depressant into potentiating action, a comparative study between structure and function was done.

1. RESULTS

1.1 PRIMARY STRUCTURE INSPECTION OF CGRP FRAGMENTS

Inspection of the CGRP fragment primary sequences (Figure 13) showed one major difference between $CGRP_{1-7}$ and $CGRP_{1-6}$, namely the presence of a disulphide bridge between Cys2 and Cys7. While the $CGRP_{1-7}$ structure features as a closed ring, in $CGRP_{1-6}$ the absence of the cysteine in position 7 transforms the disulphide ring into a linear chain. This suggested that the presence of the disulphide bridge is crucial for producing the depressant effect on nAChRs, while an open configuration like the one of $CGRP_{1-6}$ is responsible for enhancing nAChR function.

Consistent with this idea, we predicted that a seven amino acid chain similar to the one of $CGRP_{1-7}$ but lacking a cyclic structure should yield a nAChR potentiating peptide and, on the other hand, a peptide which retains the disulphide ring should maintain the $CGRP_{1-7}$ inhibitory effect. This hypothesis was tested by synthesising two new peptide fragments, one replacing Cys7 with Ala (termed $CGRP_{1-7A}$) and the other deleting Ser1 but retaining Cys2 and Cys7 (termed $CGRP_{2-7}$). The two peptide fragments were tested on rat cromaffin cells. As a result, $CGRP_{1-7A}$ was observed to behave like its shorter length counterpart $CGRP_{1-6}$ in potentiating nAChRs (although with somewhat reduced potency), while $CGRP_{2-7}$ retained (albeit weakly) the depressant action of the longer compound $CGRP_{1-7}$.

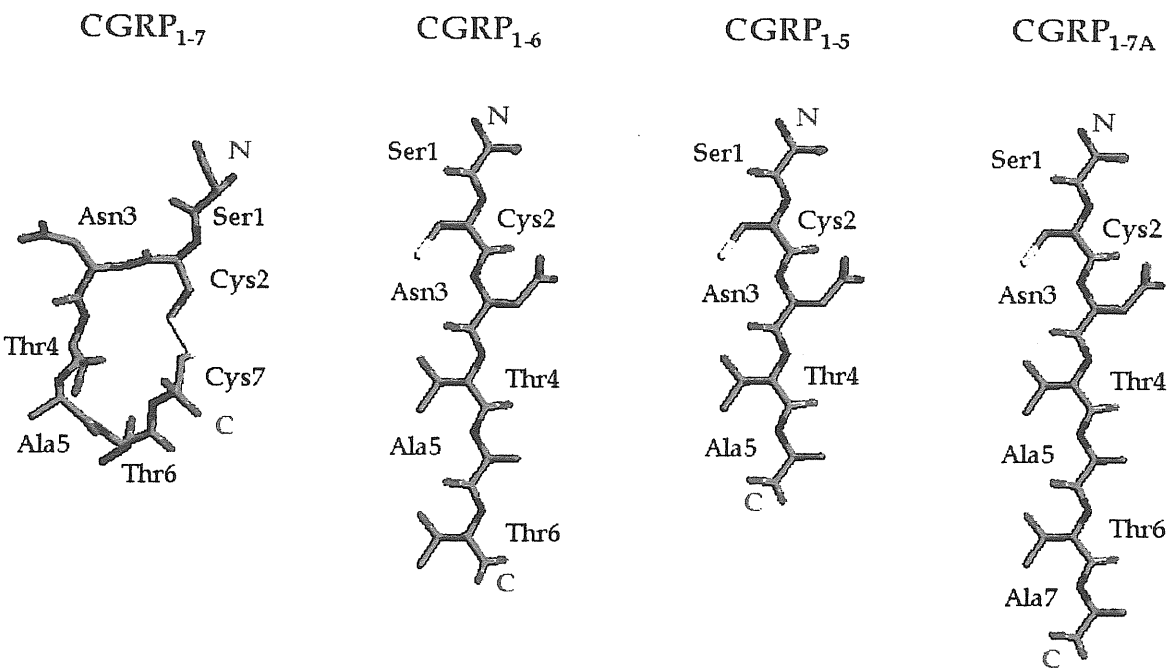

FIGURE 13. Initial MD structures of the peptides $CGRP_{1-7}$ (note disulphide bond), **$CGRP_{1-7A}$, $CGRP_{1-6}$, $CGRP_{1-5}$.**

In the attempt to understand more about into the structure-activity relation of these peptides, we subsequently performed a three-dimensional structure investigation.

1.2 3D STRUCTURE INVESTIGATION

The major goal of our study was to relate the structural properties of the peptides in solution to their modulatory properties on nAChRs. To this aim, we have performed a combination of computational and experimental techniques, that is molecular dynamics, which can provide atomic structural models, and circular dichroism measurements, which can provide insights into the relative preponderance of various secondary structures for each peptide in solution (Impellizzeri G, 1998 and refs. therein).

1.2.1 COMPUTATIONAL DETAILS

STRUCTURAL MODELS

We investigated the three-dimensional structure of four CGRP terminal fragments (see Figure 13), namely (i) $CGRP_{1-7}$, in which Cys_2 and Cys_7 form a disulfide bridge, (ii)

$CGRP_{1-7A}$, which is the same as $CGRP_{1-7}$ except that Ala replaced Cys_7, (iii) $CGRP_{1-6}$ and (iv) $CGRP_{1-5}$. The initial structural model of $CGRP_{1-7}$ was built through a systematic search of the Protein Data Bank (Berman et al., 2002) for a protein containing a ring of six amino acids closed up by a disulphide bridge. We selected the X-ray structure of progastricsin (Moore et al., 1995; Protein Data Bank accession number 1HTR) as its residues Cys45-Gln46-Ser47-Gln48-Ala49-Cys50 form a six-membered disulphide ring. These residues were found to display a very good Ramachandran plot (Ramachandran and Sasisekharan, 1968), indicative of a highly plausible spatial conformation of this protein. To build the $CGRP_{1-7}$ model, we replaced Gln46, Ser47, Gln48 and Ala49 with Asn, Thr, Ala and Thr, respectively. A Ser residue was attached to Cys45; NH_3^+ and COO^- terminal groups were added.

The initial models of $CGRP_{1-7A}$, $CGRP_{1-6}$ or $CGRP_{1-5}$ were, instead, constructed starting from a linear configuration (i.e. backbone dihedral angles $\phi = \psi = 180°$). Then, for each peptide a simulated-annealing procedure (similar to that of Daura et al., 1998) was performed for each peptide in three steps: (i) MD simulations in vacuum at 1000 K temperature for 10 ps; (ii) eight structurally different conformers, selected from this simulation, were cooled from 600 K to 0.5 K in 1.5 ns; and finally (iii) the lowest-energy models were used for the MD simulation in water.

The four CGRP terminal fragments were finally inserted in a water cubic box of about 30x30x30 $Å^3$ and MD simulation were further performed.

COMPUTATIONAL SETUP

The AMBER (Cornell et al., 1995; www.amber.ucsf.edu/amber/) or TIP3P (Jorgensen et al., 1983) force-fields were used to describe the inter-atomic potential energy functions of peptides or water, respectively. The dielectric constant was set to 1. The time-step integration of the Newton equation of motion was set to 1.5 fs. Temperature (298 K) and pressure (1 bar) were kept constant by coupling the peptide/water systems to a Berendsen bath algorithm (Berendsen et al., 1984) with 1.0 ps relaxation time. van der Waals interactions were truncated up to a spherical, residue-based cut-off of 12 Å. Periodic boundary conditions (Allen and Tildesley, 1987) were imposed to avoid

problems due to the small dimensions of the system. Electrostatic interactions were calculated using the Ewald particle mesh method (Essman et al., 1995).

MOLECULAR DYNAMICS CALCULATIONS

The simulation procedure was carried out as follows. First, the solvent underwent energy minimization and was equilibrated (with a molecular dynamics process) with the peptide for 30 ps at constant volume. Subsequently, the entire system was heated for 0.12 ns from 0 to 298 K, at 1 bar pressure. Finally, 10 ns molecular dynamics simulations at 298 K temperature and 1 bar pressure were performed. All calculations were carried out with the SANDER module of the AMBER5 suite of programs (Case et al., 1997) running on a four-processor SGI Origin 200 parallel machine. 10 ns simulation for each peptide required approximately 20 days of calculations.

1.2.2 COMPUTATIONAL AND EXPERIMENTAL RESULTS

MD STRUCTURE OF CGRP FRAGMENTS

The structural properties of the four peptides $CGRP_{1-7}$, $CGRP_{1-6}$, $CGRP_{1-5}$ and $CGRP_{1-7A}$ are hereafter described as a result of our MD investigation in aqueous solution.

Figure 14 A shows the structure of the $CGRP_{1-7}$ in aqueous solution. A six amino acid ring results from the disulphide bridge (yellow sticks) between Cys2 and Cys7. An inner ring hydrogen bond (see dashed line in Figure 14 A) between the backbone carbonyl of Thr4 and the backbone amide of Cys7 was found throughout all dynamics simulation (the distance, *d*, between [O(Thr4)-NH(Cys7)] was 2.4±0.3 Å). The conformation of $CGRP_{1-7}$ backbone was relatively rigid (R_G = 0.75±0.03 Å). Some flexibility was observed on the plane orthogonal to the inner hydrogen bond. Water molecules were not found within the ring. All side-chains and carbonylic oxygen atoms were outwardly directed away from the ring.

Investigation on $CGRP_{1-6}$ showed that an H-bond between Ser1 backbone carbonyl oxygen and the Thr4 NH group (indicated by thick dashed line in Figure 14 B) was formed after few ns. Two additional hydrogen bonds (O(Cys2)-NH(Thr6) and O(Ser1)-NH(Ala5)) appeared weaker (see thinner dashed lines in Figure 14 B) as they broke and

immediately reformed several times during the dynamics. The resulting backbone geometry in terms of torsion angles was that of an α-helix (Creighton, 1993). The molecular shape was rather flexible (R_G = 0.64±0.05 Å).

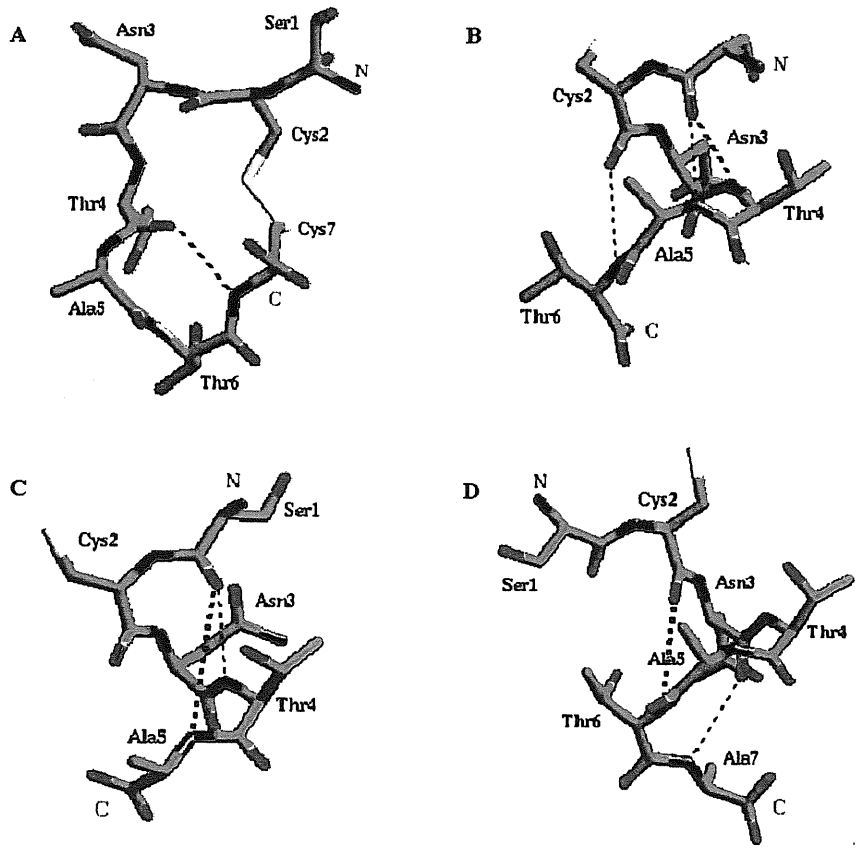

FIGURE 14. Schematic conformations of the four peptides in aqueous solution as obtained with molecular dynamics calculations. Hydrogen atoms are not displayed for sake of clarity. Hydrogen bonds are indicated as dashed lines of different thickness according to the strength of the bond. (**A**) $CGRP_{1-7}$, (**B**) $CGRP_{1-6}$, (**C**) $CGRP_{1-5}$ and (**D**) $CGRP_{1-7A}$. Atoms are colored using the following code: oxygen (red), nitrogen (blue) carbon (green) and sulphide (yellow).

Also in the case of $CGRP_{1-5}$ the Ser_1 backbone carbonyl oxygen formed a stable hydrogen bond (thick dashed line in Figure 14 C) with Ala_5 (d[O(Ser1)-NH(Ala5)] =2.8±1.5 Å) after few ns and a further, albeit weak, hydrogen bond (see thin dashed line in Figure 14 C) with Thr4. As a result, also the $CGRP_{1-5}$ adopted a rather flexible shape (R_G = 0.66±0.04 Å).

$CGRP_{1-7A}$ was finally characterised by the hydrogen bond between O(Cys2) and NH(Thr6) (d[O(Cys2)-NH(Thr6)] = 3.2±0.4 Å; see thick line in Figure 14 D) that stabilised the Cys2-Thr6 backbone structure. An additional, weak hydrogen bond (see

thin line in Figure 14 D) between Asn3 carbonyl oxygen and Ala7 formed and broke several times during simulations. Thus, while the Cys2-Ala7 backbone adopted an α-helix conformation, the N-terminal residue (Ser1) turned away from the main peptide structure to interact with water. The resulting backbone geometry was rather flexible (R_G = 0.59±0.04 Å).

COMPARISON BETWEEN PEPTIDES STRUCTURES

In conclusion, simulation data highlighted that the AChR-depressant $CGRP_{1-7}$ possessed a ring structure stabilised by a hydrogen bond, while the AChR-enhancing peptides preferentially displayed a flexible shape, in which α-helix structural elements could be formed and broken during the dynamics. The spatial alignment of $CGRP_{1-6}$ and $CGRP_{1-5}$ (Figure 15 A) suggests that the $CGRP_{1-6}$ structure (blue) was rather similar to that of $CGRP_{1-5}$ (yellow), with only a significant difference in peptide length.

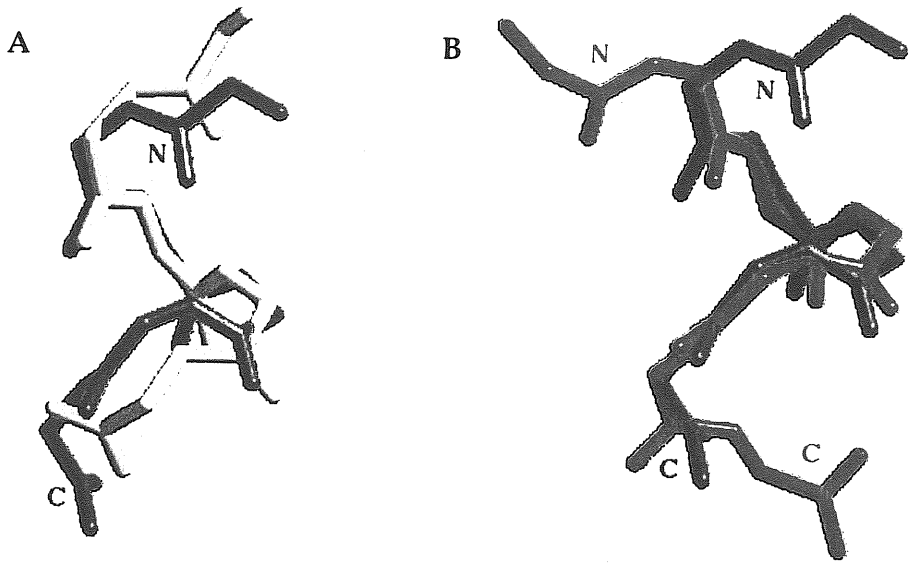

FIGURE 15. Spatial alignment of $CGRP_{1-6}$, $_{1-5}$ or $_{1-7A}$ backbones. **A**: comparison of $CGRP_{1-6}$ backbone (blue) with the one of $CGRP_{1-5}$ (yellow). **B**: comparison of $CGRP_{1-6}$ backbone (blue) with the one of $CGRP_{1-7A}$ (magenta).

By fitting $CGRP_{1-5}$ alongside with the corresponding five amino acids of $CGRP_{1-6}$, it became clear that $CGRP_{1-5}$ had a more extended conformation along the α helix axis (Figure 15 A), possibly because of the lower number of hydrogen bonds between its backbone atoms. $CGRP_{1-6}$ (blue) and $CGRP_{1-7A}$ (magenta) were also rather similar

(Figure 15 B): their structures differed only for the conformation assumed by their N-terminal residues, that in the case of $CGRP_{1-6}$ was constrained to the backbone by the two hydrogen bonds.

CD SPECTRA OF $CGRP_{1-7}$ AND $CGRP_{1-6}$

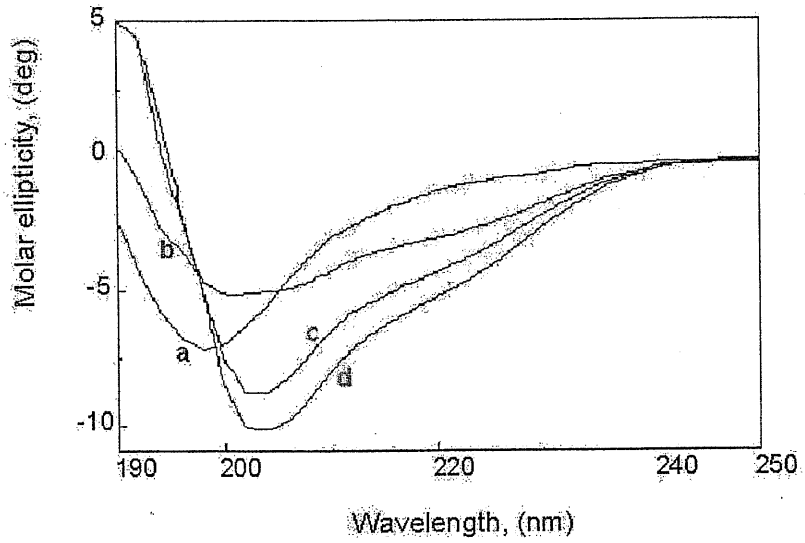

FIGURE 16. CD spectra of $CGRP_{1-6}$ and $CGRP_{1-7}$. a) record of $CGRP_{1-6}$ in phosphate buffer at 20 C; b) record of $CGRP_{1-6}$ in phosphate buffer/TFE (50/50 %); c) record of $CGRP_{1-7}$ in phosphate buffer; d) record of $CGRP_{1-7}$ in phosphate buffer/TFE (50/50 %).

To verify our computational results, a secondary structure investigation of $CGRP_{1-7}$ and $CGRP_{1-6}$ by circular dicronism measurements was performed. The peptides CD spectra in aqueous salt solution (containing 25 mM phosphate buffer and 4 mM NaCl at pH 7.4) were significantly different, suggesting underlying dissimilarities in their structure (Figure 16). Indeed, the spectrum of $CGRP_{1-6}$ (see record marked *a* in Figure 16) showing a negative band peak at 198 nm is diagnostic of an essentially "disordered" conformation; its CD intensity at 220 nm was very low. In contrast, the spectrum of $CGRP_{1-7}$ (see record marked *c* in Figure 16) was characterised by a negative band at 204 nm with a hump around 220 nm, the latter feature being indicative of some structural organisation. Further data were obtained by recording the CD spectra of the two peptides in 50 % TFE/water solution. The spectrum of $CGRP_{1-6}$ was largely affected (see trace labelled *b* in Figure 16) as the negative band was shifted to 202 nm and

development of a negative hump around 220 nm appeared. Conversely, the conformation of $CGRP_{1-7}$ in solution was only slightly changed by switching to the TFE/water medium (see trace labelled *d* in Figure 16).

The CD spectrum of an α-helix is characterised by two minima at 222 nm and 206 nm, and a maximum at 193 nm in solution (Impellizzeri G, 1998). Thus, any increase in ellipticity absolute values observed at 222 nm when passing from water to a semi-hydrophobic solvent (50% water/TFE) should indicate larger α-helical content of the test samples. Since the random coil conformation generates a very low signal at 222 nm, $CGRP_{1-6}$ has some propensity for helix formation.

2. DISCUSSION

The structure/function relation of a series CGRP fragments (Figure 13) was characterised by computer simulation techniques.

Experimentally, it has been shown that discrete changes in the amino acid composition of the CGRP N-terminal sequence may induce different effects on nAChRs. Indeed, in sharp contrast with the $CGRP_{1-7}$ depressing action on nAChRs (Giniatullin et al., 1999), $CGRP_{1-6}$ exhibited a selective, rapid and reversible potentiating modulation (Di Angelantonio et al., 2002). Equimolar concentrations of $CGRP_{1-6}$ and $CGRP_{1-7}$, co-applied to the same cell, left nicotine-induced submaximal currents unchanged. Deleting one amino acid from the COO^- end of the $CGRP_{1-6}$ sequence clearly yielded the compound $CGRP_{1-5}$ still endowed with potentiating activity on nAChRs (although with reduced potency). Significant although slight, potentiation was also retained by the $CGRP_{1-4}$ fragment and lost with $CGRP_{1-3}$ (Di Angelantonio et al., 2002).

The major difference between $CGRP_{1-7}$ and $CGRP_{1-6}$ is the presence of a disulphide bridge between Cys_2 and Cys_7, which determines the closed ring structure of $CGRP_{1-7}$ (Figure 13). Thus, $CGRP_{1-6}$ is expected to be more flexible than $CGRP_{1-7}$. This realisation led to synthesis of a seven amino acid peptide analogous to $CGRP_{1-7}$ except that the terminal Cys_7 was replaced by Ala and was thus devoid of the disulphide bridge. This new compound, termed $CGRP_{1-7A}$, was observed to behave like its shorter length

counterpart $CGRP_{1-6}$ in potentiating nAChRs although with somewhat reduced potency (Di Angelantonio et al., 2002).

In order to shed light on the changes of structural determinants upon discrete changes in amino acid composition, MD simulations of all of these peptides were carried out in aqueous solution.

MD simulations indicated that the ring structure of $CGRP_{1-7}$ was stabilised by an inner ring hydrogen bond (Figure 14). This interaction ensured a rather rigid structure, in agreement with CD results (Di Angelantonio et al., 2002). The rather rigid structure was presumably responsible for blocking agonist binding to nAChRs and was indeed the molecular determinant of the antagonist activity of the native CGRP itself (Giniatullin et al., 1999).

$CGRP_{1-6}$, $CGRP_{1-5}$ and $CGRP_{1-7A}$ turned out to be structurally similar and preferentially adopted a flexible structure, partly with α-helix conformation (Figure 14 and 15). Most of the H-bond interactions stabilising the secondary structure motif were lost and reformed within the time scale investigated.

The calculated α-helix character was more pronounced than that indicated by CD measurements (Di Angelantonio et al., 2002) performed on one of these peptides ($CGRP_{1-6}$). Indeed, from CD spectra $CGRP_{1-6}$ mostly assumed a random coil conformation. The discrepancy between theory and experiment may be ascribed to the different time scales investigated as MD simulations are in the order of ns, whereas CD spectra obtain structural data averaged over a few tens of seconds. Thus, the MD sampling might have been predominantly oriented to a certain conformation present in water solution, namely a highly flexible α-helix. A small amount of such a conformation (10-15%) is indeed compatible with the CD results (Rees and Reed, 1997).

On the basis of CD data, the propensity of $CGRP_{1-6}$ for α-helix formation increased when the solvent was changed from water to a semi-hydrophobic one (TFE/water). This result suggests that at the level of the nAChR binding sites, which is expected to be a low dielectric medium, the population of α-helix structures might become relevant for biological responses. Thus, the MD helical conformation of $CGRP_{1-6}$ was used as starting structures for the docking calculations, which are here presented.

STRUCTURAL MODELS OF nAChR AND INTERACTION WITH LIGANDS

To shed light on the structural reason underlying the different modulatory effects of the CGRP N-terminal fragments on nAChRs, a structural model of the ligand-binding domain of the receptor is required. In this thesis, I have exploited the similarity between the receptor ligand-binding domain and the acetylcholine-binding protein (AChBP) of snail *Lymnaea stagnalis* (Smit et al., 2001), the structure of which has been recently determined by X-ray diffraction (Brejc et al., 2001). AChBP aligns the N-terminal domain of all ligand-gated ion channels (Introduction, Figure 4). Furthermore, almost all residues relevant for ligands binding that are conserved within the nAChR family were present in AChBP. In fact, nAChR agonists and competitive antagonists, such as acetylcholine, nicotine, d-tubocurarine and α-bungarotoxin bind also to AChBP (Smit et al., 2001).

α3β4 and α4β2 are the neuronal nicotinic receptors most populated in rat cromaffin cells (see Introduction; Campos-Caro et al., 1997). The binding domains of these receptors were then constructed on the basis of the AChBP X-ray structure, using comparative modelling and molecular dynamics techniques. From now on, α3β4 and α4β2 will refer only to the ligand binding domain of the nicotinic receptors subtypes composed by $(\alpha3)_2(\beta4)_3$ and $(\alpha4)_2(\beta2)_3$ subunits.

1. RESULTS

1.1 STRUCTURAL MODELS OF NACHRS IN RAT CROMAFFIN CELLS

1.1.1 STRUCTURAL ALIGMENT AND MOLECULAR MODELLING PROCEDURE

The complete sequence of AChBP was aligned to that of the amino-terminal domain of the rat subunits α3, α4, β2 and β4, using the CLUSTALX program (Thompson et al.,

1997). This multiple alignment was manually improved by including structural information of the template (see Methods for details). Figure 17 shows the receptor secondary structure as obtained by our modelling and comprising α-helices (H) and β-sheets (B) with reference to the position of the aminoacids within the AChBP sequence.

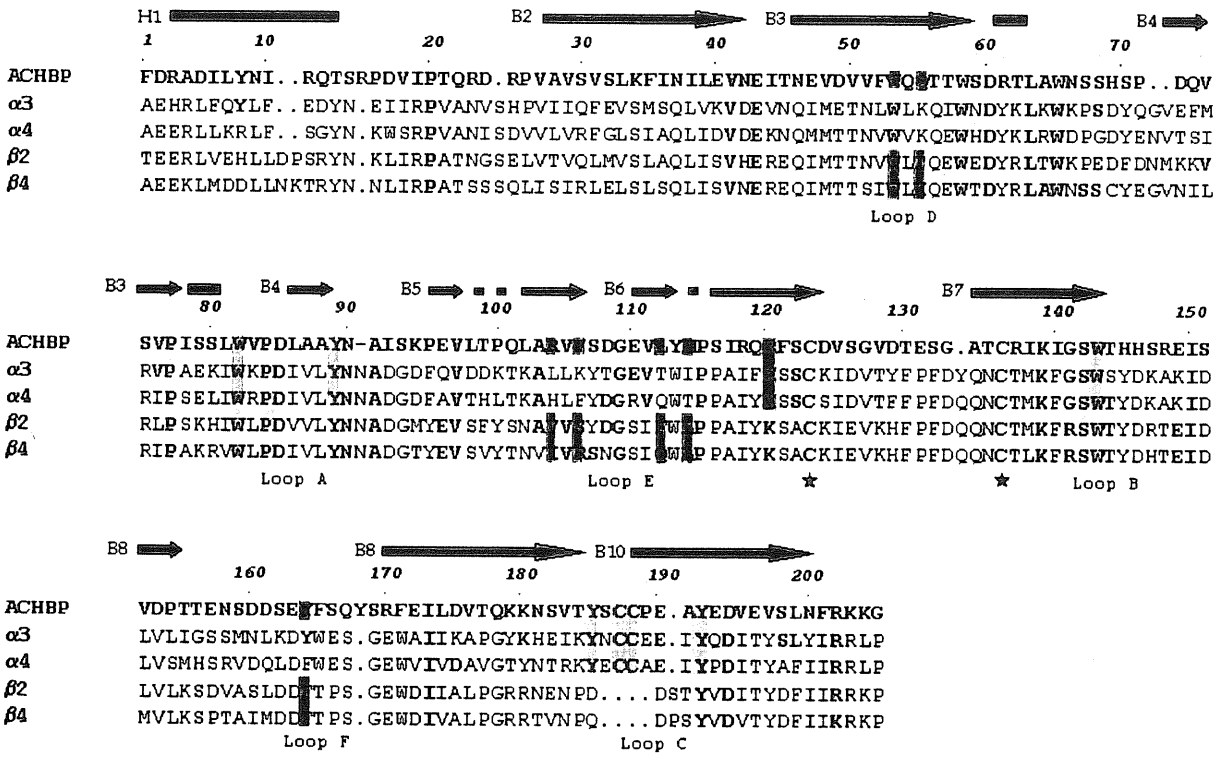

FIGURE 17. Sequence alignment between AChBP and amino-terminal domains of rat α3, α4, β2 and β4 nAChR subunits. The top line (blue) presents the secondary structure of AChBP: bars indicate α-helices and arrows β-sheets. Only 22-20% of residues present in α-β N-terminal segments of the nAChRs are conserved in the AChBP. Residues conserved in all aligned segments are labeled in light green. Residues involved in the agonist/antagonist binding site of the α and β component are labeled grey and blue, respectively. The residue known to bind the allosteric agent is depicted in red. Asterisks indicate the beginning and end of the Cys-loop. The loops indicated in the bottom line are referred to residues belonging to the agonist binding site. Numbering is that of AChBP (Brejc et al 2001).

The resulting sequence identities of α and β subunits were found to be 22% and 20%, respectively. The final alignment did not differ significantly from those of Brejc et al. (2001) and of Le Novere et al. (2002). Larger differences were found between our alignment and that of Schapira et al. (2002).

The three-dimensional structure of α3β4 was built with the MODELLER program (Sali and Blundell, 1993). The program constructs backbone and side-chains based on the 3D

structure of the template and the sequence alignment (see Methods). The structural model with the highest MODELLER score (Sanchez and Sali, 1997) was refined by imposing symmetry constraints for the two α and the three β subunits and by loop structural improvements during the calculation. The resulting model exhibited a good Ramachandran plot (Ramachandran and Sasisekharan, 1968).

The structure of α4β2 was reported by Le Novere et al. (2002), while carrying out my work. As the procedure adopted to construct the model was practically the same as the one used here, I used Le Novere's model (http://www.pauster.fr/recherche/banques/LGIC/LGIC.html).

Using AMBER program (Case et al., 1997), the two structural models underwent energy minimization, initially by the procedure of 1,000 steps of steepest descent and subsequently by the method of 2,000 steps of conjugate gradient algorithms. Then, the position of the side-chains was relaxed by 30 ps of MD at low temperature (50 K), while the backbone positions were harmonically constrained.

1.1.2 Comparison between AChBP structure and α3β4/α4β2 models

Overall structures

As expected from the relatively low number of insertions/deletions in the alignment, the α3β4 and α4β2 structures did not differ largely form the template (Figure 18 A). The domains were barrels of 80 Å diameter and 63 Å height with a central irregular pore of variable diameter from 10 to 15 Å. The structures confirmed for nAChRs an immunoglobulin fold (Corringer et al., 2000) mostly composed of β-strands (Figure 18 B). The secondary structure elements of the template were mostly preserved. Only small differences were observed in the β subunits; in particular α-helix H1 was shorter, B6 was disrupted in two parts and the loop between β-sheet B8 and B9 was longer than in the template.

The sequence alignment (Figure 17) showed that most of the conserved residues (20%-22%) were hydrophobic. As expected, these residues were mainly located in the core region of the subunits. The charge residues, mainly distributed over the external side of the pentamer, were not well conserved even within the nicotinic receptors family.

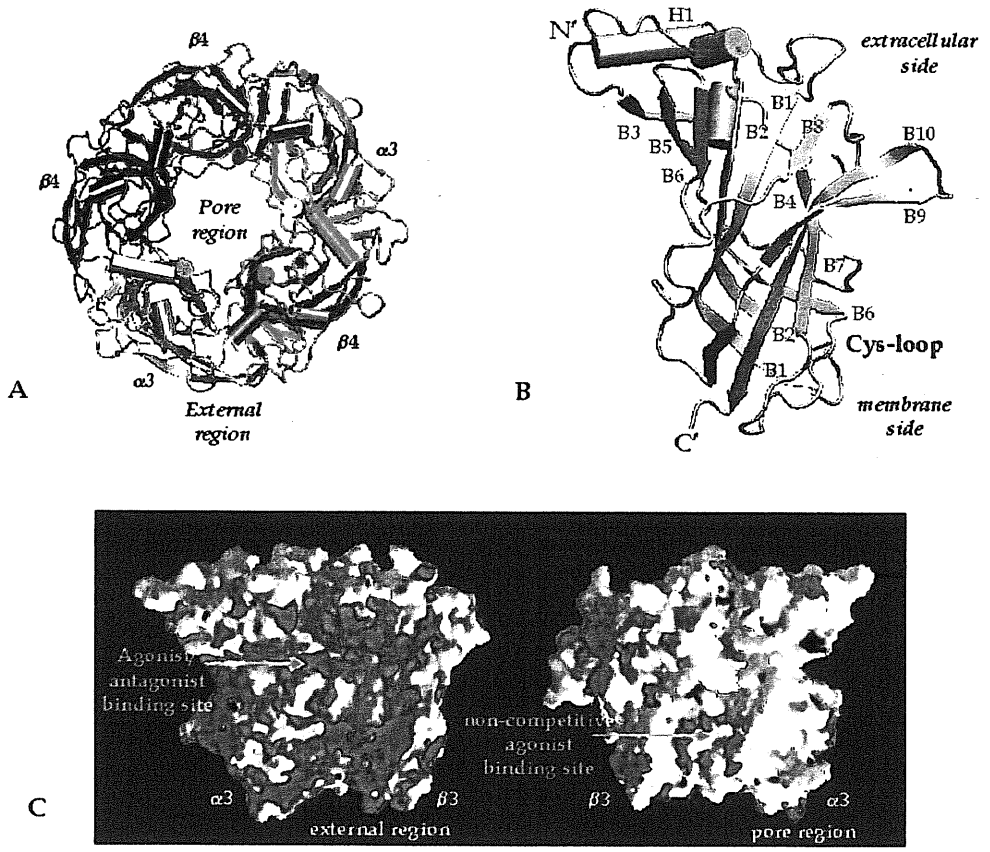

FIGURE 18. **α3β4 model**. **A**: Top view of the pentameric structure. The model has the shape of a barrel of 80 Å diameter and 63 Å height, with a central irregular pore of variable diameter (10-15 Å). **B**: Secondary structure of the α3 subunit. It is composed by one α-helix (H1) and ten β-sheets (B1-B10). Two very small α-helices are also present. C: Color-coded calculated electrostatic potential at the surface of one α3β4 pair of subunits. External and pore sides are shown, outlining the amphipatic profile of the nicotinic receptor N-terminal domain. The prevalence of negatively charged residues is apparent. The binding site location of full and allosteric agonists is indicated within the external and pore region, respectively. Red, blue and white colors indicate negative, positive and neutral regions.

Although the identity percentage between α's and β's nicotinic receptor subunits is high (62% and 69%, respectively), the overall charge of each subunit appreciably varies (-5,-5,-9 and -2 for α3, α4, β2 and β4 respectively, compared with -9 of each AChBP subunit). The electrostatic potential over the receptor surface (Figure 18 C) confirms its negatively charge profile in the external side, while the core region is mostly hydrophobic.

In our models, like in the AChBP, the subunits interfaces were formed entirely by loops on one side and mostly by secondary structure elements on the opposite side. The

residues at the interface were however not well conserved neither between nAChR subunits and AChBP, nor within nicotinic receptor family. In particular, salt bridges crossing α/β and β/α interfaces in both α3β4 and α4β2 models mainly involved not aligned residues (Table I).

TABLE I. SALT BRIGES AT SUBUNIT INTERFACES.†

α3β4			α4β2			AChPB		
atom name		d(Å)	atom name		d(Å)	Atom name		d(Å)
αArg17	βGlu1	2.7	+αArg17	βGlu2	2.7	+Glu149	–Arg3	2.8
αArg78	βGlu2	2.8	αLys61	βGlu1	2.8	+Glu149	–Arg104	2.9
αGlu117	βGlu110	2.7	αAsp86	βArg78	2.7			
			αAsp149	βLys76	2.7			
βGlu10	αArg13	3.1	βArg45	αGlu172	2.8	+Glu149	–Arg3	2.8
βAsp88	αLys104	2.8	βAsp88	αArg76	2.7	+Glu149	–Arg104	2.9

†Salt bridges crossing α/β (+/–) and β/α (–/+) interfaces in α3β4, α4β2 and AChBP. Interactions mainly involved not aligned residues.

The Cys-loop (i.e. loop characterised by the presence of a disulphide bond between two β-sheets B6 and B7 in Figure 18, see also Introduction Section), is known to be important for the complete nAChR assembly (Green and Wanamaker, 1998). The loop was not conserved in the AChBP: while the Cys-loop of α3β4 and α4β2 contains 13 residues and is hydrophobic, the one of the AChBP is 12 residues long and has a hydrophilic profile. Notice that, in the α3β4 and α4β2 receptors, the loop is located at the bottom of the ligand-binding domain, close to the membrane, suggesting its potential role in the interaction with the transmembrane region of the receptors. This function is absent in AChBP which is soluble protein.

Several other regions (such as 1-20 and 152-170 segments in Figure 17) were not homologous with those of the AChBP. The expected accuracy of the models in those regions was therefore lower than for the general structure.

COMPETITIVE AGONIST/ANTAGONIST BINDING SITES

The agonist binding region of nAChRs is well defined, since several photoaffinity labelling and mutagenesis experiments done on muscle type or *Torpedo* nicotinic receptors identified most residues involved in binding (see Karlin, 2002 for a recent review). In α3β4 and α4β2 (Le Novere et al., 2002) models (as well as in their template)

these residues, mostly aromatic, formed a small hydrophobic cavity at the interface between α and β subunits (Figure 19). In both models, seven residues of the α-subunit, namely αTyr90 (loop A), αTrp146 and αTyr148 (loop B) and αTyr187, αCys189, αCys190 and αTyr194 (loop C), formed the principal component of the binding site, while five residues on the β-subunit, namely βTrp55 (loop D), β_2Val106/β_4Ile106, β_2Ser108/β_4Arg108 β_2Phe114/β_4Gln114 and βLeu116 (loop E), formed the complementary component. The residues of the α-subunit were highly conserved within nAChRs family and AChBP. Conversely, only βTrp55 was conserved within the β subunits (see Figure 17).

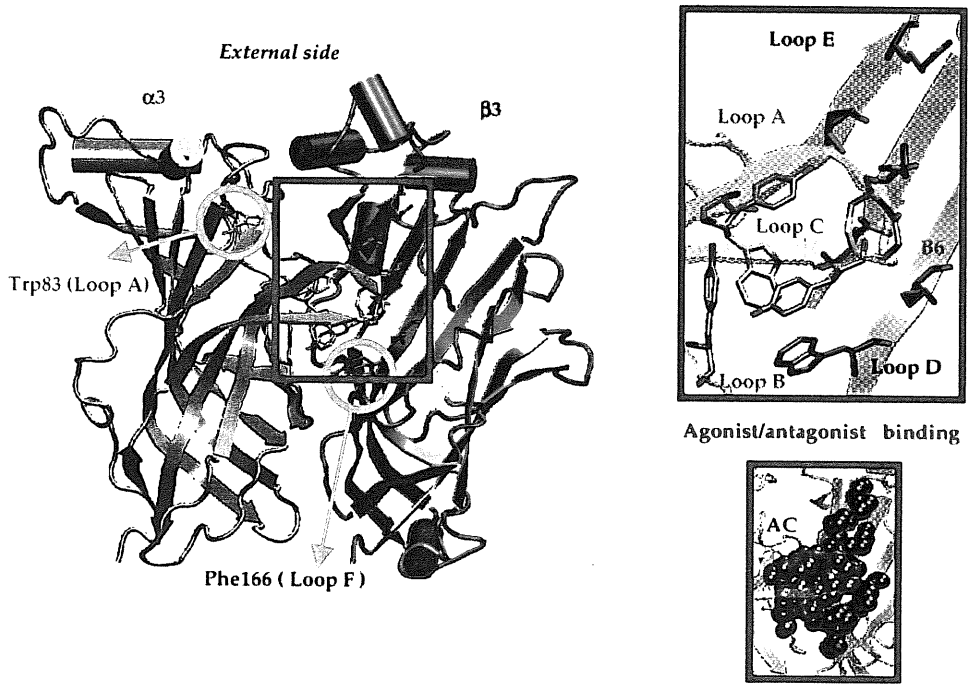

FIGURE 19. Agonist/antagonist binding site in α3β4 model. Seven residues of the α-subunit (gray) on loops A, B and C formed the principal component of the binding site, while five residues of the β-subunit (blue) on loops D and E formed the complementary component. This arrangement yields a small hydrophobic cavity on the external side at the interface between α and β subunits.

The residues involved in ligand binding were experimentally characterised either for changing the agonist/antagonist affinity or for inhibition of channel gating. In our models, some of these side chains were not involved in the binding site structure. For these residues experimental findings could be rationalise on the basis of our models.

Residue αTrp83 (loop A), which was identified by labelling studies as important for agonist binding (Galzi et al., 1990), in the present model was located outside the binding pocket (Figure 19) being, instead, involved in hydrophobic core formation, perhaps to stabilize the binding site structure.

Experimental studies on *Torpedo* receptors suggest an additional residue (on loop F; see Figure 17) to be important for agonist binding (Czajkowski and Karlin, 1995). In our alignment this would correspond to βPhe166, which was clearly far away from the binding site (Figure 19). Note however that the relatively low resolution of the crystal structure in this region makes the structural analysis difficult (Brejc et al., 2001).

Moreover, the loop F has low sequence conservation in the nicotinic family (Brejc et al., 2001) and, in the δ subunit of the *Torpedo* receptor, it corresponds to an aspartate (δAsp182). This and other aspartic residues present in the *Torpedo* receptor along and near loop F are reported to decrease the affinity of ACh (Czajkowski and Karlin, 1995; Martin et al., 1996).

Their role, which is probably to stabilize the agonist cationic charge by long range interactions, could not be fulfilled in our neuronal receptors by the corresponding residues because they were absent from β subunits. In the present study long range electrostatic stabilization of the ACh charge was provided by two other aspartates from the principal component, namely αAsp149 (loop B) and αAsp197 (loop C), in full agreement with mutagenesis experiments (Sugiyama et al., 1996; Osaka et al., 1998). These residues were the source of the negative electrostatic potential which characterized the agonist binding site, as detected by electrostatic calculations (see Figure 18 C) and as expected from experimental findings and theoretical studies (Stauffer and Karlin, 1994).

ALLOSTERIC AGONIST BINDING SITE

The location of the allosteric binding site(s) remains uncertain. Photoaffinity labelling experiments have shown that eserine labels α_1Lys125 of the *Torpedo* receptor (Schrattenholz et al., 1993). On the basis of the current subunit alignment (see Figure 17) the residue α_1Lys125 of the *Torpedo* receptor corresponds to αLys122 for the nAChRs

and +Arg120 for the AChBP, which could be found on the B6 β-sheet of the nAChR α subunits or the corresponding AChBP (+) subunit (Figure 20).

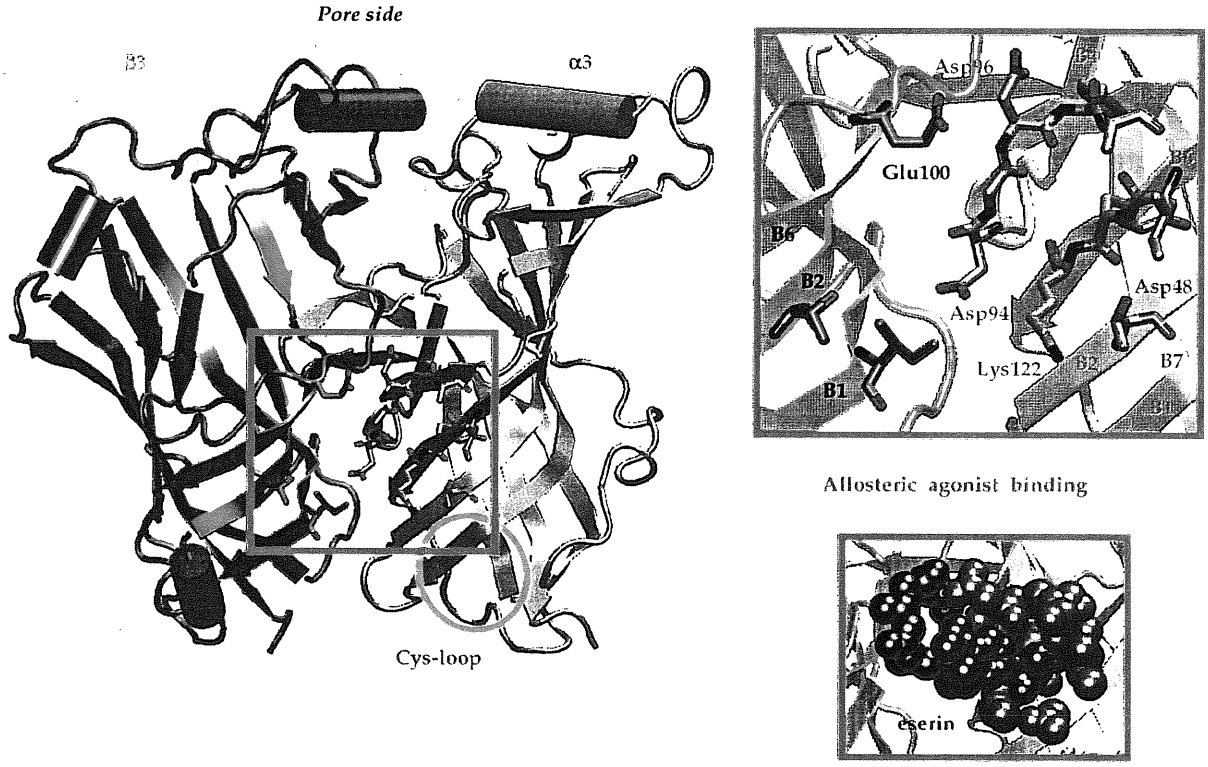

FIGURE 20. Allosteric agonist binding site in α3β4 models. The suggested binding region is located around αLys122, between segments of β-sheets B1, B2, B6 and B5 on the α subunit (gray) and β-sheets B1, B2 and B6 of the β subunit (blue). Residues involved in eserine binding are shown as sticks and are observed within the pore region.

Unlike the external location of the agonist binding site (see Figure 19), the allosteric binding site was internally located between the B2 and B5 β-sheets, thus not far from the subunit interface (Figure 20). The region within 14 Å from αLys122 of nAChRs was mostly composed by four segments of the α subunit, namely α_2Ile38/α_4Val38-αAsp41 (B1 β-sheet), αAsn44-αAsn50 (B2 β-sheet), αAla119-αCys125 (B6 β-sheet), and αLeu89-αPhe97 (B5 β-sheet) plus some residues of the β component facing the subunit interface (namely on B1, B2 and B6 β-sheets). αLys122 made a salt bridge with αGlu48 (B2 β-sheet) in the α3β4 structural model and with αAsp39 (B1 β-sheets) in α4β2 and AChBP. The region adjacent to αLys122 is relatively hydrophobic, as shown by the electrostatic potential in Figure 18 C. The αLeu89-αPhe97 segment (B5 β-sheet), which is completely

charge profile for the binding of a hydrophobic molecule, such as eserine. In fact, it was an amphipathic segment in which non-polar residues faced the external surface of the pore and polar or charged side chains pointed toward the internal core of the subunit. Based on the fact that allosteric agents (such as eserine or galanthamine) are in general hydrophobic molecules, Arias (2000) suggested that their binding pocket was located between of the hydrophobic segments 118-124 and 130-137 of the *Torpedo* α1 subunit. However, our model reveals that this region is far away (more than 14 Å) from αLys122 (Figure 18 B), making Arias's hypothesis unsuitable for mammalian nAChRs.

1.3 BINDING OF LIGANDS TO α3β4 AND α4β2 RECEPTORS

Some molecules were docked on the AChBP crystal structure as well as on the α3β4 and α4β2 nicotinic receptor models. These ligands included agonists (ACh, nicotine and cytisine), competitive antagonist ($CGRP_{1-7}$) and allosteric agonist (eserine and $CGRP_{1-6}$). Also muscarine, which is a cholinergic drug that acts as selective agonist on muscarinic acetylcholine receptors, but does not affect nicotinic acetylcholine receptors, was docked in order to test the selectivity of our model. Comparison with experimental data was carried out whenever possible.

1.3.1 COMPUTATIONAL DETAILS

LIGAND STRUCTURE AND PARAMETRIZATION

Figure 21 shows the chemical structures of the ligands here investigated. Full agonists (ACh, nicotine, cytisine) as well as muscarine are small compounds (26, 27, 29, 32 atoms for ACh, nicotine, cytisine, muscarine), positively charged at physiological pH (Lide, 2001) and characterized by an ammonium group which is quaternary for ACh and muscarine, tertiary for cytisine, and binary for nicotine. ACh is aliphatic with an ester group at its tail; nicotine is more hydrophobic because of the piridine group substituting in position meta a pentameric ring; cytisine has the most rigid structure conferred by three condensed rings; muscarine is polar with a hydrofuranic group at its tail. Eserine is larger (41 atoms) and contains a hydrophobic moiety (three condensed rings) plus a polar tail.

The peptide fragments $CGRP_{1-6}$ and $CGRP_{1-7}$ were the largest ligands here studied. Their structural properties were investigated in the Results (Section 1).

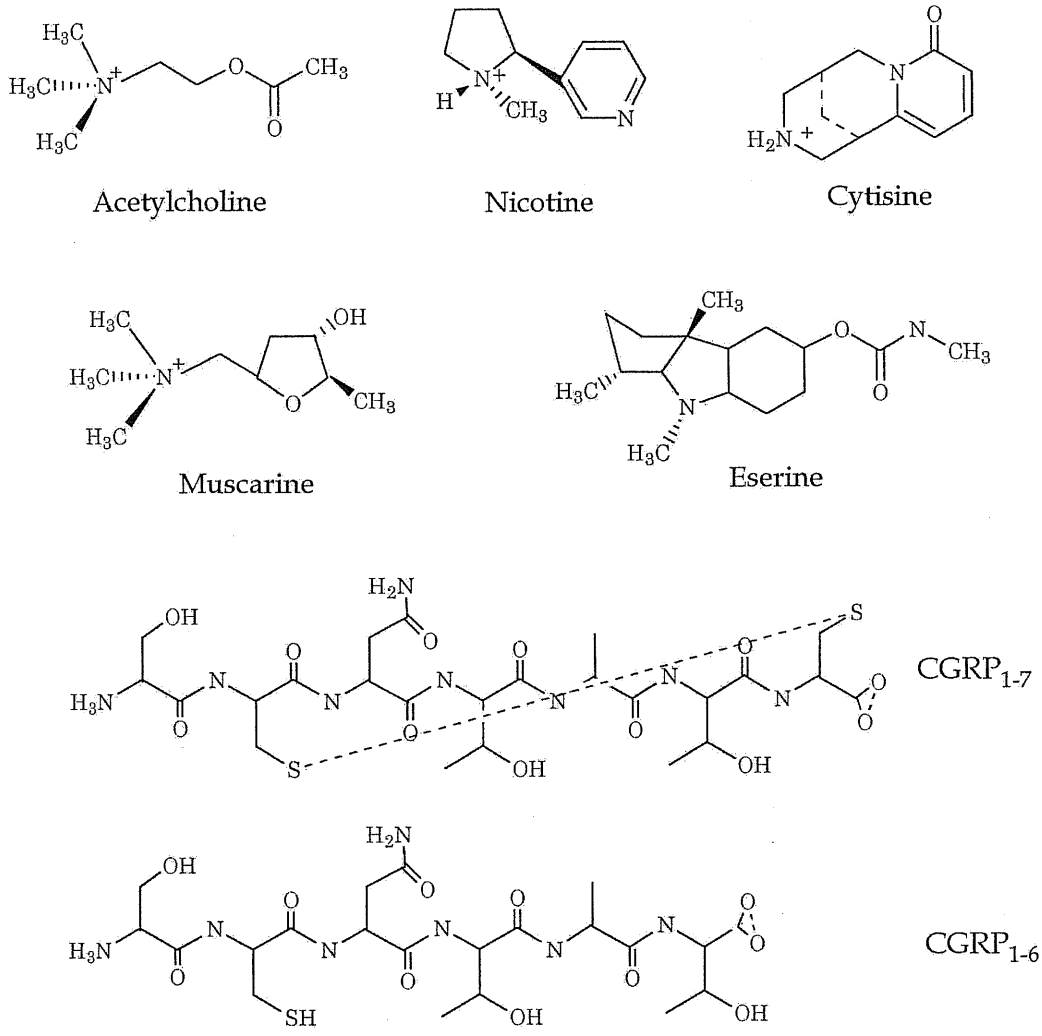

FIGURE 21. Chemical formula of the nAChR ligands investigated. They comprise full agonists (ACh, nicotine and cytisine), competitive antagonist ($CGRP_{1-7}$), allosteric agonist (eserine and $CGRP_{1-6}$) and muscarine, which is a cholinergic drug that acts as selective agonist on muscarinic acetylcholine receptors.

The initial 3D conformation of ACh, nicotine, cytisine, muscarine and eserine was selected from the X-ray structures found in the Cambridge Structural Database (CSD; http://www.ccdc.cam.ac.uk/). Since CSD shows consistently reliable structures for nicotine, cytisine or eserine, the ones with the smallest R-factors were selected. Their CSD entries were DOXSIS (Barlow et al., 1986) FITPIHO2 (Barlow and Johnson, 1989) and ESEIN10 (Pauling and Petcher, 1973), respectively. ACh and muscarine were

instead found in multiple configurations, which were all considered here. These had CSD entries: ACHOLC (Herdklotz and Sass, 1970), ACCHOBII (Svinning and Sourum, 1975) ACHTPB (Datta et al., 1980) and GEBMEF (Frydenvang et al., 1988) for ACh; HABNON (Frydenvang, 1990) and HABNUT (Frydenvang, 1990) for muscarine. The geometry of all ligands was optimized using ab initio methods as implemented in Gaussian98 package (Frisch and et al., 2001) on the basis of the density function theory (DFT; Hohenberg and Kohn, 1964). A total charge equal to +1 was assigned to ACh, nicotine, cytisine and muscarine.

The geometry of $CGRP_{1-7}$ and $CGRP_{1-6}$ was that obtained at the final MD snapshot.

Topology and force field parameters were assigned to all compounds from equivalent atom types present in the AMBER databases (Cornell et al., 1995). Atomic partial charges were calculated according to the standard AMBER procedure. First, the electrostatic potential (ESP) of each molecule was calculated using Gaussian98 package (Frisch and et al., 2001) and adopting the RHF Hamiltonian with 6-31G* basis set. Then, a set of charges which would fit the electrostatic potential (RESP) was determined (Bayly et al., 1993; Cornell et al., 1995). For nicotine, cytisine and eserine only the optimised structure was considered. For ACh and muscarine, final partial charges were average values obtained on the basis of all conformations considered here.

$CGRP_{1-7}$ and $CGRP_{1-6}$ partial charges and force field parameters have been described in Results (Section 1).

BINDING SITES STRUCTURE AND PARAMETRIZATION

Since binding sites were located at each (+)(–) or αβ subunit pair, for computational simplicity only a single pair of subunits was considered for docking. The agonist binding site was defined by the region which included the residues listed below (see Results Section) with a margin of ± 6 Å. The allosteric agonist binding site was defined by residues within a 12 Å sphere centered on αLys122 (+Lys120).

Since the receptor models were obtained in their free state, e.g. not in complex with a ligand, a MD protocol using the AMBER program (Case et al., 1997) was carried out to relax the binding site structure before docking. First, a 50 ps MD simulation of the receptor capped with a 15 Å water sphere around the binding site was performed.

Then, docking of cytisine or eserine inside their respective binding pockets (see below for docking details) was carried out followed by a 50 ps MD simulation of each ligand/receptor complex. Cytisine was chosen for this simulation in view of its large size. The MD calculations were run simulating low constant temperature (50 K) and constraining the position of the backbone atoms. The final MD structure of the receptors was used for docking studies.

The program used for docking was DOCK (Ewing and Kuntz, 1997) which includes several steps for binding site parameterization. First, the molecular surfaces (MS) of the protein binding cavities were built using Connolly's MS algorithm (Connolly, 1983) with a probe atom of 1.0 Å radius and a dot density of 4 points/Å. Then, the program SPHGEN (Ewing and Kuntz, 1997) was used to fill the cavities with spheres having variable radii (1.0-4.0 Å). Full electrostatic calculations were done to increase calculation accuracy. The AMBER force field (Cornell et al., 1995) provided receptor parameters (atomic van der Waals radii, well depths and partial charges).

DOCKING PROCEDURE

For each ligand and each receptor a three steps docking procedure, which included DOCK runs, cluster analysis and MD simulations, was implemented.

First, using the DOCK program (Ewing and Kuntz, 1997), four docking runs were performed starting from different initial conditions and treating the ligand as a flexible molecule. Each run supplied 50-150 possible configurations for each pair of ligand/receptor, with free energies of binding ranging from -6 to -65 kcal/mol. The configurations of each ligand were subsequently clustered in several classes, depending on their conformational similarity. Each class grouped ligand structures differing by less than 2 Å rmsd value from its neighboring conformation. Sampling was done by a 0 K temperature Monte Carlo simulation. Each class was scored on the basis of the number of its constituents and their binding free energies. The structure with the best score was selected for each ligand/receptor pair (see Table II for free energy values). Finally, the structure of selected ligand-protein complexes was optimized through a short (30 ps) MD simulation. The latter was performed at room temperature using the AMBER program (Case et al., 1997; see below for computational details). Since water

could not be included in DOCK runs, to estimate the possible contribution of water molecules to stabilizing the binding configuration, a sphere of 100 water molecules around the ligand was added to the ligand/receptor complex. During the simulation, the receptor residues were constrained with a force constant K=0.01 kcal/mol/Å^2 when the distance from the ligand was less than 10 Å, with K=1.0 kcal/mol/Å^2 between 10 Å and 20 Å and with K=10.0 kcal/mol/Å^2 at distances larger than 20 Å.

TABLE II. BEST SCORES FOR DOCKING.†

Ligand	α3β4			α4β2			AChPB		
	E_{TOT}	E_{ELE}	E_{VAN}	E_{TOT}	E_{ELE}	E_{VAN}	E_{TOT}	E_{ELE}	E_{VAN}
Acetylcholine	-26	-8	--19	-26	-9	-20	-28	-9	-20
Nicotine	-26	-5	-25	-20	-5	-20	-23	-5	-22
Cytisine	-33	-6	-27	-34	-9	-24	-31	-5	-26
Muscarine	-8	-12	-5	-14	-9	-13	-17	-5	-20
$CGRP_{1-7}$	-66	-24	-23	-65	-28	-26	-62	-24	-22
Eserine	--25	-17	-5	-25	-18	-4	-26	-17	-6

†The free energy scores of selected configurations are reported in kcal/mol. For each ligand and each binding site, the total free energy, as well as single electrostatic and van der Waals contributions are reported.

1.3.2 LIGAND/RECEPTOR COMPLEXES

The docking results obtained for each ligand within each receptor were investigated analyzing mainly two aspects: number and goodness of the obtained classes and the structural properties of the ligand/receptor complex. Comparison between binding modes of different ligands were done on the basis of their free energies of binding and their electrostatics properties.

ACETYLCHOLINE

Two main conformers were determined from cluster characterisation, sharing a common position of the ACh ammonium group, but differing for orientation of the tail within the binding pocket.

Our results showed that ACh binds to the three receptors in a similar fashion. In α3β4 and α4β2, the quaternary ammonium group formed cation-π interaction with the aromatic ring of αTrp146 (Figure 22 left and Table III), consistently with ab initio quantum mechanics calculations and molecular neurobiology experiments (Zhong et al., 1998a). The ACh ammonium group was also stabilized by long range electrostatic

interactions with the αTyr90 side chain, as previously predicted by photoaffinity labelling experiments (Cohen et al., 1991; Sine et al., 1994), and by water molecules present in the binding pocket. Other three aromatic residues, namely αTyr187, αTyr194 and βTrp55, capped the α3β4 and α4β2 binding pocket over the ACh positively charge moiety at 5-6 Å distance. The pharmacological effect of mutation of these residues is directly associated with reduced ACh binding affinity (Sine et al., 1994; Corringer et al., 1999). In the AChBP, ACh ammonium group formed cation-π interactions with +Tyr185, +Tyr192 and –Trp53 aromatic side chains and electrostatic interactions with +Tyr89, with no interaction with water. For the three binding structure examined the ACh ester moiety established hydrophobic interactions with the αCys189-αCys190 loop (in accordance with mutagenesis experiments; Karlin, 1969), and with aromatic rings (α_3Tyr194, β_2Phe114 and +Trp143).

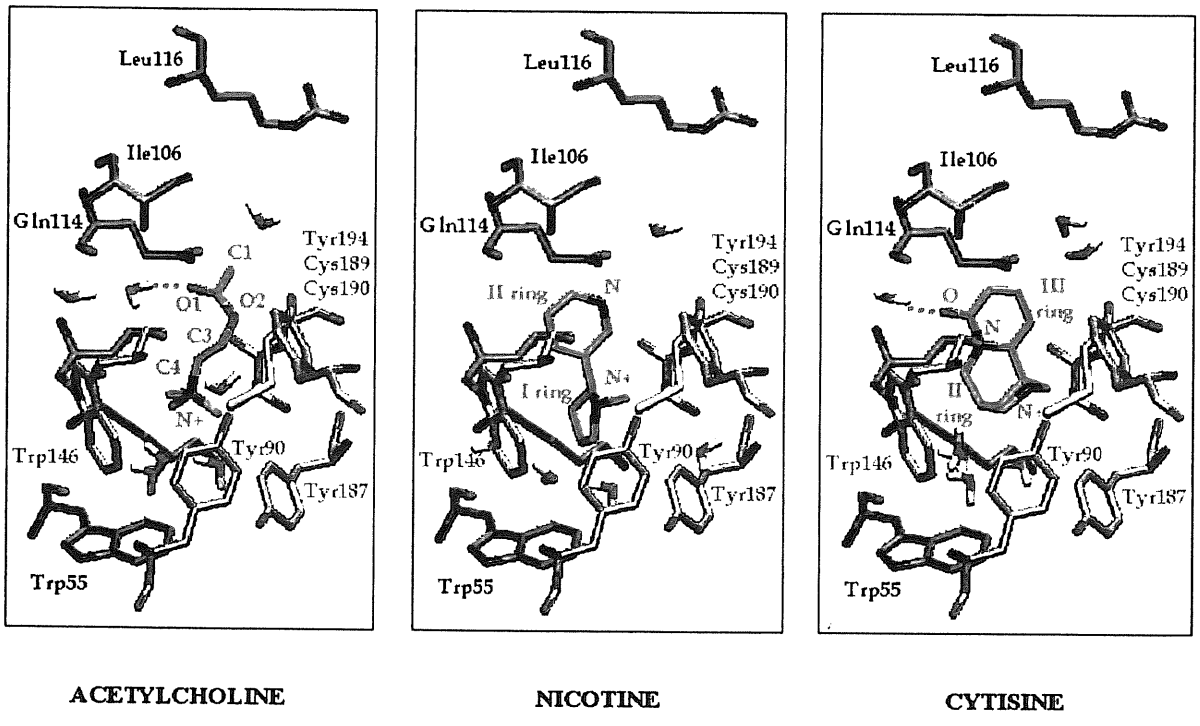

FIGURE 22. Full agonist binding to the α3β4 receptor. The binding conformation of the structure complexing ACh (left), nicotine (middle) or cytisine (right) is represented along the barrel axis of the pentameric receptor. Note that all side chains are in the same position.

TABLE III. SELECTED LIGAND RECEPTOR DISTANCES.†

Ligand	α3β4		α4β2		AChPB	
Atom name	atom name	d(Å)	atom name	d(Å)	atom name	d(Å)
			Acetylcholine			
N^+	αTrp146(ring)	4.8	αTrp146(ring)	4.5	+Tyr185(ring)	4.8
	αTyr90(OH)	4.3	αTyr90(OH)	4.7	+Tyr192(ring)	4.6
	αTrp146(O)	4.3	αTrp146(O)	4.2	–Trp53(ring)	4.6
	$3H_2O$(O)	<5.0	H_2O(O)	3.9	+Tyr89(OH)	4.3
C_4	αCys189(S)	3.5	-	-	-	-
C_3	αTrp146(ring)	3.7	Cys189(S)	3.7	+Trp143(ring)	3.5
C_1	βLeu116(C_δ)	4.4	βPhe114(ring)	4.0	-	-
O	H_2O(O)	2.8	H_2O(O)	3.1	-	-
			Nicotine			
N^+	αTrp194(ring)	4.8	αTrp146(ring)	4.8	–Trp53(ring)	4.8
	αTyr90(OH)	4.4	αTyr90(OH)	4.3	-	-
	H_2O(O)	4.8	αTrp146(O)	4.2	-	-
	-	-	$3H_2O$(O)	<5.0	-	-
Ring	αTrp146(ring)	3.6	αTyr187(ring ⊥)	3.4	+Tyr89(ring ⊥)	4.7
	αCys189(S)	3.5	-	-	+Trp143(ring)	4.7
	-	-	-	-	+Tyr185(ring ⊥)	4.3
	-	-	-	-	+Tyr192(ring)	4.2
N	βLeu116(O)	2.8	-	-	+Tyr192(OH)	3.2
	αTyr194(OH)	3.2	-	-	-	-
Ring	αTrp146(O)	2.8	βPhe114(ring)	3.4	+Cyx188(S)	3.4
	βLeu116(C_δ)	4.0	αCys189(S)	3.9	–Met114(S)	3.9
			Cytisine			
N^+	αTyr194(ring)	3.8	αTyr194(ring)	3.4	+Tyr89(OH)	3.1
	αTyr90(OH)	4.3	αTyr90(OH)	3.1	+Ser142(O)	3.6
	αSer145(O)	4.2	αTrp146(O)	3.1	H_2O(O)	4.4
	αTrp146(O)	3.1	H_2O(O)	4.7	-	-
Ring(I)	-	-	αTyr187(ring ⊥)	4.0	+Tyr89(ring ⊥)	3.7
	-	-	-	-	+Tyr185(ring)	4.2
	-	-	-	-	+Tyr192(ring ⊥)	4.2
Ring(I)	αTrp146(ring ⊥)	3.7	αTrp146(ring ⊥)	3.8	–Trp53(ring ⊥)	3.8
	αCys190(S)	4.0	βLeu116(C_δ)	3.4	+Trp143(O)	2.9
Ring(III)	βLeu116(C_δ)	3.6	βPhe114(ring)	4.0	+Cyx189(S)	4.0
	βIle106(C_δ)	3.3	αCys190(S)	3.5	–Met114(S)	3.9
O	H_2O(O)	3.2	H_2O(O)	2.7	+Trp143(ring)	2.9

†The final MD ligand-residue distances within 5 Å for each ligand interacting with α3β4, α4β2 and AChBP binding pocket by polar, H-bond, cation-π and van der Waals interactions are reported.

αTyr194 has been predicted to play a role in binding of the ACh ester group (Grutter et al., 2000). The carbonyl oxygen of the ACh ester moiety formed an H-bond with one water molecule in the case of α3β4 and α4β2 receptors (Figure 22 left and Table III).

In conclusion, our results show considerable homologies in the ACh binding to the nAChR and AChBP sites. The main difference was in the number of cation-π interactions stabilizing the ammonium group, which was higher for the AChBP. No room was available for water molecules within the AChBP binding pocket, whereas for nAChRs the ACh bond was stabilized by water molecules.

NICOTINE

For α3β4, α4β2 and AChBP binding sites, our clustering analysis found several conformers with similar binding modes for the ammonium group, though with differing orientation of the two nicotine rings.

On α3β4 and α4β2, the nicotine ammonium formed a cation-π interaction with α_3Trp195 and α_4Trp146, and long range electrostatic interaction with αTyr90 side chain (Figure 22, middle and Table III) in accordance with the experimentally characterized residues essential for nicotine binding (Kearney et al., 1996; Galzi et al., 1991b). In the present study nicotine was observed to interact with 1-3 water molecules. van der Waals interactions stabilized the first and second ring in both nicotinic receptors. On α3β4 receptors the nitrogen atom of the second ring formed a hydrogen bond with βLeu116(O) and αTyr194(OH) residues. Likewise, nicotine binding to AChBP was stabilized by van der Waals interactions mostly involving aromatic side chains. A cation-π interaction with –Trp53 was also observed (Table III). The importance of this residue has been predicted by mutagenesis experiments reporting the reduction in agonist binding and agonist-induced channel activation (Chiara et al., 1998).

CYTISINE

As cytisine structure is more rigid with respect to ACh and nicotine (Figure 21), a smaller number of binding conformers was expected. Consistently, from clustering only two main conformers were obtained. The cytisine binding type was also similar for the three binding sites.

Cytisine ammonium group bound the same region as ACh and nicotine (Table III and Figure 22, right and), forming a cation-π interaction with the ring of βTyr194. An H-bond between cytisine oxygen and one water molecule was present on α3β4 and α4β2

receptors, but not on AChBP. Several main chain and side chain oxygen atoms stabilized the ammonium group through long range electrostatic interactions (Table III) and several hydrophobic residues made van der Waals contacts with the three cytisine rings. In absence of mutagenesis or photoaffinity labelling data, our findings provide the first clues to cytisine binding to nicotinic receptors.

MUSCARINE

The calculated binding free energies for AChBP and α4β2 were small (Table II). In α3β4 site, the ligand did not bind at all. For AChBP and α4β2, the clustering generated a large number of classes which markedly differed for binding of both ammonium group and pentameric ring. In conclusion, our results suggested low affinity of muscarine to nicotinic receptors, in agreement with lack of agonist activity on nicotinic receptors.

$CGRP_{1-7}$

$CGRP_{1-7}$ MD structure turned out to be too large to fit into the receptors binding sites. Indeed, its volume (660 ± 10 $Å^3$) was much larger than that of the agonists (115 ± 1 $Å^3$, 168 ± 1 $Å^3$ and 180 ± 1 $Å^3$ for ACh, nicotine and cytisine, respectively). Consistently, docking runs provided structural models in which the peptide structure was located outside the binding pocket.

Clustering provided several possible configurations for the antagonist-protein complexes in which the $CGRP_{1-7}$ externally bound to the agonist pocket at either the top (only in the case of AChBP) or the bottom of the site (Figure 19). For α3β4 and AChBP we obtained a spread distribution of classes, while for α4β2 four main binding conformers were generated.

The selected configurations for α3β4 and AChBP bound to the long loop between β-sheets B8 and B9 at the interface region of the β subunit (Figure 19). $CGRP_{1-7}$ bound to α4β2 receptor between loop C on the α subunit and the external side of loop B8-B9 on the β subunit (Figure 23 left). In particular, the N-terminal made a salt bridge with βAsp168 (d(Ser1(N^+),βAsp168(O_δ))=2.8 Å and C-terminal bound to the side chain of αArg185 (d(Cys7(O^-),αArg185 (N_δ))=2.8 Å).

Our calculations therefore support the idea that $CGRP_{1-7}$ blocks the nicotinic receptor function by external binding of the peptide, preventing the access of agonists to the binding site. Under the assumption that agonist access to the binding site occurs by the opening of loop C (Grutter and Changeux, 2001), $CGRP_{1-7}$ binding at to α4β2 prevents loop C motion. However, a final resolution of the mechanism of action of $CGRP_{1-7}$ could not be given at this stage when neither the state of the AChBP crystal structure, nor the access mechanism of agonist are definitively clear. Experimental investigations into the $CGRP_{1-7}$ binding at molecular level could improve the accuracy of a computational study.

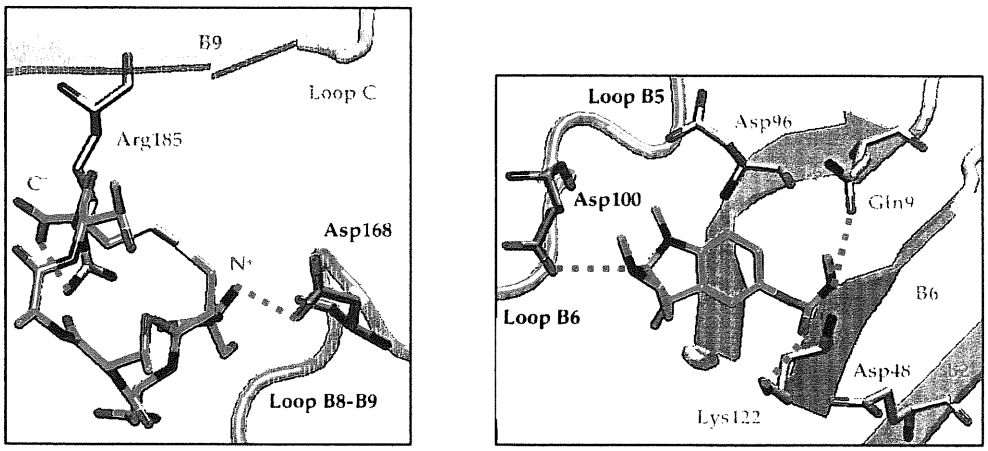

CGRP1-7 ESERIN

FIGURE 23. $CGRP_{1-7}$ and eserine binding to α4β2 and α3β4, respectively. $CGRP_{1-7}$ (left) binds between loop C on the α subunit and the external side of loop B8-B9 on the β subunit. Eserine (right) rings interacted hydrophobically with the main chain of β-sheet B5, whereas the rest was stabilised by van der Waals interactions with αIle120, αPhe121 (B6) and βIle113 (B6), and electrostatic interactions with αGlu48 (B2), αAsp96 (B5), αLys122 (B6) and βGlu98 (B5).

ESERINE

From cluster analysis a large number of conformers were found for α4β2 and AChBP, whereas for α3β4 receptor the 50% of eserine configurations fell in the same class. The selected eserine/protein complexes were very similar, although the binding site of allosteric agonists was a quite large region.

The free energy values characterising the eserine binding were lower than standard agonists ones (Table II). Its binding site was exposed to solvent and consequently only one site of the molecule interacted with the protein (Figure 20). The binding region was

located between β-sheet B5 and B6 of α and β subunits. Specifically, two rings of the ligand faced the main chain of β-sheet B5, between αAsp94 and αGlu98. The ligand formed van der Waals interactions with αIle120, αPhe121 (B6) and βIle113 (Loop B6), and electrostatic interactions with αGlu48 (B2), αAsp96 (B5), αLys122 (B6) and βGlu100 (Loop B5).

BINDING OF $CGRP_{1-6}$

Experimental studies on neuronal nicotinic receptors have shown a potentiation of nicotine-evoked responses by $CGRP_{1-6}$ (Di Angelantonio et al., 2002). The action of this N-terminal fragment was compared with the pharmacological profile of a typical allosteric agonist, the eserine. The data showed that $CGRP_{1-6}$ and eserine had distinct actions on nAChRs. Since $CGRP_{1-6}$ and $CGRP_{1-7}$ were observed to have a competitive action on nicotinic receptors, they could also share the binding region. Starting from this hypothesis $CGRP_{1-6}$ docking was performed on the region around the agonist binding site. Binding affinity scores were similar to the $CGRP_{1-7}$, however from clustering the obtained distribution of binding conformers were too large to give any definitive response. Experimental investigations on the $CGRP_{1-6}$ binding at molecular level could give a basis for further computational study.

2. DISCUSSION

The structural basis of the different modulatory effects of CGRP N-terminal ligands on nAChRs was subsequently investigated by constructing three-dimensional models of receptor/ligand complexes. Indeed, the similarity between the ligand binding domain of nAChRs and the X-ray structure of the acetylcholine-binding protein from snail *Lymnaea stagnalis* (Smit et al., 2001), has allowed construction of the N-terminal domain of two subtypes of nAChRs, namely α3β4 and α4β2. These two receptors are representative samples of the neuronal nicotinic receptors located in rat cromaffin cells (Campos-Caro et al., 1997; S. Di Angelantonio and A. Nistri, unpublished; Di Angelantonio, 2002). Agonists, antagonists, and allosteric agonists have been subsequently docked on these models. The study presented hereafter focuses first, on

the structural model of the receptors and then, on the structure of the ligand/receptor complexes.

2.1 OVERALL STRUCTURE OF RECEPTORS

As expected from the low number of insertions/deletions in the sequence alignment (see Figure 17), the overall structure of the α3β4 and α4β2 models did not differ largely from that of the template: a pentameric barrel with a central irregular pore (Figure 18 A). Most conserved residues (20-22% with the α and β subunits, respectively) were hydrophobic and located in the pore region of the pentameric structure. The residues at the interface were not well conserved between nAChRs and AChBP or within the nicotinic receptor family. Several other regions in α3β4 and α4β2, among which the Cys-loop (Figure 18 B), exhibited no sequence homology with AChBP and the expected accuracy of the models in those regions was therefore lower than for the rest of the structure. Finally, the electrostatic potential over the receptor surface (Figure 18 C) outlined an amphipatic profile, as it was negatively charged on the external side and mostly hydrophobic in the core region.

2.1.1 AGONIST/ANTAGONIST BINDING SITES

The agonist/antagonist binding site in the α3β4 and α4β2 (Le Novere et al., 2002) models (like those in the AChBP) were located at the external interface between α and β subunits and were mostly formed by aromatic residues (Figure 19). The residues of the α (or principal) component were highly conserved within the nAChRs family, whereas βTrp55 was the only common residue within the nAChR complementary β component. These models were fully consistent with photoaffinity labelling and mutagenesis experiments (see Karlin, 2002 for a review). Indeed, those experiments show that most residues affecting the agonist or antagonist binding properties as well as the receptor gating mechanism, were located at the binding site of our models (see Results, Section 2.2.2). Furthermore, our models proposed a plausible structural role for αTyr83 residue important for the biological function, but not located in the binding site. The models provide a functional role for αAsp149 (loop B) and αAsp197 (loop C), located at 7-8 Å

from the binding site and presumably useful for electrostatic stabilization of the agonist, in accordance with experimental evidence (Sugiyama et al., 1996; Osaka et al., 1998). In fact, they were the source of the negative electrostatic potential observed at the agonist binding site (Figure 18 C), as suggested by experimental findings (Stauffer and Karlin, 1994).

In summary, the binding site appears to be made up by a conserved core of aromatic residues with variable nearby amino acids plus several amino acids from the non conserved loop E and F, located on the β-subunits. The latter might confer individual pharmacological properties to each receptor subtype (Corringer et al., 2000).

2.1.2 ALLOSTERIC AGONIST BINDING SITES

The allosteric agonist binding sites have not been firmly identified. α_1Lys125 in the *Torpedo* receptor is the only residue known to bind allosteric agonists such as eserine (Schrattenholz et al., 1993). In our model, this residue was located in the pore region of the pentameric domain, on the B5 β-sheet, not far away from the subunit interface. Thus, a plausible allosteric agonist binding site could be the region between β-sheets B2, B5 and B6 of the α subunit and β-sheets B5 and B6 of the β-component (Figure 20). This finding contrasts with the predictions of Arias (2000), who postulated that the binding pocket was located in a gorge within the Cys-loop. Indeed, the region within the Cys-loop was far away (more than 14 Å) from αLys122.

2.2 BINDING OF LIGANDS TO α3β4 AND α4β2 RECEPTORS

A selected set of ligands (Figure 21), including $CGRP_{1-6}$ and $CGRP_{1-7}$, were docked on the α3β4 and α4β2 nicotinic receptor models as well as on the AChBP X-ray structure. Comparisons between binding modes of different ligands were made in terms of their binding free energies of the ligand/receptor contacts and of their electrostatics properties.

2.2.1 BINDING OF THE AGONISTS ACH, NICOTINE, CYTISINE

Our calculations showed that the ammonium group in each ligand bound within the same region of the binding pocket, as predicted previously by several experimental studies (Karlin, 2002). This group may be stabilised by the negatively charged electrostatic potential generated mostly by αAsp86 (loop A), αAsp196 (loop C) and αAsp149 (loop B). Interestingly, the role of αAsp86, which is highly conserved within the ligand gated ion channel family, had not been previously detected by experimental studies.

ACh bound the three receptor binding sites in a similar fashion. This result was consistent with experimental data, which predicted the same selective orientation within its binding site (Corringer et al., 2000; Karlin, 2002). The ammonium group formed cation-π and long range electrostatic interactions with αTrp146 and αTyr90, respectively (Figure 22 and Table III), in agreement with photoaffinity labelling experiments (Cohen et al., 1991; Sine et al., 1994). Furthermore, αTyr194 and βTrp55, which seem to have an important role in the gating mechanism (Akk and Auerbach, 1999; Xie and Cohen, 2001), limited the nicotinic receptor binding pocket without direct interaction with ACh. The ACh ester moiety interacted with the Cys loop and with aromatic rings as αTyr194 in accordance with experimental data (Karlin, 1969; Grutter et al., 2000). Finally, both ammonium group and ester tail interacted with water molecules. ACh bound the AChBP with relatively similar characteristics, the major difference consisting in its higher number of cation-π interactions. In fact, in the AChBP, the ammonium group was strictly bound within the hydrophobic pocket preventing access to water molecules.

The other full agonists investigated here (nicotine and cytisine) exhibited conformations quite similar to those of ACh (Figure 22 and Table III). Specifically, their ammonium group bound the same ACh region and was stabilized by at least a cation-π interaction (with either αTrp194 or αTrp146). Also several water molecules were essential to stabilize the ligand/receptor complexes. While the role of some aromatic residues facing the binding site is experimentally characterized for nicotine binding (Kearney et al., 1996; Galzi et al., 1991b), our findings with cytisine are the only available data for this commonly used agonist, owing to lack of mutagenesis or photoaffinity labelling results.

The structural properties of ACh or nicotine complexed with the α4β2 receptor are similar to those obtained in recent molecular modelling studies (Schapira et al., 2002; Le Novere et al., 2002). However, it is interesting to point out some significant differences. Le Novere et al. (2002) did not consider water molecules in their agonists binding studies, in contrast with our investigation in which their role was found to be important. Those authors also predicted higher affinity of nicotine for the receptor containing β2 instead of β4 subunit, since γTyr117 (known to be important in nicotine binding to the *Torpedo* receptor) is transformed into phenylalanine and glutamine in β2 and β4 subunits, respectively. This difference was not observed in our receptor models (α4β2 and α3β4) bound by nicotine. Indeed, in our complexes the van der Waals interactions which in the β2 subunit involved β_2Phe114 were replaced by β_4Leu116.

Although Shapira et al (2002) considered the role of water molecules, their study presumed that only one water molecule was accommodated around each ligand. Specifically, they considered a water molecule H-bound to the ACh ester oxygen and the nicotine pyridine nitrogen, as it was obtained by our docking studies. However, they did not detect the important role of several other water molecules in stabilizing the agonist ammonium groups. Beside, the ACh ester moiety in the model by Shapira et al (2002) was not engaged in the interaction with the Cys-loop, as obtained in our complexes and previously suggested by photoaffinity labelling (Grutter et al., 2000).

The estimated binding free energies of the three agonists were very similar (Table II), varying from -34 kcal/mol for cytisine binding to α4β2 to –20 kcal/mol for nicotine binding to α4β2. Although, their values must be considered qualitatively because of the simplified computational approach used here, the obtained ranking order of binding efficiencies (namely cytisine, ACh and nicotine) was consistent with experimental findings (Di Angelantonio et al., 2000; Free et al., 2002). The reliability of these calculated affinities with the present computational setup was further tested by performing docking runs with muscarine. This compound is a cholinergic drug that acts as selective agonist on muscarinic ACh receptors and does not activate nicotinic receptors. The binding free energies obtained turned out to be small (Table II) and the number of conformations

adopted was very large. These two independent features fully validated the selectivity of our binding site model and substantiated the computational approach used here.

2.2.2 BINDING OF AN ALLOSTERIC AGONIST.

Eserine is an allosteric agonist whose effect on nAChRs of cromaffin cells was well characterised (Di Angelantonio et al., 2002). Eserine turned out to bind to the gorge between β-sheet B5 and B6 of the α subunit, at the interface with β (Figure 23). Remarkable is that the segment B5 contains αTyr90 residue, which is one of the side chains participating in the agonist binding site (loop A). At speculative level, we might suggest that β-sheet B5 could have the allosteric role to connect allosteric agonist binding site with the agonist one.

2.2.3 BINDING OF THE $CGRP_{1-7}$ AND $CGRP_{1-6}$ PEPTIDES.

$CGRP_{1-7}$ is an antagonist of nicotinic receptors. Its MD structures turned out to be too large to fit into the receptor binding sites. Consistently, docking runs provided structural models in which the peptide bound to the external surface of the receptor, near the binding pocket. Specifically in the α4β2 receptor, the peptide was bound in such a way to prevent loop C motion (Figure 23). If the agonists access to binding site occurs by the opening of loop C (Grutter and Changeux, 2001; Karlin, 2002), the antagonist role of $CGRP_{1-7}$ could be interpreted as preventing the agonist binding. However, experimental investigations on the $CGRP_{1-7}$ binding at molecular level might help to improve the accuracy of a computational study.

$CGRP_{1-6}$ is distinct from a typical allosteric agonist (eserine) and compete with the antagonist $CGRP_{1-7}$ (Di Angelantonio et al., 2002). Experimental data therefore suggest a common binding site for the two CGRP fragments. Although the binding affinity scores were very similar to the one of $CGRP_{1-7}$, a main $CGRP_{1-6}$/receptor complex configuration could not be selected. Further experimental information on the $CGRP_{1-6}$ binding is required to restrain the docking on a smaller binding region and to provide a reliable model for the peptide/receptor complex.

CALCIUM BINDING TO CA^{2+}-ATPASE

1. RESULTS

Molecular modelling was used to investigate structure/function relation in protein complexes involved in the calcium binding process (Introduction, Figure 7). Two Ca^{2+} ions bind to the protein. The first Ca^{2+} ion binds to one of the two binding sites (site I of H_2E_2), inducing a conformational change in the protein (HCaE′ state), which has large affinity for calcium ion in the second binding site, site II. Binding of the second calcium ion causes the formation of the Ca_2E_1 state.

Our investigation was subdivided in three steps. First, we studied structural and dynamical features of the protein in its Ca_2E_1 state. Subsequently, we constructed the structural models of the H_2E_2 and HCaE′ complexes, which are the other key intermediates of the Ca^{2+} binding process. Finally, we addressed the issue on how Ca^{2+} can reach the binding sites and we investigated the possible Ca^{2+} binding sites on the outer mouth of the cytoplasmic channel.

1.1 CA_2E_1 MODEL: CALCIUM BINDING SITES

First, we constructed a model of the Ca_2E_1 state based on the X-ray structure resolved by Toyoshima et al. (2000) (Introduction, Figure 9) and we investigated its structural and dynamic aspects performing MD simulations of the protein in a water/membrane environment. In particular, the attention was focussed on calcium binding site properties and on the main differences with the X-ray structure.

1.1.1 COMPUTATIONAL DETAILS

STRUCTURAL MODEL

The Ca_2E_1 model was based on the at 2.6 Å resolution crystal structure of the calcium ATPase of skeletal muscle sarcoplasmic reticulum [Toyoshima et al., 2000; Protein Data

Bank, (Berman et al., 2002) accession number 1EUL]. It features a transmembrane region, composed by ten α-helices, and a cytoplasmic headpiece consisting of three well-separated domains (labeled as P, N and A in Figure 9 in Introduction). The Ca_2E_1 model included only the phosphorylation and transmembrane regions (Figure 24). Inclusion of the nucleotide-binding and actuator domains, would have substantially increased the computational effort without affecting significantly the dynamic and electrostatic properties of the TM domain. Indeed, the N and A domains are attached to P and TM only by few loops (Toyoshima et al., 2000; East, 2000). Furthermore, the electric field turns out not to vary significantly upon inclusion of these two domains, as suggested by electrostatics calculations based on the Poisson-Boltzmann equation (data not shown).

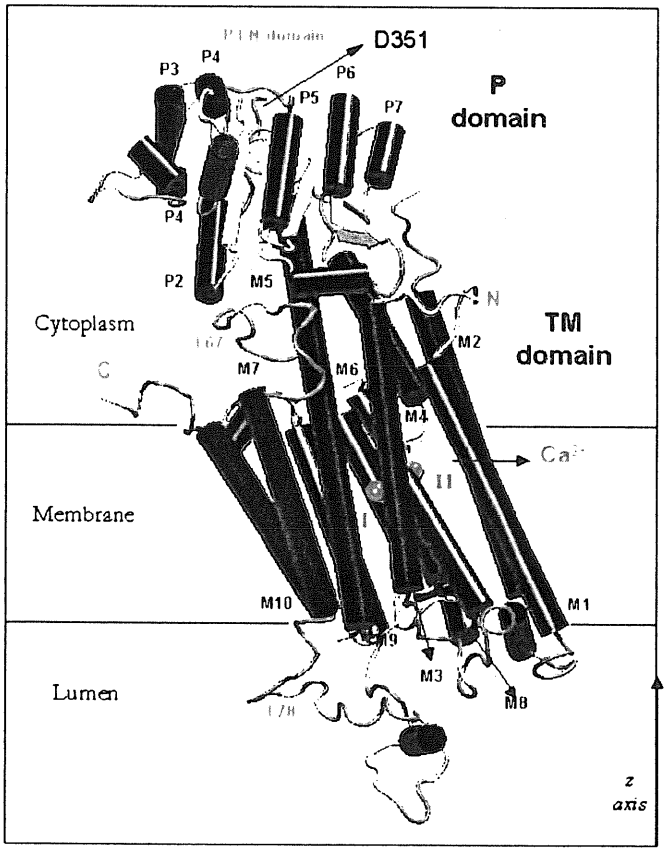

FIGURE 24. Structure of the Ca_2E_1 model. This model, which comprises the P and TM domains, is immersed in a cytoplasmic/membrane environment, mimicked by a water/n-octane bilayer. The thickness of the organic liquid is 30 Å (Moore et al., 1998). The structure after 2.0 ns of MD is shown. The axis z is orthogonal to the plane defined by the water/n-octane interface. The complex is schematically represented. ϑ-helices and selected loops are labelled.

His residues were protonated according to their plausible H-bond pattern in the protein: His278, His284, His868, His880 and His882 were assumed to be protonated on the N_ε nitrogen, His872 and His944 on the N_δ nitrogen and His683 was assumed to be diprotonated. Thirty-five water molecules were added to the transmembrane solvent accessible space (Hua et al., 2000) taking care to avoid non-physical contacts with the protein frame.

Ca_2E_1 contained two Ca^{2+} in the binding sites as in the crystal structure (Figure 24). The highly negative charge of the model (-23) was counterbalanced by adding K^+ counterions, located at least 8 Å far from any negatively charged group of the protein. The model was immersed in a cytoplasmic/membrane environment, mimicked by a water/*n*-octane bilayer enclosed in a 85x62x107 $Å^3$ box. This computational set-up has been successfully used as membrane model for a variety of channels, namely synthetic ion channels (Zhong et al., 1998b), HIV-1 Vpu protein (Moore et al., 1998) and the KcsA potassium channel (Guidoni et al., 1999). The thickness of the octane slab was set at 30 Å (Nagle and Tristram-Nagle, 2000). The protein was oriented inside the membrane as suggested by Toyoshima et al. (Toyoshima et al., 2000) so that in the lumen side all loops (except L78) were inside the transmembrane region, and in the cytoplasmic side Asp59 of ϑ-helix M1 and Ala988 of C-terminus were exposed to solvent (Figure 24). The system was composed by ≈ 56,000 atoms.

Molecular Dynamics calculations

The simulation was carried out with the SANDER module of AMBER5 package (Case et al., 1997) running on a four-processor SGI Origin 200 parallel computer.

For the protein, the metal ions, *n*-octane and water, the AMBER force field (Cornell et al., 1995), the Aqvist parameters (Aqvist, 1990), the OPTS (Kaminski et al., 1994; Chen et al., 1998) and the TIP3P (Jorgensen et al., 1983) force fields were used, respectively.

Periodic boundary conditions were applied. Long-range electrostatic interactions were calculated using the Ewald particle mesh method (Essman et al., 1995), assuming the dielectric constant equal to 1. All bonds were constrained by SHAKE algorithm (Ryckaert et al., 1977) during the dynamics. The time integration step was set equal to 1.5 fs. Constant temperature and pressure simulations were achieved by coupling the

systems with a Berendsen bath (Berendsen et al., 1984) with 2 ps relaxation time. The MD protocols were the following: (i) 0.2 ns of MD of the solvent at 600 K constant temperature. No phase mixing was observed. (ii) Energy minimisation of the entire system. (iii) MD of the entire system in which temperature was increased from 0 to 300 K steps of 15 ps. (iv) 2 ns of MD simulations of the entire system at constant temperature (300 K) and pressure (1 Atm). Only the last 1.5 ns of dynamics were collected for analysis.

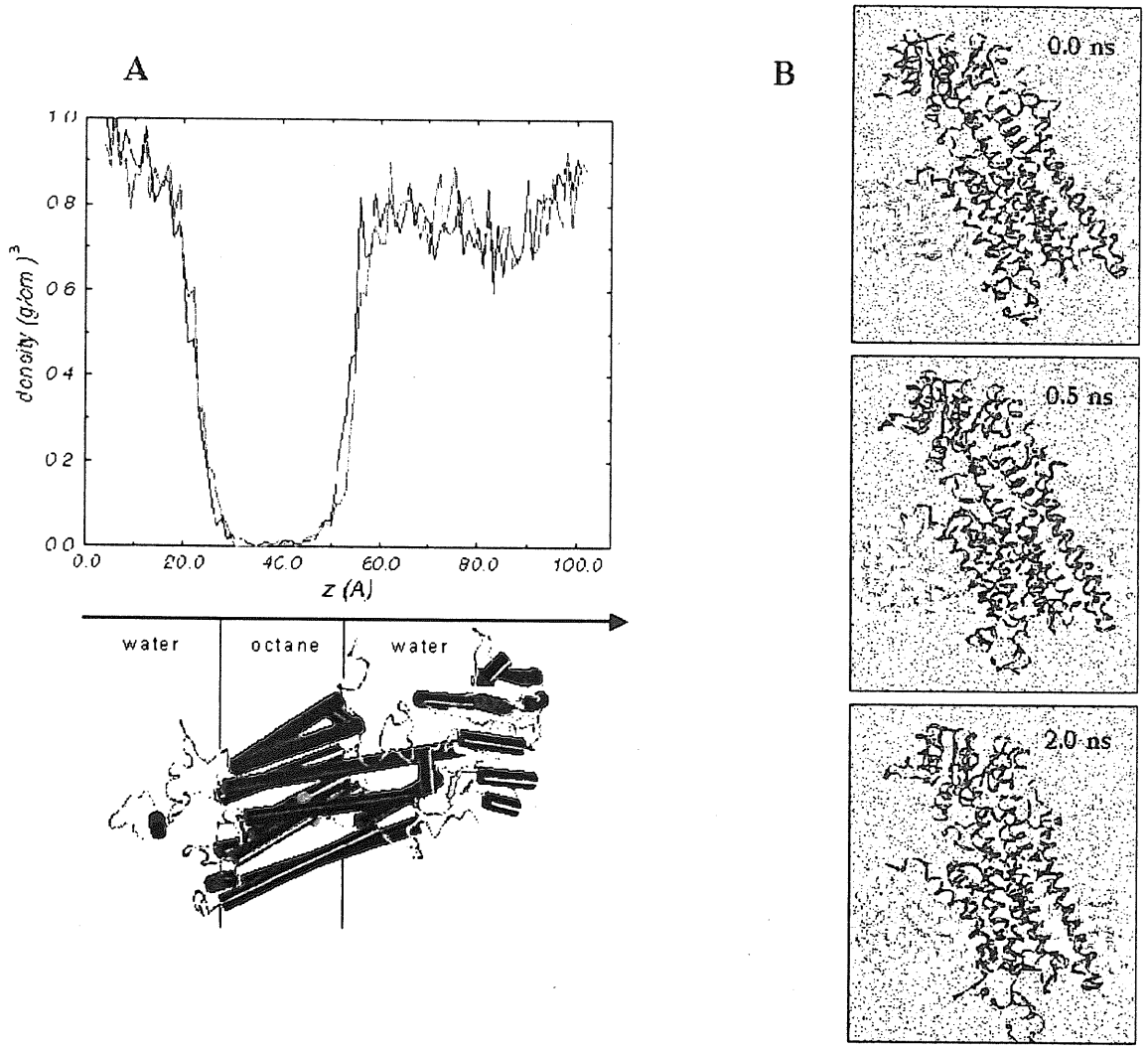

FIGURE 25. Water/n-octane bilayer. A: Water density of model Ca_2E_1 plotted as a function of the axis z, which is orthogonal to the water/octane interface. The density is plotted for t=0.0 ns (blue) and t=2.0 ns (red). A simulation box containing the Ca_2E_1 model is also shown below the plot as scheme of comparison of the water/octane distribution within our system B: MD snapshots of the Ca_2E_1 model immersed in the water/n-octane bilayer, at 0.0 ns, 0.5 ns and 2.0 ns.

The octane slab thickness did not change during simulation, as shown by a comparison of the water density profile in initial and final MD snapshots (Figure 25). During the dynamics, 5 water molecules left TM domain and diffused towards lumen bulk water.

1.1.2 Dynamical properties of the structural model

The thickness of the n-octane slab did not change significantly during the simulation, as shown by a comparison of the water density profile in initial and final MD snapshots (Figure 25 A). However, the initial orientation of the protein complex with respect to the water-membrane mimic environment, suggested by Toyoshima et al. (2000) changed in the first 0.5 ns (Figure 25 B). As a result, in TM domain Ca^{2+} located in site II turned out to be closer to the bulk water in the lumen side than in the X-ray structure; furthermore, all loops located on the lumen side (L12, L34, L78 and L910) moved from the membrane mimic region to the bulk water.

During the rest of the dynamics (1.5 ns) the protein did not change orientation (Figure 25B). The complex experienced small fluctuations with respect to its initial configuration (Table IV) and its motion was mostly due to the TM loops fluctuations.

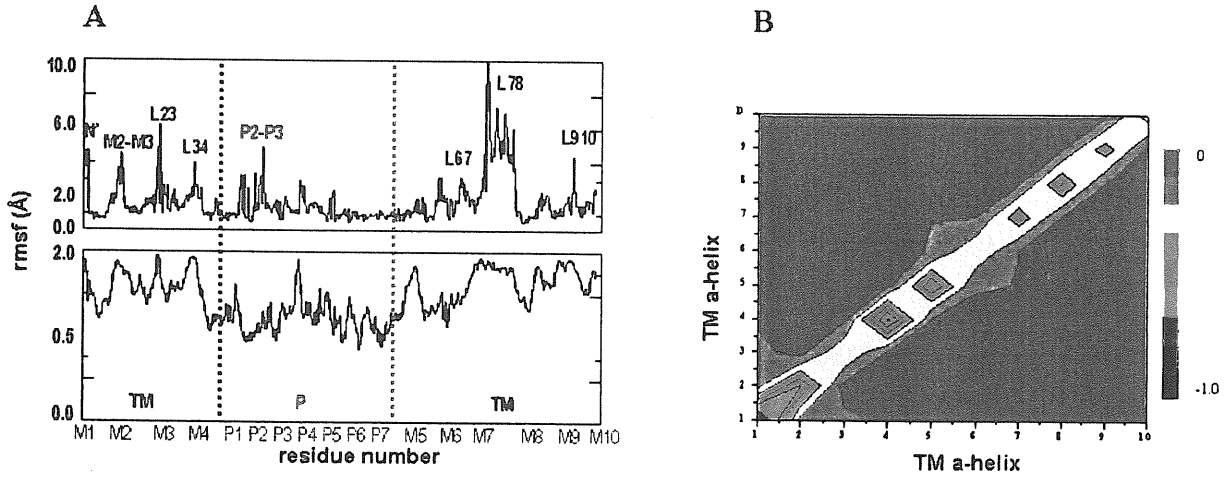

FIGURE 26. **Molecular dynamics of Ca_2E_1.** A: Comparison between MD-averaged rmsf values per residue (top) with those derived from the B-factors of the X-ray structure (Toyoshima et al 2000) (bottom). The most mobile regions are labelled in blue and red for TM and P domains, respectively. B: Electrostatic interactions between the 10 α-helices of the TM domain. As the energies are evaluated using a single point charge model, the values reported here have been normalised. Colour calibration scale, from black to red, corresponds interaction energy variation between the α-helices, form its maximum (-1) to its minimum (0) value.

TABLE IV. SELECTED MD-AVERAGED PROPERTIES.†

Property	Ca_2E_1	H_2E_2	HCaE′
Rmsd	2.5 ± 0.3	1.7 ± 0.3	1.5 ± 0.2
Rmsd of TM	2.8 ± 0.4	1.6 ± 0.2	1.6 ± 0.2
Rmsd of P	1.3±0.1	1.6 ± 0.4	1.2 ± 0.2
R_g	30.2±0.1	30.11±0.08	29.99±0.08

†MD-averaged rmsd (Å) and gyration radius (Å) of Ca_2E_1, H_2E_2 and HCaE′ structural models. Standard deviations are also reported.

TABLE V. SELECTED MD-AVERAGED DISTANCES.†

Distances	X-ray	Ca_2E_1	HCaE′ (H_2E_2)
$Ca(I)^{2+}$-$Ca(II)^{2+}$	5.7	6.5 ± 0.2	-
$Ca(I)^{2+}$-$O_{\delta1}$(D904)	2.7	2.6 ± 0.1	2.6 ± 0.1
$Ca(I)^{2+}$-$O_{\delta2}$(D904)	-	-	2.6 ± 0.1
$Ca(I)^{2+}$-$O_{\gamma1}$(T799)	2.2	2.9 ± 0.1	2.9 ± 0.1
$Ca(I)^{2+}$-$O_{\gamma1}$(E800)	2.2	2.6 ± 0.1	-
$Ca(I)^{2+}$-$O_{\gamma1}$(E771)	2.7	2.7 ± 0.1	2.6 ± 0.1
$Ca(I)^{2+}$-$O_{\gamma2}$(E771)	-	-	3.3 ± 0.6
$Ca(I)^{2+}$-$O_{\delta1}$(N768)	2.4	2.6 ± 0.1	2.7 ± 0.1
$Ca(I)^{2+}$-O(W1)	-	2.7 ± 0.2	2.8 ± 0.1
$Ca(I)^{2+}$-O(W2)	-	3.0 ± 0.5	3.2 ± 0.7
$Ca(I)^{2+}$-O(W3)	-	4.3 ± 1.5	2.7 ± 0.1
$Ca(II)^{2+}$-$O_{\gamma2}$ (E800)	2.3	2.6 ± 0.1	-
$Ca(II)^{2+}$-$O_{\delta1}$(N796)	2.2	2.6 ± 0.1	-
$Ca(II)^{2+}$-$O_{\gamma1}$(E309)	2.1	3.0 ± 0.8	-
$Ca(II)^{2+}$-$O_{\gamma2}$(E309)	2.7	2.6 ± 0.1	-
$Ca(II)^{2+}$-O(I307)	2.5	2.6 ± 0.1	-
$Ca(II)^{2+}$-O(A305)	2.6	2.8 ± 0.2	-
$Ca(II)^{2+}$-O(V304)	2.4	2.7 ± 0.1	-
$Ca(II)^{2+}$-$O_{\gamma1}$(E58)	5.1	2.6 ± 0.1	-
$O2_\delta$(D315)-N_ζ(K684)	2.9	2.9 ± 0.4	3.6 ± 0.7 (3.6 ± 0.7)
D345(M5)-L211(P2)	3.0	2.9 ± 0.2	2.9 ± 0.2 (2.9± 0.1)

†Comparison of selected distances (Å) between X-ray structure (Toyoshima et al., 2000) in the Ca_2E_1 conformation and MD-averaged structures of models Ca_2E_1, HCaE′ and H_2E_2. Standard deviations are also reported. The values in brackets refer to H_2E_2.

The gyration radius exhibited low fluctuations (Table IV) indicating that the protein was rather compact. The final MD structure, as well as structures selected during the dynamics, exhibited a good Ramachandran plot (Ramachandran & Sasisekharan 1968).

The P domain experienced small fluctuations (Table IV). The α-helix P4 and terminal chains between α-helices P2 and P3 (Figure 24) turned out to be the most flexible groups, as shown by Figure 26 A. During the dynamics, the secondary structure elements were conserved and the essential residue Asp351 maintained its salt bridge with Lys684 (Table V). The link between P and TM domains is established by a H-bond between residues on α-helices P2 and M5. This interaction was fully conserved during the dynamics (Table V).

Secondary structure elements of TM domain were fully maintained, as visible from our rmsf plot (upper plot in Figure 26 A) and according to the rmsf plot derived by the Debye-Waller factors of the X-ray structure (Hua et al., 2000) (bottom plot in Figure 26 A). As expected, some of the loops in the structure, especially the longest loop of the protein L78, exhibited large rmsf values (Figure 26 A). In contrast, L67, which is known to be essential for the enzyme functionality, was relatively rigid.

The electrostatic interaction between the TM α-helices, estimated with a single point charge method, showed that the only significant interactions occurred between α-helices M1, M2 and M3 (Figure 26 B).

The large-scale motions of the protein complex were investigated in terms of eigenvectors of the covariance matrix of the C_α atoms. The four largest eigenvectors, which span as much as 70% of the total motion, were considered here (Figure 27 A). The first and second largest eigenvectors involved a local motion of L12, L34 and L78 from TM domain. The largest eigenvectors involving the entire complex (namely the third and the fourth eigenvectors) are represented in Figure 27 B: in this motion, the TM and P domains rotate independently and in opposite direction around two axes, one parallel and the other orthogonal to the membrane plane.

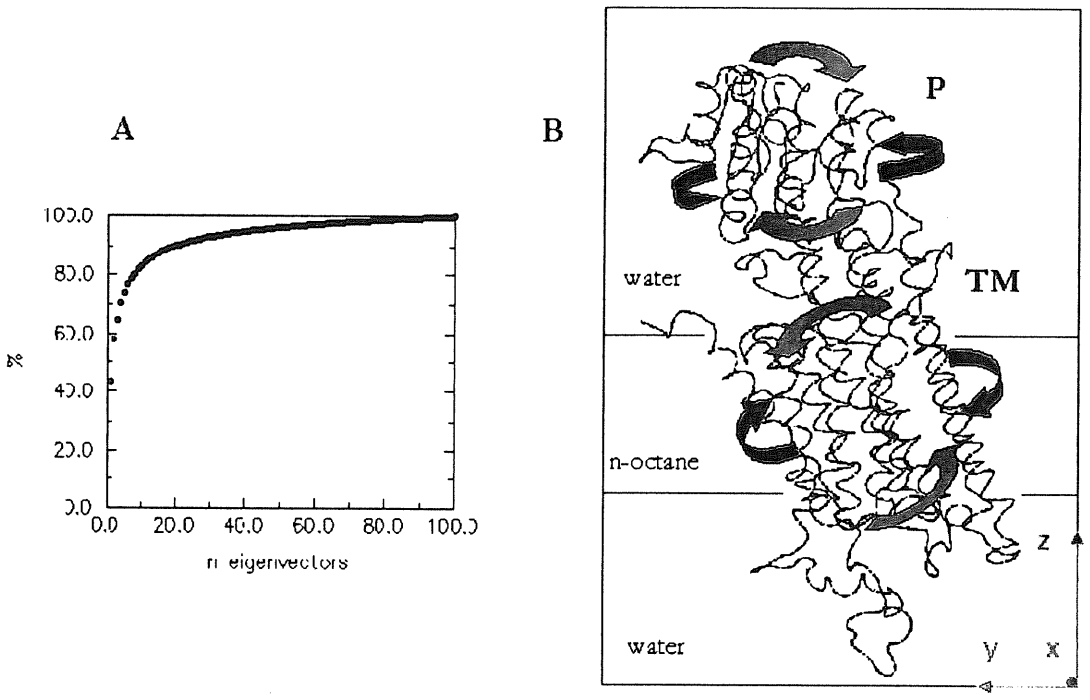

FIGURE 27. Large scale motions of Ca_2E_1. A: Fraction of protein motion $[(\lambda_n 100)/(\sum_n \lambda_n)$, n=1,100] plotted as a function of the essential eigenvalues (λ_n) number (n). The largest four eigenvectors cover as much as ~70% of the total motion. **B**: The largest eigenvectors involving the entire complex are represented schematically in blue (third) and green (fourth largest eigenvector) colours.

Several water molecules, not present in the PDB file (Toyoshima et al., 2000), turned out to be ordered during the last 1.5 ns of dynamics (Figure 27). They formed hydrogen bonds with the protein frame and interacted with the $Ca(I)^{2+}$ ion (Figure 27 and Table V). The coordination of $Ca(II)^{2+}$ was completed by Glu58, not acting as a ligand in the X-ray structure (Table V). As a result, the MD-averaged coordination numbers and metal-donor distances were larger than those of the X-ray structure (see Table VI). These structural parameters were more similar to those of Ca^{2+} in aqueous solution as obtained with the same computational set-up in this work (Table VI). These discrepancies might be ascribed to the lack of a polarization term in our force field, which is know to overestimate the coordination number for a divalent ion like Ca^{2+} (Weinstein and Mehler, 1994; Marchand and Roux, 1998). The distance between the two calcium ions was larger than that of the X-ray (Table V).

TABLE VI. COORDINATION OF CALCIUM IONS †

Model	N coord	d(Å)
$Ca^{2+}(I) - Ca_2E_1$	8.4 ± 0.6	2.7± 0.1
$Ca^{2+}(II) - Ca_2E_1$	8.1 ± 0.3	2.6 ± 0.2
$Ca^{2+}(I)$ – HcaE′	8.3 ± 0.5	2.7 ± 0.1
Ca^{2+} - water	8.7 ± 0.5	2.7 ± 0.1
$Ca^{2+}(I)$ - X-ray	5	2.5 ± 0.3
$Ca^{2+}(II)$ – X-ray	6	2.5 ± 0.3

†Calcium ions in Ca_2E_1 and HCaE′ models. The MD-averaged coordination number and metal-donor atom distances are compared with those of Ca^{2+} ion aqueous solution (this work) and with the correspondent values in the X-ray structure (Toyoshima et al., 2000).

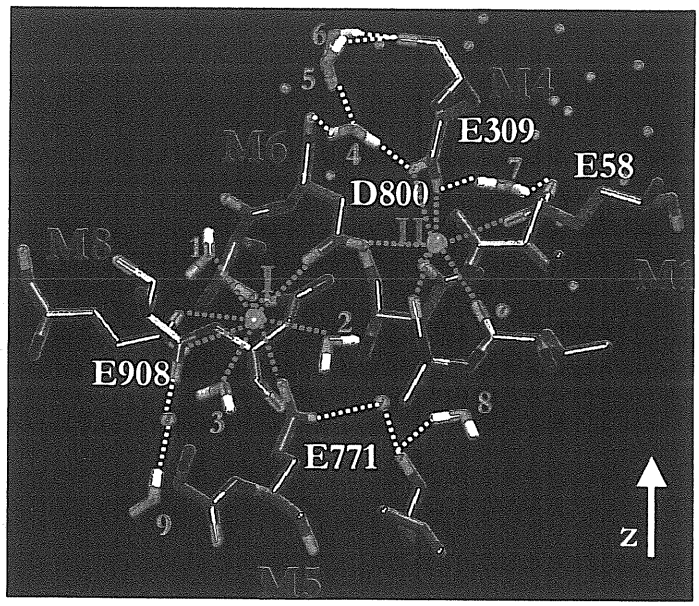

FIGURE 28. Structure of the calcium binding sites. Snapshot at 2.0 ns of dynamics. The calcium ions (spheres coloured in green) lie side-by-side near the centre of M4, M5, M6 and M8 α-helices. E908/E771 bind to $Ca(I)^{2+}$, E309/E58 bind to $Ca(II)^{2+}$. D800 binds to both ions. Water molecules (red spheres) located within 10 Å from the metal ions are also shown. Those found to be ordered during the dynamics, are numbered and represented with their hydrogen atoms (red and white).

1.2 TM CONFORMATIONAL CHANGES DURING CALCIUM BINDING PROCESS: H_2E_2 AND HCAE′ MODELS

Possible conformational changes of the protein transmembrane region during the calcium binding process were next investigated. This was done by constructing structural models (H_2E_2 and HCaE′) of the intermediate and final calcium binding step and comparing them with Ca_2E_1 model.

1.2.1 COMPUTATIONAL DETAILS

STRUCTURAL MODELS

Both H_2E_2 and HCaE′ models were based on the Ca_2E_1 structure after 2 ns of MD simulation.

First we constructed H_2E_2, which contains no calcium at the binding sites. The M6 and M4 α-helices were constrained to a wound conformation (see below for details), as previously suggested (McIntosh, 2000; MacLennan and Green, 2000) on the basis of time-resolved Fourier transformed infrared difference spectroscopy (Troullier et al., 1996) and NMR (Soulie et al., 1999) studies. Asp800 and Glu309, that bind respectively $Ca(I)^{2+}$ and $Ca(II)^{2+}$ in Ca_2E_1 (Figure 27), were considered protonated to take into account the presence of two extra protons in the binding site (see Introduction; Yu and Inesi, 1993). Finally to ensure electro-neutrality to the system, two more potassium ions were added.

HCaE′ model contained, instead, only one Ca^{2+} located at site I. It was built as model H_2E_2, except that: (i) only Glu309 was protonated; (ii) one more potassium was added; (iii) only the M4 α-helix was constrained to a wound conformation (Inesi et al., 1980).

MOLECULAR DYNAMICS CALCULATIONS

α-Helices M4 (for both models) and M6 (for H_2E_2) were wound by performing the following MD runs at low-temperature (100 K): (i) 60 ps of constrained MD simulation on α-helices M4 (for HCaE′) and M4/M6 (for H_2E_2). Harmonic constraints were imposed onto the backbone dihedral angles ϕ and ψ (Creighton, 1993) and onto the H-bonds involving the α-helices (Case et al., 1997). The harmonic force constant K assumed increasingly larger values. Specifically we considered five steps 12 ps long in which K increased from 0.1 to 1.0, 10, 100 and 200 kcal $mol^{-1}Å^{-2}$ for bonds and kcal $mol^{-1}deg^{-2}$ for angles. The rest of the protein was kept fixed. (ii) The entire protein was slowly allowed to relax by performing 60 ps of restrained MD simulation, during which α-helix M4 (and M6 for H_2E_2) was harmonically-restrained to its wound conformation (force constant 200 kcal $mol^{-1}Å^{-2}$ [deg^{-2}]) and the rest of the protein was harmonically restrained to its position (the protein force constant varied as follows: 50, 10, 5, 1.0 and

0.1 kcal $mol^{-1}Å^{-2}$ in 5 steps of 12 ps each). (iii) 60 ps of constrained dynamics in which the force constants of the α-helices were slowly decreased from 200 to 100, 10, 1.0 and 0.1 kcal $mol^{-1}Å^{-2}$ [deg^{-2}] in 5 steps of 12 ps each, while the rest of the protein was unconstrained.

At the end of this procedure, α-helix M4 (and M6 for H_2E_2) resulted to be wound and the structures exhibited a good Ramachandran plot. Both systems underwent, finally, 1.0 ns of unconstrained dynamics. Only the last 0.6 ns of dynamics were collected for analysis. Final configurations are shown in Figure 29.

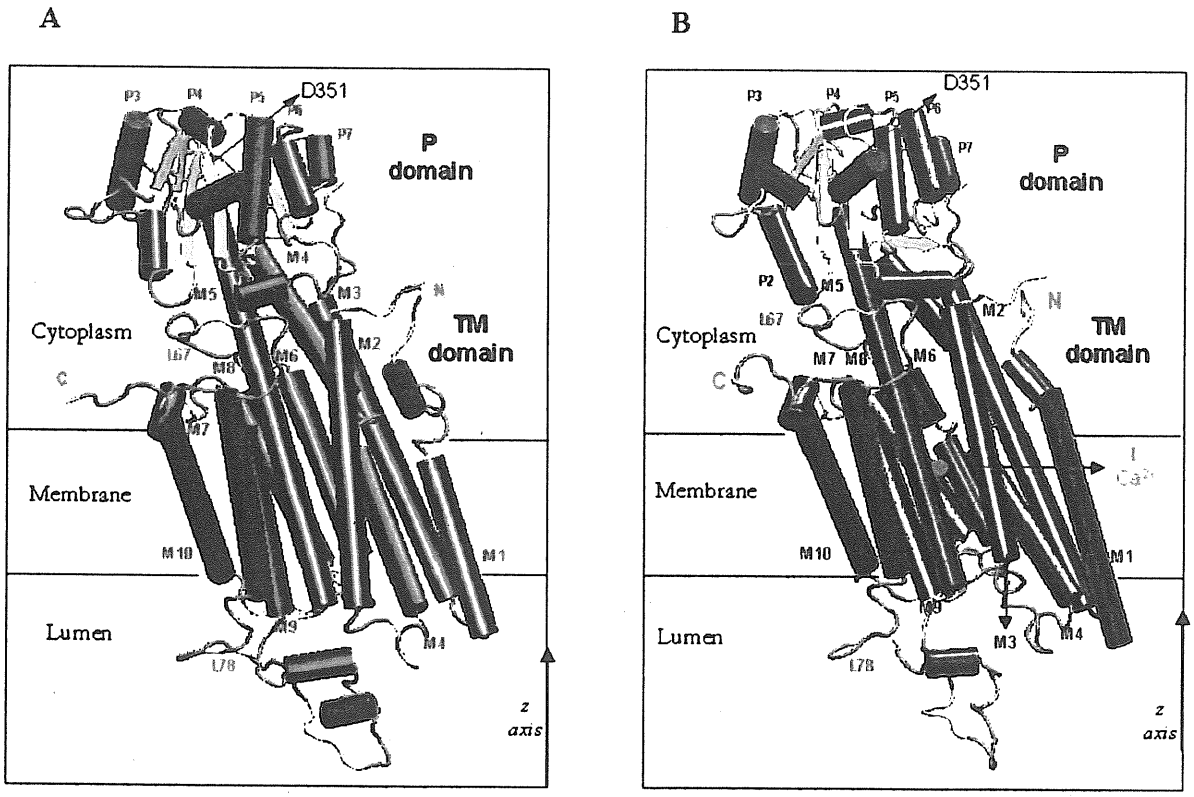

FIGURE 29. H_2E (A) and HCaE′ (B) models. Snapshot at 1 ns of molecular dynamics simulation. In first model any calcium ions are bound, while in the second one ion (green sphere) occupies the I binding site.

1.2.2 COMPARISON BETWEEN Ca_2E_1, HCaE′ AND H_2E_2 STRUCTURAL MODELS

In these models, Ca^{2+} was either absent (H_2E_2) or only $Ca(I)^{2+}$ was present (HCaE′). The M4 α-helix (and M6 for H_2E_2) was constrained wound. The largest conformational

changes on passing from Ca_2E_1 to HCaE' and then to H_2E_2 are visible in Figure 30. The two models were rather stable during the dynamics, as suggested by rmsd values with respect to the structural model obtained after 180ps of constrained dynamics (see rmsd values in Table IV). Overall, the MD structures appeared to be similar to that of Ca_2E_1, as indicated by a comparison between the gyration radii (Table IV).

The structural determinants of the P domain for both models were very similar to those observed for Ca_2E_1. The H-bond interaction between TM and P domains was fully maintained (Table V), while the Asp351/Lys684 salt bridge at times turned out to be mediated by a water molecule (Table V). The relative orientation between α-helices M4 and M5 and the P domain did not exhibit significant differences.

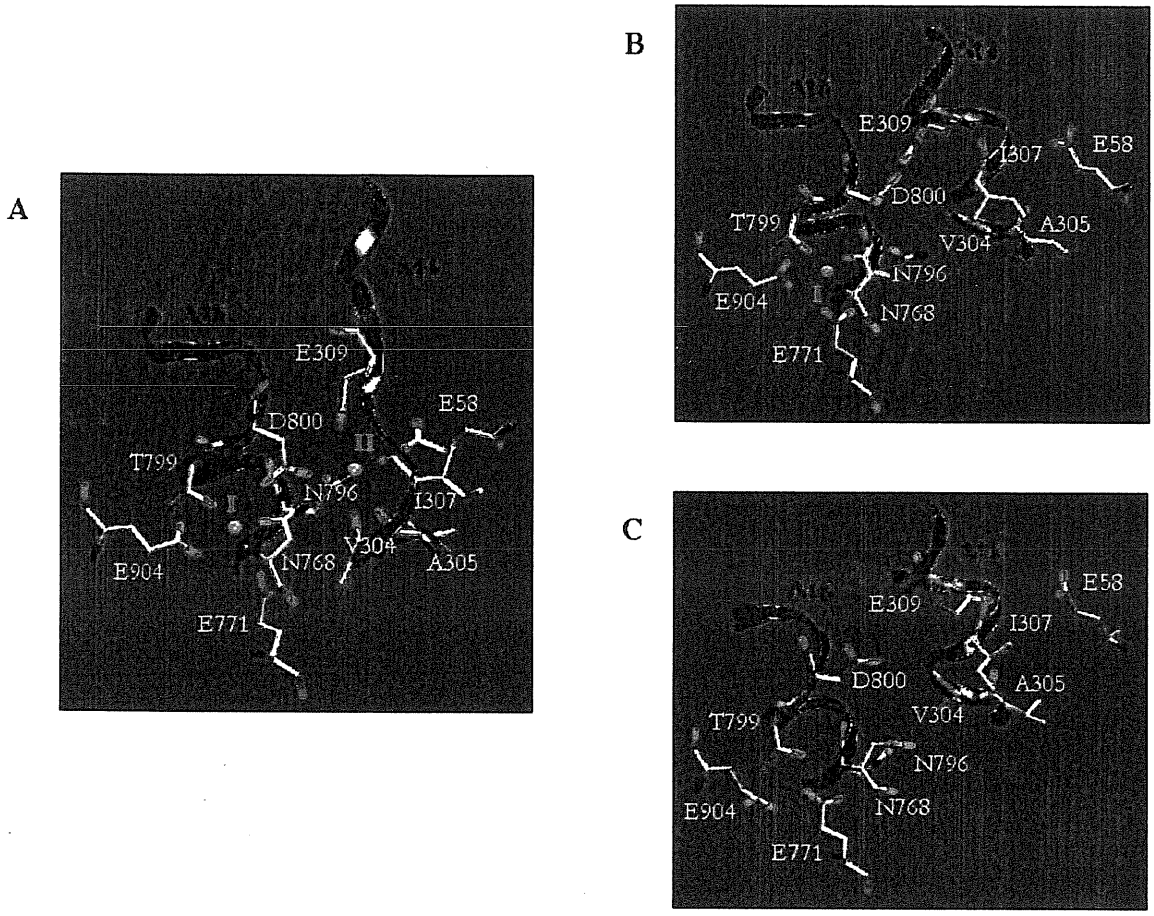

FIGURE 30. Ca^{2+} binding sites in Ca_2E_1 (A), HCaE' (B) and H_2E_2 (C). The residues binding calcium ions are indicated. For sake of simplicity, water molecules are not shown. Both M4 and M6 α-helices are unwound and two metal binding sites are present in (A). α-helix M4 is wound and only site I is present in (B). M4 and M6 α-helices are both wound and the metal binding sites are not present in (C).

In contrast, TM α-helices around the two binding sites and loops between them were mostly affected in their lumenal half. The orientation of M1-M3 α-helices was different with respect to the Ca_2E_1 model (Figure 24 and 29). In particular, M1 tilted and M2-M3 shifted far away from M4. In H_2E_2, also the α-helix M6 was wound, without inducing any important rearrangement of the protein 3D structure.

As expected, the absence of metal ions from either both sites of H_2E_2 or site II of HCaE', affected the structure of the binding sites (Figure 30). HCaE' was fairly similar to that of Ca_2E_1, however Asp800 did not bind the metal ion, Glu771 acted as a bidentate ligand and few water molecules interacted with $Ca(I)^{2+}$ (Table V).

1.3 CALCIUM BINDING TO THE TRANSMEMBRANE SITES

The last part of our investigation focused on the interactions between the calcium ions and the protein residues located, either in the binding sites (inner pathways), or in the outer mouth of the protein (outer binding). As mentioned in the Introduction, two mechanisms are in principle possible for the calcium binding process (McIntosh, 2000): either the first ion binds directly to site I of H_2E_2 as site II is not properly formed, or it binds to site II of H_2E_2 and then moves to site I. In both cases, the second ion subsequently binds to site II of HCaE'. Of these two possible mechanisms, only the first one appears to be consistent with the cooperativity of Ca^{2+} binding to the protein (Inesi et al., 1980). Starting from this assumption, only the first mechanism was here investigated. By electrostatic modelling we examined if this mechanism was feasible and looked for possible pathways for Ca^{2+} binding to the protein. Furthermore, with several MD simulations we searched for residues which could interact with calcium ions during the outer binding process.

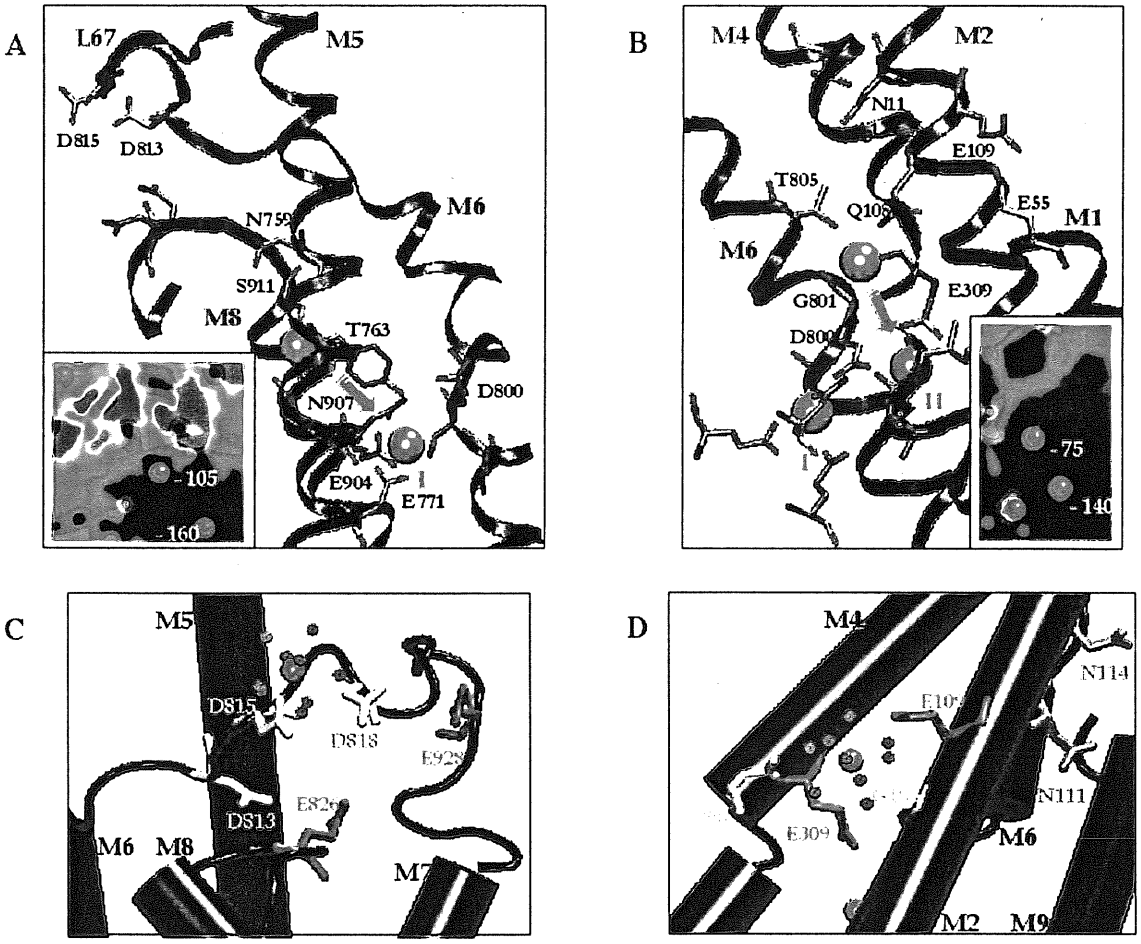

FIGURE 31. **Calcium pathways.** Calcium pathways for HCaE′ (**A**) and Ca_2E_1 (**B**) and models around sites I and II, respectively. The electrostatic slices display the electrostatic potential energies on surfaces crossing the position of the calcium ions. The potential energies values are expressed in kcal/mol and the colours range varies from blue (E < -20 kcal/mol) to red (E > 20 kcal/mol). Calcium outer binding to H_2E_2 (**C**) and HCaE′ (**D**). Final position of calcium ions (green spheres) in the outer mouth of models $H_2E_2(Ca^{2+})$ (**C**) and HCaE′(Ca^{2+}) (**D**). Specifically, the ions were located at about 4-5 Å far away from Asp815/Asp818 of loop L67 (**C**) and Gly105/Glu109 of ϑ-helix M2 and Pro308/Glu309 of ϑ-helix M4 (**D**). Their first hydration shell is shown (red spheres).

1.3.1 INNER CALCIUM PATWAYS

Under the assumption that the conformational changes around the binding sites occur before calcium binding (Inesi et al., 1980), the Ca^{2+} pathways in the TM region close to the metal sites were identified by performing electrostatic calculations on HCaE′ (for site I) and Ca_2E_1 (for site II; Figure 31). The pathways were constructed by connecting sites of minimum of the electrostatic potential energy, namely: (i) for the pathway leading to site I (Figure 31 A-B), in proximity of Asn759, Phe763 (α-helix M5), Ser911

and Asn907 (α-helix M8); (ii) for the pathway leading to site II (Figure 31 B), in proximity of Gln108 (α-helix M2), Asp800, Gly801 and Thr805 (α-helix M6) as well as residues belonging to the unwound part of ϑ-helices M4 (Gly310, Glu309).

1.3.2 OUTER CALCIUM BINDING

STRUCTURAL MODELS

To investigate the binding of the first Ca^{2+} to the outer mouth of the channel, we performed MD simulations of models with the protein in the H_2E_2 conformation (thus without calcium ions at the binding sites, see Figure 4 in Introduction) and one calcium ion on the cytoplasmic side (namely $H_2E_2(Ca^{2+})$). As the outcome of the simulation is expected to depend significantly on the initial conditions, several initial locations of calcium ion in the cytoplasmic space were considered (Table VII). Specifically, the ions were located in proximity of L67 loop, which is essential for Ca^{2+} binding (Falson et al., 1997; Menguy et al., 1998; Zhang et al., 2000; Zhang et al., 2001), in regions of highly negative electrostatic potential as calculated by the Poisson-Bolzmann equation (see below).

The binding of the second Ca^{2+} to the outer mouth of the channel was investigated by adding one calcium ion to the cytoplasmic space in the HCaE′ model (thus with one Ca^{2+} ion in site I), namely the HCaE′(Ca^{2+}) model. Also in this case, several models differing for the position of the metal ion in the cytoplasmatic region were considered (Table VII). Our electrostatic calculations suggested that residues between M4 and M2 might play an important role for the binding. Furthermore, activity measurements of Asn114Ala and Asn111Ala mutants (Clarke et al., 1989) suggested that residues Asn111 and Asn114 were also important. Thus, the second Ca^{2+} was located either between M4 and M2 α-helices or in the proximity of residues Asn111and Asn114.

Solvent equilibration for these HCaE′(Ca^{2+}) and $H_2E_2(Ca^{2+})$ models was carried out for 20 ps. This was followed by 0.6 ns of MD at room temperature and pressure.

TABLE VII. INITIAL POSITIONS OF CYTOPLASMIC Ca^{2+} †

H_2E_2	d(Å)	HcaE′	d(Å)
$Ca(1)^{2+}$ - O_Y(E749)	6.2	$Ca(1)^{2+}$ - O_Y(E55)	6.3
$Ca(1)^{2+}$ - O_δ(D813)	5.8	$Ca(1)^{2+}$ - O_Y(E109)	6.4
$Ca(2)^{2+}$ - O_δ(D815)	7.2	$Ca(2)^{2+}$ - O_Y(E109)	7.1
$Ca(2)^{2+}$ - O_δ(D818)	7.8	$Ca(3)^{2+}$ - O_δ(D111)	6.9
$Ca(3)^{2+}$ - O_δ(D815)	6.3	$Ca(3)^{2+}$ - N_δ(N114)	5.8
$Ca(3)^{2+}$ - O_δ(D818)	5.7	$Ca(4)^{2+}$ - O_δ(N114)	6.3
$Ca(4)^{2+}$ - O_Y(E826)	5.9		
$Ca(4)^{2+}$ - O_Y(E928)	6.2		

†Distances between initial positions of Ca^{2+} ions (Å) located in the outer mouth of H_2E_2 and HCaE′ models and selected residues.

Ca^{2+}/PROTEIN INTERACTIONS

The pathways for calcium ions in the outer mouth of the channel are difficult to be determined at the present stage. Here we attempted to identify specific regions in the outer mouth which might be involved in the permeation process, under the assumption that the conformational changes around the binding sites occur after cytoplasmic calcium binding to the protein (Inesi et al., 1980). Electrostatic calculations (performed in the present study) and mutagenesis experiments suggest that Asp813, Asp815 and Asp818 might be involved in the outer binding of the first ion (Figure 31 A; Falson et al., 1997; Zhang et al., 2000; Menguy et al., 1998; Zhang et al., 2001), plus Asn111, Asn114 (Clarke et al., 1989) and Glu309 (Vilsen and Andersen, 1998) in the binding of the second ion (Figure 31 B). One calcium ion was then added to different locations in the solvent of H_2E_2 and HCaE′ (models $H_2E_2(Ca^{2+})$ and HCaE′(Ca^{2+})). As a result of MD calculations of these models, the cytoplasmic calcium ion either diffused away in the cytoplasmic water, or formed stable water-mediated interactions with the protein (Figure 31 C and D). These interactions involved Asp815/Asp818 of L67 (Figure 31 C) for the binding of the first calcium ion and Gly105/Glu109 of α-helix M2 and Glu309/Pro308 of α-helix M4 (Figure 31 D) for the binding of the second calcium ion.

2. DISCUSSION

Structural and dynamical aspects of the sarcoplasmic reticulum Ca^{2+}-ATPase in Ca_2E_1, HCaE′ and H_2E_2 states of its functional cycle (Introduction, Figure 7), as well as calcium

binding to states HCaE′ and H_2E_2 were investigated. Calculations were based on the X-ray structure of the protein in its unphosphorylated calcium-bound state (Toyoshima et al., 2000).

2.1 BINDING SITES IN THE CA_2E_1 STRUCTURAL MODEL

The P and TM domains of the Ca_2E_1 model were investigated by carrying out MD simulations of the complex in a membrane mimic environment (Figure 24). The structure of Ca_2E_1 was stable in the timescale investigated (2 ns). In particular, the secondary structure was fully maintained. However, the membrane environment oriented in a different fashion than that suggested by crystallographers (Toyoshima et al., 2000), and as a consequence, also the orientation of calcium ions (Figure 25) was diverse from that previously proposed (Lee and East, 2001).

The mobility of the TM domain loops was markedly different, as shown by the rmsf plots per residue derived from our calculations and from the Debye-Waller factors of the X-ray structure (Figure 26). The longest lumenal loop L78 was rather mobile, while loop L67, which is known to be essential for the enzyme functionality (Falson et al., 1997; Menguy et al., 1998), was relatively rigid.

Large-scale motion analysis suggests that the TM and P domains rotate independently and in opposite direction around two axes (x and z in Fig. 27B). Thus, in spite of the interaction between M5 (TM domain) with the P2 (P domain) these domains appear to be free to move independently. Our results therefore support the idea that domain P is flexible in presence of Ca^{2+} and before ATP-hydrolysis (Toyoshima et al., 2000).

Novel information has been obtained on the hydration of the calcium binding sites and on the metal coordination (Figure 28 and Table VI). In particular, few water molecules, not detected in the X-ray structure (Toyoshima et al., 2000), were observed to be ordered around the two binding sites and three of them bound Ca^{2+} at site I. Beside, with respect to the X-ray structure also Glu58 contributed to Ca^{2+} coordination in site II. As a result, the MD structural properties of the metal ion coordination polyhedra resembled those of Ca^{2+} in its inner hydration shell.

2.2 H_2E_2 AND HCAE′ STRUCTURAL MODELS

The H_2E_2 and HCaE′ models were built starting from the Ca_2E_1 structure after 2 ns of MD. In these models, α-helix M4 (and M6 in H_2E_2) was imposed to be in a wound conformation. A structural change of the protein at the level of the two binding sites was also previously proposed (McIntosh, 2000; MacLennan and Green, 2000) on the basis of spectroscopic data (Troullier et al., 1996; Soulie et al., 1999).

Overall, our MD structures exhibited a slightly lower α-helical content than Ca_2E_1 model. Indeed, M1 and M4 α-helices were found to bend during simulation in both models (Figure 29). This fact may be consistent with the decrease of α-helical content upon Ca^{2+} release observed by CD spectroscopy (Girardet and Dupont, 1992).

M4 and M6 winding affected the structure of the metal binding sites (Figure 30). The empty sites were disrupted, like in a variety of other metallo-proteins. Furthermore, the orientation of the α-helices at the binding sites changed with respect to the Ca_2E_1 conformation. M4 winding caused M1 tilting and M2/M3 shifting far away from the binding sites. These findings are consistent with the proposal that relatively large-scale movements of all Ca^{2+}-ATPase domains accompany the binding of calcium (Ogawa et al., 1998; Stokes et al., 1999). The rearrangement of M1-M3 α-helices, which are connected to domain A, might be responsible for domain A motions, as previously postulated (Toyoshima et al., 2000) and accord with experimental observations (Juul et al., 1995). TM α-helices and loops were mostly affected in their lumenal portion.

2.3 CALCIUM BINDING TO THE PROTEIN

Calcium binding to the protein was investigated using electrostatic modelling and MD simulations, under the assumption that the conformational changes around the binding sites occur *before* calcium binding to the TM sites and *after* cytoplasmic calcium binding to the outer mouth of the protein, consistently with the cooperativity of the binding process (Inesi et al., 1980). As a consequence, the calcium pathways in the TM region in close proximity to the metal binding sites were identified by performing electrostatic calculations for HCaE′ (for site I) and Ca_2E_1 (for site II), whereas calcium binding to the region of the solvent in the outer mouth of the protein was investigated by MD

simulations for H_2E_2 when binding the first ion and for HCaE′ when binding the second Ca^{2+}.

As a result, Poisson-Boltzmann electrostatic calculations indicated that calcium binds to sites I and II through two specific pathways (Figure 31 A and B). Furthermore, within the limitation of our MD approach (the results are dependent on the initial conditions since Ca^{2+} diffusion is slow), our simulations allowed identifying the residues for outer Ca^{2+} binding. Because of the limited sampling of configurations performed, our calculations are not exhaustive.

In particular, residues Asp815 and Asp818 (L67) (Figure 31 C) seem to be involved in the first calcium binding to H_2E_2, while residues Gly105, Glu109 (M2), Pro308 and Glu309 (M4) (Figure 31 D) seem to be relevant for the outer binding of the second ion to HCaE′. These findings appear to be consistent with the experimentally-observed low-affinity for calcium of the D813A/D818A and D813A/D815A/D818A mutants (Falson et al., 1997; Menguy et al., 1998; Zhang et al., 2001). A very recent study with NMR and mass spectrometry techniques indicates involvement of the cytoplasmic loop L67 in the Ca^{2+} entry mechanism, by forming an entrance in preceding steps and before subsequent high affinity binding of Ca^{2+} inside the membrane (Menguy et al., 2002). Thus, theory and experiments suggest that the region 808-818 (loop L67) is essential for Ca^{2+} binding to site I. In addition, our calculations point out the relevance of Glu309 for Ca^{2+} binding to site II, in accordance with mutagenesis experiments on this position (Vilsen and Andersen, 1998).

2.4 COMPARISON BETWEEN E_2(TG) X-RAY STRUCTURE AND H_2E_2 STRUCTURAL MODEL

Very recently the X-ray structure of the protein in absence of Ca^{2+} ions and in the presence of the potent inhibitor thapsigargin (TG) has been solved at 3.1 Å resolution (Toyoshima and Nomura, 2002). TG fixes the protein in the state E_2(TG) which is analogous to H_2E_2 (Sagara and Inesi, 1991). Comparison between these two Ca^{2+}-free structures may help to validate the accuracy of our predictions. It must be kept in mind that some differences between the two models may also arise by the presence of TG in the crystal structure, which was not present in our model.

Hereafter, I will first describe the conformational changes between the Ca^{2+}-free ($E_2(TG)$) and Ca^{2+}-bound (Ca_2E_1) crystal structure, in cytoplasmic and transmembrane domains. Differences with our Ca^{2+}-free model (H_2E_2) will be pointed out. Then, I will compare conformational changes in $E_2(TG)$ and H_2E_2 around binding sites. Finally, I will re-analyse our results on the calcium pathways in light of the new structure.

2.4.1 CYTOPLASMIC HEADPIECE

The $E_2(TG)$ structure is very different from that in the Ca_2E_1 state (see Figure 33) and the movements of cytoplasmic domains are even larger than the one predicted before with a Ca^{2+}-free low resolution structure (see Introduction, Figure 10; Zhang et al., 1998; Toyoshima et al., 2000).

In particular, comparison between the two crystal structures shows that N domain inclines nearly 90° with respect to the membrane, A domain rotates by about 110° horizontally and P domain inclines by 30° relative to the membrane (Figure 32). The overall motion of N and A cytoplasmic domains was not observable in our model, since we considered only P and TM domains. However, also the rearrangement of P domain could not be detected because of the timescale, too short for such large motions.

Despite the detected large movements of the cytoplasmic headpiece, in $E_2(TG)$ the structure of the P domain remain virtually the same of the one in Ca_2E_1 (rmsd = 0.63 Å). This feature characterizes also our model (rmsd = 0.9 ± 0.3 Å).

2.4.2 TRASMEMBRANE DOMAIN

In $E_2(TG)$, Ca^{2+}-binding accompanies dramatic rearrangements of six (M1-M6) out of ten transmembrane α-helices. Specifically, M1 and M2 move upwards (+z direction, towards the cytoplasm) whereas M3 and M4 shift downwards. M1 unfolds and bends within the membrane region. M5 and M3 are strongly curved but in opposite directions, and M6 winds (Figure 32). Also in our H_2E_2 model, the α-helices M1-M3 are the most affected by M4 and M6 α-helices winding. In particular, α-helix M1 bends at the cytoplasmic half, in accordance with experimental data (Figure 29). On the contrary, the M5 conserves its initial orientation. Some of the differences between our conclusions

conclusions and the experimental structural data may be caused by the absence of the TG ligand, which binds between M3, M5 and M7 helices (near the cytoplasmic surface of the membrane, Figure 32) and therefore it could have affected the M5 conformation.

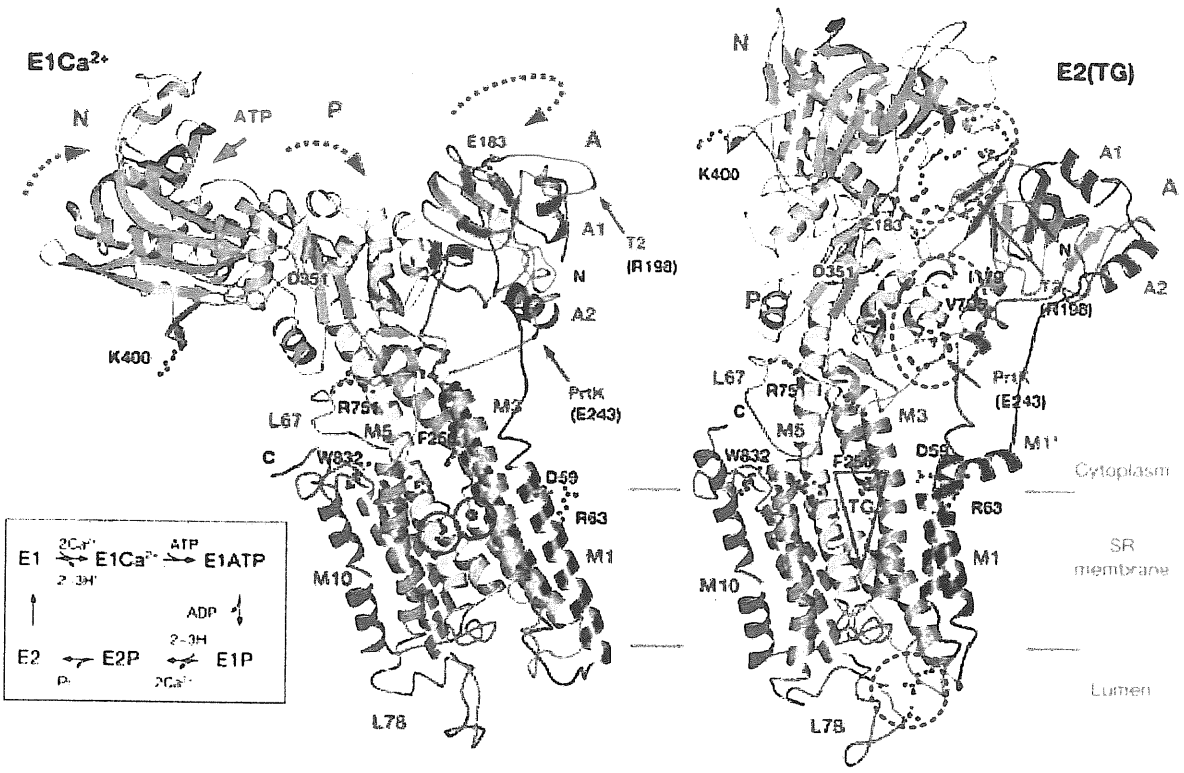

FIGURE 32. Ca^{2+}-ATPase in the Ca^{2+}-bound form (Ca_2E_1) and that in the absence of Ca^{2+} but in the presence of thapsigargin (E_2(TG); Toyoshima and Nomura, 2002). Inset, a simplified reaction scheme (showing only the forward direction). Colours change gradually from the amino terminus (blue) to the carboxy terminus (red). Two purple spheres (circled) in Ca_2E_1 represent bound Ca^{2+}. Red circles in E_2(TG) indicate extra hydrogen bonds in E_2(TG). Large arrows in Ca_2E_1 indicate the direction of movement of the cytoplasmic domains during the change from Ca_2E_1 to E_2(TG). Principal residues are marked: E183 (A domain), F256 (thapsigargin-binding site), D351 (P domain, phosphorylation site), K400 (N domain, phospholamban-binding site) and R751 (linking M5 and the loop (L67) connecting M6 and M7).

2.4.3 CA^{2+}-BINDING SITES

In both crystal and theoretical model structures, release of Ca^{2+} causes a rearrangement of the helices involved in calcium binding, namely M4 and M6 (Figure 30 and 33). In site I, α-helix M6 winds in both cases at the level of residue Asp800, which, as a result, points away from the active site. However, in H_2E_2 M6 winding occurs towards the upper cytoplamic half of the helix, whereas in E_2(TG) occurs towards the lumen half. In

site II, α-helix M4 shifts in both structures downwards relative to the calcium bound protein. The helices are also more elongated. However, in H_2E_2 M4 partially forms an helix whereas it does not change configuration in E_2(TG). Residue Glu309, which in Ca_2E_1 state bind the II metal ion, points away from the binding site towards the cytoplasmic water in both structures. This confirms that Glu309 could have an important role in cytoplasmic calcium trapping, as observed in our simulation and in accordance with experimental results (Vilsen and Andersen, 1998).

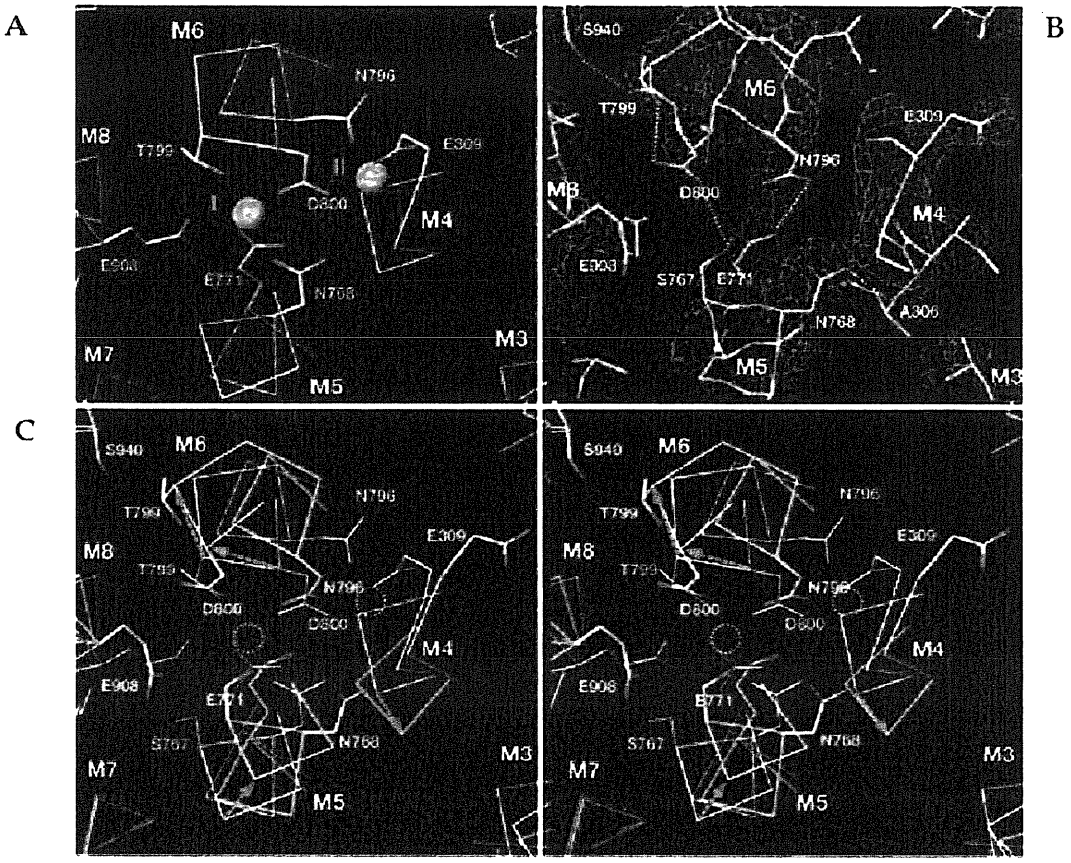

FIGURE 33. **Conformation changes around the Ca^{2+}-binding sites** (Toyoshima and Nomura, 2002).**A**: Cα trace and the side chains of the coordinating residues in Ca_2E_1. **B:** composite omit map and the model for the corresponding area in E2(TG). **C**: stereo view of the composite of the models for Ca_2E_1 (violet) and E2(TG) (atom colour). The viewing direction is approximately down the M5 helix in Ca_2E_1 Two bound Ca appear as cyan spheres (**A**) or circles (**C**). Dashed lines in b show potential hydrogen bonds. Orange arrows in c show the movements of the corresponding residues during the change from Ca_2E_1 to E2(TG).

2.4.4 Ca^{2+} PATHWAYS

E_2(TG) structure does not clearly show any ion pathway to the transmembrane binding sites. In fact, E_2 is believed to have low-affinity for the Ca^{2+}-binding sites exposed to the lumen and high-affinity for the two cytoplasmic sites (see Introduction, Figure 8; de Meis and Vianna, 1979). However, the inner pathway for calcium it known to be formed within the structure after a conformational change caused by the outer binding of the first calcium (Toyoshima and Nomura, 2002). In our study we supposed that changes around the binding sites occur *before* calcium binding to the TM sites and *after* cytoplasmic calcium binding to the outer mouth of the protein.

In our study we supported the hypothesis of the existence of two transport calcium pathways, one for each binding site. In particular, the first calcium was supposed to bind to the protein around loop L67, in accordance with several experiments (see also the most recent NMR and mass spectroscopy study Menguy et al., 2002). Then MD calculations suggest that the first calcium binds to outer mouth of the protein interacting with cytoplasmic residues Asp815 and Asp818 (loop L67). In the E_2(TG), although loop L67 moves with respect to α-helix M5, its structure is quite conserved (rmsd = 1.2 Å with respect to Ca_2E_1 conformation). As a result, Asp815 and Asp818 are still near enough (about 5 Å far away) to form a cytoplasmic binding site for calcium, in according with our calculations.

For the outer binding of the second calcium, our electrostatic calculations points out the existence of a highly attractive region for cations between α-helices M4 and M2. Our MD simulations consistently suggest outer binding of the second metal ion to Glu309 (M4), which in the model as well as in the X-ray structure points towards the cytoplasmic side. In the E_2(TG) structure, a water accessible channel lined by negatively charged residues and leading to the carboxyl group of Glu309 has been observed. The crystallographers (Toyoshima and Nomura, 2002) suggest that the first event in the calcium binding could be the interaction with Glu309, followed by a conformational change of the side chain to deliver the calcium ion to the transmembrane binding cavity. These hypotheses are in full agreements with our findings.

CONCLUSIONS

My theoretical work has provided novel information concerning the structure of fundamental domains of membrane proteins handling Ca^{2+} in excitable cells. One of these proteins, namely the nAChR, is highly permeable to Ca^{2+}, once activated by agonist molecules, and thus generates elevated intracellular Ca^{2+} which, in addition to being a charge carrier, can modulate intracellular enzymes. However, any persistent rise in Ca^{2+} is toxic to cells as it then activates proteolytic enzymes. Hence, cells have developed a number of intracellular processes to keep internal Ca^{2+} levels low. The Ca^{2+} pump is an essential member of the family of processes preserving Ca^{2+} homeostasis. These membrane proteins are therefore both very important for Ca^{2+} signalling although they operate within distinct cell compartments and with different properties. The present project has theoretically investigated a number of characteristics which make such proteins special Ca^{2+} operators. In detail, the main conclusions are listed below.

Study of the structural and binding properties of ligands modulating neuronal nicotinic receptor showed that:

(a) $CGRP_{1-6}$ and shorter peptides are characterised by a α-helix propensity in sharp contrast with the relatively rigid ring structure of $CGRP_{1-7}$.

(b) Electrostatic and structural properties of competitive agonist/antagonist and allosteric agonists binding sites were characterized in nicotinic receptors α3β4 and α4β2 models and compared to the available experimental data.

(c) The selectivity of the α3β4 and α4β2 binding sites, where the studied agonists bind with common properties, were validated. A possible mechanism for the antagonist action of $CGRP_{1-7}$ and a possible site of binding for allosteric agonists, such as eserine, were also suggested.

Investigation on the key intermediates of the calcium pump during the Ca^{2+} binding process mainly provided information on:

(d) Hydration of the two Ca^{2+} binding sites so far not available from X-ray structure.

(e) Protein structural rearrangements around the calcium binding sites in the presence of only one ion or in the absence of both. The latter model is fairly consistent with the X-ray structure appeared in literature after finishing this work.

(f) Specific pathways for calcium. These ions seem to reach their binding sites via two pathways. Some residues responsible for the first binding of cytoplasmic Ca^{2+} ions in the outer mouth of the protein have been porposed.

NOTE

All the work reported in the present thesis has been published in the articles listed below or will be submitted soon to international scientific journals.

Di Angelantonio S, Costa V, Carloni P, Messori L, Nistri A (2002) A novel class of peptides with facilitating action on neuronal nicotinic receptors of rat chromaffin cells in vitro: functional and molecular dynamics studies. Mol Pharmacol 61: 43-54.

Costa V, Carloni P (2002) Calcium binding to the transmembrane domain of the sarcoplasmic reticulum Ca^{2+}-ATPase: insights from molecular modelling. Proteins SFG, in press.

ACKNOWLEDGMENTS

I wish to express my graditude to Prof. Paolo Carloni and Prof. Andrea Nistri for their careful supervision and all the stimulating discussions.

I am very grateful to Dr. Andrea Cavalli for his teaching and his kind support during all the thesis period. I also thank Dr. Silvia Di Angelantonio with whom I had a nice collaboration.

Many thanks to Marco Punta, Matteo Dal Peraro, Sergio Pantano and Stefano Piana for helpful discussions and encouragements.

Finally, I wish to thank all my friends and in particular Laura, Cristina, Fabiana and Nico, who shared with me these nice years in Trieste.

BIBLIOGRAPHY

Adams DJ, Dwyer TM, Hille B (1980) The permeability of endplate channels to monovalent and divalent metal cations. J Gen Physiol 75: 493-510.

Ahmed Z, Reid DG, Watts A, Middleton DA (2000) A solid-state NMR study of the phospholamban transmembrane domain: local structure and interactions with Ca(2+)-ATPase. Biochim Biophys Acta 1468: 187-198.

Akabas MH, Karlin A (1995) Identification of acetylcholine receptor channel-lining residues in the M1 segment of the alpha-subunit. Biochemistry 34: 12496-12500.

Akabas MH, Kaufmann C, Archdeacon P, Karlin A (1994) Identification of acetylcholine receptor channel-lining residues in the entire M2 segment of the alpha subunit. Neuron 13: 919-927.

Akk G, Auerbach A (1999) Activation of muscle nicotinic acetylcholine receptor channels by nicotinic and muscarinic agonists. Br J Pharmacol 128: 1467-1476.

Albuquerque EX, Alkondon M, Pereira EF, Castro NG, Schrattenholz A, Barbosa CT, Bonfante-Cabarcas R, Aracava Y, Eisenberg HM, Maelicke A (1997a) Properties of neuronal nicotinic acetylcholine receptors: pharmacological characterization and modulation of synaptic function. J Pharmacol Exp Ther 280: 1117-1136.

Albuquerque EX, Alkondon M, Pereira EF, Castro NG, Schrattenholz A, Barbosa CT, Bonfante-Cabarcas R, Aracava Y, Eisenberg HM, Maelicke A (1997b) Properties of neuronal nicotinic acetylcholine receptors: pharmacological characterization and modulation of synaptic function. J Pharmacol Exp Ther 280: 1117-1136.

Allen FH, Bellard S, Brice MD, Cartwright BA, Doubleday A, Higgs H, Hummelink T, Hummelink-Peters BG, Kennard O, Motherwell WDS, Rodgers JR, Watson DG (1979) The Cambridge Crystallographic Data Centre: computer-based search, retrieval, analysis and display of information. Acta Crystallogr B 35: 2331-2339.

Allen MP, Tildesley DJ (1987) Computer Simulation of Liquids, Oxford University Press, New York 1987. New York, NY: Oxford University Press.

Amadei A, Linssen A, Berendsen H (1993) Essential dynamics of the protein. Proteins 17: 412-425.

Andersen JP, Vilsen B, Collins JH, Jorgensen PL (1986) Localization of E1-E2 conformational transitions of sarcoplasmic reticulum Ca-ATPase by tryptic cleavage and hydrophobic labeling. J Membr Biol 93: 85-92.

Andersen JP, Vilsen B (1994) Amino acids Asn796 and Thr799 of the Ca(2+)-ATPase of sarcoplasmic reticulum bind Ca2+ at different sites. J Biol Chem 269: 15931-15936.

Andersen JP, Vilsen B (1995) Structure-function relationships of cation translocation by Ca(2+)- and Na+, K(+)-ATPases studied by site-directed mutagenesis. FEBS Lett 359: 101-106.

Aqvist J (1990) Ion-Water interaction Potentials Derived from Free Energy Perturbation Simulations. J Phys Chem 94: 8021-8024.

Aravind L, Galperin MY, Koonin EV (1998) The catalytic domain of the P-type ATPase has the haloacid dehalogenase fold. Trends Biochem Sci 23: 127-129.

Arias HR (1997) Topology of ligand binding sites on the nicotinic acetylcholine receptor. Brain Res Brain Res Rev 25: 133-191.

Arias HR (2000) Localization of agonist and competitive antagonist binding sites on nicotinic acetylcholine receptors. Neurochem Int 36: 595-645.

Armstrong N, Gouaux E (2000) Mechanisms for activation and antagonism of an AMPA-sensitive glutamate receptor: crystal structures of the GluR2 ligand binding core. Neuron 28: 165-181.

Asahi M, Kimura Y, Kurzydlowski K, Tada M, MacLennan DH (1999) Transmembrane helix M6 in sarco(endo)plasmic reticulum Ca(2+)-ATPase forms a functional interaction site with phospholamban. Evidence for physical interactions at other sites. J Biol Chem 274: 32855-32862.

Barlow RB, Howard JAK, Johnson O (1986) Acta Crystallogr C 42: 852.

Barlow RB, Johnson O (1989) Relations between structure and nicotine-like activity: X-ray crystal structure analysis of (-)-cytisine and (-)-lobeline hydrochloride and a comparison with (-)-nicotine and other nicotine-like compounds. Br J Pharmacol 98: 799-808.

Bayly C, Cieplack P., Cornell W., Kollman P.A. (1993) A well-behaved electrostatic potential based method using charge restraints deriving atomic charges: the RESP model. J Phys Chem 97: 10269-10280.

Berendsen HJC, Postma JPM, van Gunsteren WF, DiNola A, Haak JR (1984) Molecular dynamics with coupling to an external bath. J Chem Phys 81: 3684-3690.

Berman HM, Battistuz T, Bhat TN, Bluhm WF, Bourne PE, Burkhardt K, Feng Z, Gilliland GL, Iype L, Jain S, Fagan P, Marvin J, Padilla D, Ravichandran V, Schneider B, Thanki N, Weissig H, Westbrook JD, Zardecki C (2002) The Protein Data Bank. Acta Crystallogr D Biol Crystallogr 58: 899-907.

Berman MC, King SB (1990) Stoichiometries of calcium and strontium transport coupled to ATP and acetyl phosphate hydrolysis by skeletal sarcoplasmic reticulum. Biochim Biophys Acta 1029: 235-240.

Berridge MJ, Bootman MD, Lipp P (1998) Calcium--a life and death signal. Nature 395: 645-648.

Blount P, Merlie JP (1989) Molecular basis of the two nonequivalent ligand binding sites of the muscle nicotinic acetylcholine receptor. Neuron 3: 349-357.

Blundell TL, Sibanda BL, Sternberg MJ, Thornton JM (1987) Knowledge-based prediction of protein structures and the design of novel molecules. Nature 326: 347-352.

Brandl CJ, deLeon S, Martin DR, MacLennan DH (1987) Adult forms of the Ca2+ATPase of sarcoplasmic reticulum. Expression in developing skeletal muscle. J Biol Chem 262: 3768-3774.

Brejc K, van Dijk WJ, Klaassen RV, Schuurmans M, van Der OJ, Smit AB, Sixma TK (2001) Crystal structure of an ACh-binding protein reveals the ligand-binding domain of nicotinic receptors. Nature 411: 269-276.

Brody JI, Soltys HD, Zinsser HF (1969) Folic acid deficiency in congestive heart failure. Br Heart J 31: 741-745.

Campos-Caro A, Smillie FI, Dominguez dT, Rovira JC, Vicente-Agullo F, Chapuli J, Juiz JM, Sala S, Sala F, Ballesta JJ, Criado M (1997) Neuronal nicotinic acetylcholine receptors on bovine chromaffin cells: cloning, expression, and genomic organization of receptor subunits. J Neurochem 68: 488-497.

Canti C, Bodas E, Marsal J, Solsona C (1998) Tacrine and physostigmine block nicotinic receptors in Xenopus oocytes injected with Torpedo electroplaque membranes. Eur J Pharmacol 363: 197-202.

Cantilina T, Sagara Y, Inesi G, Jones LR (1993) Comparative studies of cardiac and skeletal sarcoplasmic reticulum ATPases. Effect of a phospholamban antibody on enzyme activation by Ca2+. J Biol Chem 268: 17018-17025.

Case, D. A., Pearlman, D A, Caldwell, J W, Cheatham III, T E, Ross, W S, Simmerling, C L, Darden, T A, Merz, K M, Stanton, R V, Cheng, A L, Vincent, J J, Crowley, M F, Ferguson, D M, Radmer, R J, Singh, U C, Weiner, P K, and Kollman, P A. AMBER 5, University of California, San Francisco. 1997.

Champeil P, Gingold MP, Guillain F, Inesi G (1983) Effect of magnesium on the calcium-dependent transient kinetics of sarcoplasmic reticulum ATPase, studied by stopped flow fluorescence and phosphorylation. J Biol Chem 258: 4453-4458.

Changeux JP, Rubin MM (1968) Allosteric interactions in aspartate transcarbamylase. 3. Interpretation of experimental data in terms of the model of Monod, Wyman, and Changeux. Biochemistry 7: 553-561.

Changeux JP (1990) The TiPS lecture. The nicotinic acetylcholine receptor: an allosteric protein prototype of ligand-gated ion channels. Trends Pharmacol Sci 11: 485-492.

Changeux JP, Duclert A, Sekine S (1992) Calcitonin gene-related peptides and neuromuscular interactions. Ann N Y Acad Sci 657: 361-378.

Changeux JP (1995) Thudichum Medal Lecture. The acetylcholine receptor: a model for allosteric membrane proteins. Biochem Soc Trans 23: 195-205.

Changeux JP, Bertrand D, Corringer PJ, Dehaene S, Edelstein S, Lena C, Le Novere N, Marubio L, Picciotto M, Zoli M (1998) Brain nicotinic receptors: structure and regulation, role in learning and reinforcement. Brain Res Brain Res Rev 26: 198-216.

Chen B, Martin MG, Siepmann JI (1998) Thermodynamic properties of the Williams, OPLS-AA force fields for modeling organic liquids. J Phys Chem 102: 2578-2586.

Chen L, Sumbilla C, Lewis D, Zhong L, Strock C, Kirtley ME, Inesi G (1996) Short and long range functions of amino acids in the transmembrane region of the sarcoplasmic reticulum ATPase. A mutational study. J Biol Chem 271: 10745-10752.

Chiara DC, Middleton RE, Cohen JB (1998) Identification of tryptophan 55 as the primary site of [3H]nicotine photoincorporation in the gamma-subunit of the Torpedo nicotinic acetylcholine receptor. FEBS Lett 423: 223-226.

Chiesi M, Inesi G (1980) Adenosine 5'-triphosphate dependent fluxes of manganese and and hydrogen ions in sarcoplasmic reticulum vesicles. Biochemistry 19: 2912-2918.

Chiesi M, Inesi G (1981) Mg2+ and Mn2+ modulation of Ca2+ transport and ATPase activity in sarcoplasmic reticulum vesicles. Arch Biochem Biophys 208: 586-592.

Clapham DE (1995) Calcium signaling. Cell 80: 259-268.

Clarke DM, Maruyama K, Loo TW, Leberer E, Inesi G, MacLennan DH (1989) Functional consequences of glutamate, aspartate, glutamine, and asparagine mutations in the stalk sector of the Ca2+-ATPase of sarcoplasmic reticulum. J Biol Chem 264: 11246-11251.

Cohen BN, Labarca C, Davidson N, Lester HA (1992) Mutations in M2 alter the selectivity of the mouse nicotinic acetylcholine receptor for organic and alkali metal cations. J Gen Physiol 100: 373-400.

Cohen JB, Sharp SD, Liu WS (1991) Structure of the agonist-binding site of the nicotinic acetylcholine receptor. [3H]acetylcholine mustard identifies residues in the cation-binding subsite. J Biol Chem 266: 23354-23364.

Colquhoun D, Sakmann B (1985) Fast events in single-channel currents activated by acetylcholine and its analogues at the frog muscle end-plate. J Physiol 369: 501-557.

Colquhoun LM, Patrick JW (1997) Alpha3, beta2, and beta4 form heterotrimeric neuronal nicotinic acetylcholine receptors in Xenopus oocytes. J Neurochem 69: 2355-2362.

Conners CK, Levin ED, Sparrow E, Hinton SC, Erhardt D, Meck WH, Rose JE, March J (1996) Nicotine and attention in adult attention deficit hyperactivity disorder (ADHD). Psychopharmacol Bull 32: 67-73.

Connolly ML (1983) Analytical molecular surface calculation. J Appl Cryst 16: 548-558.

Cornell WD, Cieplak P, Bayly CI, Gould IR, Merz KM, Jr., Ferguson DM, Spellmeyer DC, Fox T, Caldwell JW, Kollman PA (1995) A second-generation force field for the simulation of proteins and nucleic acids. J Chem Phys 117: 5179-5197.

Corringer PJ, Bertrand S, Galzi JL, Devillers-Thiery A, Changeux JP, Bertrand D (1999) Molecular basis of the charge selectivity of nicotinic acetylcholine receptor and related ligand-gated ion channels. Novartis Found Symp 225: 215-224.

Corringer PJ, Le Novere N, Changeux JP (2000) Nicotinic receptors at the amino acid level. Annu Rev Pharmacol Toxicol 40: 431-458.

Cowan SW, Garavito RM, Jansonius JN, Jenkins JA, Karlsson R, Konig N, Pai EF, Pauptit RA, Rizkallah PJ, Rosenbusch JP, . (1995) The structure of OmpF porin in a tetragonal crystal form. Structure 3: 1041-1050.

Creighton TE (1993) Proteins. Structures and molecular properties. New York, NY.: W.H. Freeman and Company.

Cully DF, Vassilatis DK, Liu KK, Paress PS, Van der Ploeg LH, Schaeffer JM, Arena JP (1994) Cloning of an avermectin-sensitive glutamate-gated chloride channel from Caenorhabditis elegans. Nature 371: 707-711.

Czajkowski C, Karlin A (1995) Structure of the nicotinic receptor acetylcholine-binding site. Identification of acidic residues in the delta subunit within 0.9 nm of the 5 alpha subunit-binding. J Biol Chem 270: 3160-3164.

Damle VN, Karlin A (1980) Effects of agonists and antagonists on the reactivity of the binding site disulfide in acetylcholine receptor from Torpedo californica. Biochemistry 19: 3924-3932.

Dani JA (1989) Open channel structure and ion binding sites of the nicotinic acetylcholine receptor channel. J Neurosci 9: 884-892.

Dani JA (2001) Overview of nicotinic receptors and their roles in the central nervous system. Biol Psychiatry 49: 166-174.

Darden TA, York D (1993) Particle Mesh Ewald: an N log(N) method for Ewald sums in large systems. J Chem Phys 98: 10089-10094.

Datta N, Mondal P, Pauling P (1980) Acta Crystallogr B 36: 906.

Daura X, Jaun B, Seebach D, van Gunsteren WF, Mark AE (1998) Reversible peptide folding in solution by molecular dynamics simulation. J Mol Biol 280: 925-932.

de Meis L, Vianna AL (1979) Energy interconversion by the Ca2+-dependent ATPase of the sarcoplasmic reticulum. Annu Rev Biochem 48: 275-292.

Del Castillo J, Katz B (1957) Interaction at endplate receptors between different choline derivatives. Proc R Soc Lond B Biol Sci 146: 369-381.

Di Angelantonio S, Nistri A, Moretti M, Clementi F, Gotti C (2000) Antagonism of nicotinic receptors of rat chromaffin cells by N,N, N- trimethyl-1-(4-trans-stilbenoxy)-2-propylammonium iodide: a patch clamp and ligand binding study. Br J Pharmacol 129: 1771-1779.

Di Angelantonio, S. Characterization of neuronal nicotinic receptors of rat cromaffin cells. 2002. SISSA.

Di Angelantonio S, Costa V, Carloni P, Messori L, Nistri A (2002) A novel class of peptides with facilitating action on neuronal nicotinic receptors of rat chromaffin cells in vitro: functional and molecular dynamics studies. Mol Pharmacol 61: 43-54.

Doyle DA, Morais CJ, Pfuetzner RA, Kuo A, Gulbis JM, Cohen SL, Chait BT, MacKinnon R (1998) The structure of the potassium channel: molecular basis of K+ conduction and selectivity. Science 280: 69-77.

Dupont Y (1977) Kinetics and regulation of sarcoplasmic reticulum ATPase. Eur J Biochem 72: 185-190.

Dupont Y (1982) Low-temperature studies of the sarcoplasmic reticulum calcium pump. Mechanisms of calcium binding. Biochim Biophys Acta 688: 75-87.

East JM (2000) Sarco(endo)plasmic reticulum calcium pumps: recent advances in our understanding of structure/function and biology (review). Mol Membr Biol 17: 189-200.

Ebashi S, Lipman F (1962) Adenosine triphospate-linked concentration of calcium ions in a particulate fraction of rabbit muscle. J Cell Bio 14: 389-400.

Edelstein SJ, Schaad O, Henry E, Bertrand D, Changeux JP (1996) A kinetic mechanism for nicotinic acetylcholine receptors based on multiple allosteric transitions. Biol Cybern 75: 361-379.

Essman U, Perera L, Berkowitz ML, Darden T, Lee H, Pedersen LG (1995) A smooth particle mesh Ewald Method. J Chem Phys 103: 8577-8593.

Ewing TJA, Kuntz ID (1997) Critical Evaluation of Search Algorithms for Automated Molecular Docking and Database Screening. J Comput Chem 18: 1175-1189.

Falson P, Menguy T, Corre F, Bouneau L, de Gracia AG, Soulie S, Centeno F, Moller JV, Champeil P, le Maire M (1997) The cytoplasmic loop between putative transmembrane segments 6 and 7 in sarcoplasmic reticulum Ca2+-ATPase binds Ca2+ and is functionally important. J Biol Chem 272: 17258-17262.

Fernando VC, Weign P, Yguerabide J, Johnson DA (1994) Transverse distance between the membrane and the agonist binding sites on the Torpedo acetylcholine receptor: a fluorescence study. Biophys J 66: 674-682.

Fieber LA, Adams DJ (1991) Acetylcholine-evoked currents in cultured neurones dissociated from rat parasympathetic cardiac ganglia. J Physiol 434: 215-237.

Forge V, Mintz E, Guillain F (1993a) Ca2+ binding to sarcoplasmic reticulum ATPase revisited. I. Mechanism of affinity and cooperativity modulation by H+ and Mg2+. J Biol Chem 268: 10953-10960.

Forge V, Mintz E, Guillain F (1993b) Ca2+ binding to sarcoplasmic reticulum ATPase revisited. II. Equilibrium and kinetic evidence for a two-route mechanism. J Biol Chem 268: 10961-10968.

Free RB, Bryant DL, McKay SB, Kaser DJ, McKay DB (2002) [3H]Epibatidine binding to bovine adrenal medulla: evidence for alpha3beta4* nicotinic receptors. Neurosci Lett 318: 98-102.

Freedman R, Adams CE, Leonard S (2000) The alpha7-nicotinic acetylcholine receptor and the pathology of hippocampal interneurons in schizophrenia. J Chem Neuroanat 20: 299-306.

Frisch, M. J. et al. Gaussian 98. Gaussian, Inc., Pittsburgh PA 2001.

Frydenvang J (1990) Acta Crystallogr C 49: 985.

Frydenvang K, Gronborg L, Jensen B (1988) Structures of acetylcholine picrate and methoxycarbonylcholine picrate hemihydrate. Acta Crystallogr C 44: 841-845.

Fujimori T, Jencks WP (1992) Binding of two Sr2+ ions changes the chemical specificities for phosphorylation of the sarcoplasmic reticulum calcium ATPase through a stepwise mechanism. J Biol Chem 267: 18475-18487.

Galzi JL, Revah F, Black D, Goeldner M, Hirth C, Changeux JP (1990) Identification of a novel amino acid alpha-tyrosine 93 within the cholinergic ligands-binding sites of the acetylcholine receptor by photoaffinity labeling. Additional evidence for a three-loop model of the cholinergic ligands-binding sites. J Biol Chem 265: 10430-10437.

Galzi JL, Revah F, Bessis A, Changeux JP (1991a) Functional architecture of the nicotinic acetylcholine receptor: from electric organ to brain. Annu Rev Pharmacol Toxicol 31: 37-72.

Galzi JL, Bertrand D, Devillers-Thiery A, Revah F, Bertrand S, Changeux JP (1991b) Functional significance of aromatic amino acids from three peptide loops of the alpha 7 neuronal nicotinic receptor site investigated by site-directed mutagenesis. FEBS Lett 294: 198-202.

Galzi JL, Changeux JP (1995) Neuronal nicotinic receptors: molecular organization and regulations. Neuropharmacology 34: 563-582.

Garcia A (1992) Large-amplitude nonlinear motions in proteins. Phys Rev Lett 68: 2696-2699.

Gilson MK, Honig B (1988) Calculation of the total electrostatic energy of a macromolecular system: solvation energies, binding energies, and conformational analysis. Proteins 4: 7-18.

Giniatullin R, Di Angelantonio S, Marchetti C, Sokolova E, Khiroug L, Nistri A (1999) Calcitonin gene-related peptide rapidly downregulates nicotinic receptor function and slowly raises intracellular Ca2+ in rat chromaffin cells in vitro. J Neurosci 19: 2945-2953.

Girardet JL, Dupont Y (1992) Ellipticity changes of the sarcoplasmic reticulum Ca(2+)-ATPase induced by cation binding and phosphorylation. FEBS Lett 296: 103-106.

Gotti C, Fornasari D, Clementi F (1997) Human neuronal nicotinic receptors. Prog Neurobiol 53: 199-237.

Gray R, Rajan AS, Radcliffe KA, Yakehiro M, Dani JA (1996) Hippocampal synaptic transmission enhanced by low concentrations of nicotine. Nature 383: 713-716.

Green WN, Wanamaker CP (1998) Formation of the nicotinic acetylcholine receptor binding sites. J Neurosci 18: 5555-5564.

Grosman C, Auerbach A (2001) The dissociation of acetylcholine from open nicotinic receptor channels. Proc Natl Acad Sci U S A 98: 14102-14107.

Grutter T, Ehret-Sabatier L, Kotzyba-Hibert F, Goeldner M (2000) Photoaffinity labeling of Torpedo nicotinic receptor with the agonist [3H]DCTA: identification of amino acid residues which contribute to the binding of the ester moiety of acetylcholine. Biochemistry 39: 3034-3043.

Grutter T, Changeux JP (2001) Nicotinic receptors in wonderland. Trends Biochem Sci 26: 459-463.

Guidoni L, Torre V, Carloni P (1999) Potassium and sodium binding to the outer mouth of the K+ channel. Biochemistry 38: 8599-8604.

Guillain F, Champeil P, Lacapere JJ, Gingold MP (1984) Role of Mg2+ ions in several steps of the sarcoplasmic reticulum-ATPase cycle. Curr Top Cell Regul 24: 397-407.

Hasselbach W, Mackinose M (1961) Die Calcumpumpe der "Ersclaffungsgrana" des Muskels and ihre Abhangigkeit von der ATP-spaltung. Biochem Z 333: 518-528.

Havel TF, Snow ME (1991) A new method for building protein conformations from sequence alignments with homologues of known structure. J Mol Biol 217: 1-7.

Henderson IM, Khan YM, East JM, Lee AG (1994a) Binding of Ca2+ to the (Ca(2+)-Mg2+)-ATPase of sarcoplasmic reticulum: equilibrium studies. Biochem J 297: 615-624.

Henderson IM, Starling AP, Wictome M, East JM, Lee AG (1994b) Binding of Ca2+ to the (Ca(2+)-Mg2+)-ATPase of sarcoplasmic reticulum: kinetic studies. Biochem J 297: 625-636.

Henikoff S, Henikoff LG (1992) Amino acid substitution matrices from protein blocks. Proc Natl Acad Sci 89: 10915-10919.

Herdklotz JK, Sass RL (1970) The crystal structure of acetylcholine chloride: a new conformation for acetylcholine. Biochem Biophys Res Commun 40: 583-588.

Herz JM, Johnson DA, Taylor P (1989) Distance between the agonist and noncompetitive inhibitor sites on the nicotinic acetylcholine receptor. J Biol Chem 264: 12439-12448.

Hess GP, Udgaonkar JB, Olbricht WL (1987) Chemical kinetic measurements of transmembrane processes using rapid reaction techniques: acetylcholine receptor. Annu Rev Biophys Biophys Chem 16: 507-534.

Higgins DG, Sharp PM (1988) CLUSTAL: a package for performing multiple sequence alignment on a microcomputer. Gene 73: 237-244.

Hill TL (1960) An Introduction to Statistical Thermodynamics. Reading, MA: Addison-Wesley Publishing Company.

Hohenberg P, Kohn W (1964) Phys Rev Lett 136: B864.

Holguin JA (1986) Cooperative effects of Ca2+ and Sr2+ on sarcoplasmic reticulum adenosine triphosphatase. Arch Biochem Biophys 251: 9-16.

Holladay MW, Dart MJ, Lynch JK (1997) Neuronal nicotinic acetylcholine receptors as targets for drug discovery. J Med Chem 40: 4169-4194.

Honig B, Nicholls A (1995) Classical electrostatics in biology and chemistry. Science 268: 1144-1149.

Hua S, Inesi G, Toyoshima C (2000) Distinct topologies of. J Biol Chem 275: 30546-30550.

Hucho F, Tsetlin VI, Machold J (1996) The emerging three-dimensional structure of a receptor. The nicotinic acetylcholine receptor. Eur J Biochem 239: 539-557.

Hughes G, East JM, Lee AG (1994) The hydrophilic domain of phospholamban inhibits the Ca2+ transport step of the Ca(2+)-ATPase. Biochem J 303: 511-516.

Hughes G, Starling AP, Sharma RP, East JM, Lee AG (1996) An investigation of the mechanism of inhibition of the Ca(2+)-ATPase by phospholamban. Biochem J 318: 973-979.

Impellizzeri G PGPRREaSA (1998) Synthesis, spectroscopic characterization, and metal ion interaction of a new alpha-helical peptide. Chem Eur J 4: 1791-1798.

Inesi G, Kurzmack M, Coan C, Lewis DE (1980) Cooperative calcium binding and ATPase activation in sarcoplasmic reticulum vesicles. J Biol Chem 255: 3025-3031.

Inesi G (1987) Sequential mechanism of calcium binding and translocation in sarcoplasmic reticulum adenosine triphosphatase. J Biol Chem 262: 16338-16342.

Itier V, Bertrand D (2001) Neuronal nicotinic receptors: from protein structure to function. FEBS Lett 504: 118-125.

Jencks WP, Yang T, Peisach D, Myung J (1993) Calcium ATPase of sarcoplasmic reticulum has four binding sites for calcium. Biochemistry 32: 7030-7034.

Jones MV, Westbrook GL (1996) The impact of receptor desensitization on fast synaptic transmission. Trends Neurosci 19: 96-101.

Jones TA, Thirup S (1986) Using known substructures in protein model building and crystallography. EMBO J 5: 819-822.

Jorgensen WL, Chandrasekhar J, and Madura JD (1983) Comparison of simple potential functions for simulating liquid water. J Chem Phys 79: 926-935.

Juul B, Turc H, Durand ML, Gomez dG, Denoroy L, Moller JV, Champeil P, le Maire M (1995) Do transmembrane segments in proteolyzed sarcoplasmic reticulum Ca(2+)-ATPase retain their functional Ca2+ binding properties after removal of cytoplasmic fragments by proteinase K? J Biol Chem 270: 20123-20134.

Kaminski G, Duffy EM, Matsui T, Jorgensen WL (1994) Free energies of hydration and pure liquid properties of hydrocarbons from the OPLS all-atom model. J Phys Chem 98: 13077-13082.

Kanazawa T, Yamada A, Yamamoto T, Tonomura Y (1971) Reaction mechanism of the Ca2 plus-dependent ATPase of sarcoplasmic reticulum from skeletal mus le. V. Vectorial requirements for calcium and magnesium ions of three partial reactions of ATPase: formation and decomposition of a phosphorylated intermediate and ATP-formation from ADP and the intermediate. J Biochem (Tokyo) 70: 95-123.

Kao PN, Dwork AJ, Kaldany RR, Silver ML, Wideman J, Stein S, Karlin A (1984) Identification of the alpha subunit half-cystine specifically labeled by an affinity reagent for the acetylcholine receptor binding site. J Biol Chem 259: 11662-11665.

Kao PN, Karlin A (1986) Acetylcholine receptor binding site contains a disulfide cross-link between adjacent half-cystinyl residues. J Biol Chem 261: 8085-8088.

Kargacin ME, Ali Z, Kargacin G (1998) Anti-phospholamban and protein kinase A alter the Ca2+ sensitivity and maximum velocity of Ca2+ uptake by the cardiac sarcoplasmic reticulum. Biochem J 331 (Pt 1): 245-249.

Karlin A (1967) On the application of "a plausible model" of allosteric proteins to the receptor for acetylcholine. J Theor Biol 16: 306-320.

Karlin A (1969) Chemical modification of the active site of the acetylcholine receptor. J Gen Physiol 54: 245S-264S.

Karlin A, Akabas MH (1995) Toward a structural basis for the function of nicotinic acetylcholine receptors and their cousins. Neuron 15: 1231-1244.

Karlin A (2002) Emerging structure of the nicotinic acetylcholine receptors. Nat Rev Neurosci 3: 102-114.

Kawai H, Cao L, Dunn SM, Dryden WF, Raftery MA (2000) Interaction of a semirigid agonist with Torpedo acetylcholine receptor. Biochemistry 39: 3867-3876.

Kearney PC, Nowak MW, Zhong W, Silverman SK, Lester HA, Dougherty DA (1996) Dose-response relations for unnatural amino acids at the agonist binding site of the nicotinic acetylcholine receptor: tests with novel side chains and with several agonists. Mol Pharmacol 50: 1401-1412.

Kehoe J, McIntosh JM (1998) Two distinct nicotinic receptors, one pharmacologically similar to the vertebrate alpha7-containing receptor, mediate Cl currents in aplysia neurons. J Neurosci 18: 8198-8213.

Khan YM, East JM, Lee AG (1997) Effects of pH on phosphorylation of the Ca2+-ATPase of sarcoplasmic reticulum by inorganic phosphate. Biochem J 321 (Pt 3): 671-676.

Khiroug L, Giniatullin R, Sokolova E, Talantova M, Nistri A (1997) Imaging of intracellular calcium during desensitization of nicotinic acetylcholine receptors of rat chromaffin cells. Br J Pharmacol 122: 1323-1332.

Khiroug L, Sokolova E, Giniatullin R, Afzalov R, Nistri A (1998) Recovery from desensitization of neuronal nicotinic acetylcholine receptors of rat chromaffin cells is modulated by intracellular calcium through distinct second messengers. J Neurosci 18: 2458-2466.

Kihara T, Shimohama S, Urushitani M, Sawada H, Kimura J, Kume T, Maeda T, Akaike A (1998) Stimulation of alpha4beta2 nicotinic acetylcholine receptors inhibits beta-amyloid toxicity. Brain Res 792: 331-334.

Krauss M, Korr D, Herrmann A, Hucho F (2000) Binding properties of agonists and antagonists to distinct allosteric states of the nicotinic acetylcholine receptor are incompatible with a concerted model. J Biol Chem 275: 30196-30201.

Kuntz ID, Blaney JM, Oatley SJ, Langridge R, Ferrin TE (1982) A geometric approach to macromolecule-ligand interactions. J Mol Biol 161: 269-288.

Kurosaki T, Fukuda K, Konno T, Mori Y, Tanaka K, Mishina M, Numa S (1987) Functional properties of nicotinic acetylcholine receptor subunits expressed in various combinations. FEBS Lett 214: 253-258.

Lacapere JJ, Gingold MP, Champeil P, Guillain F (1981) Sarcoplasmic reticulum ATPase phosphorylation from inorganic phosphate in the absence of a calcium gradient. Steady state and kinetic fluorescence studies. J Biol Chem 256: 2302-2306.

Lange KW, Wells FR, Jenner P, Marsden CD (1993) Altered muscarinic and nicotinic receptor densities in cortical and subcortical brain regions in Parkinson's disease. J Neurochem 60: 197-203.

Laskowski RA, Rullmannn JA, MacArthur MW, Kaptein R, Thornton JM (1996) AQUA and PROCHECK-NMR: programs for checking the quality of protein structures solved by NMR. J Biomol NMR 8: 477-486.

Le Novere N, Corringer PJ, Changeux JP (1999) Improved secondary structure predictions for a nicotinic receptor subunit: incorporation of solvent accessibility and experimental data into a two-dimensional representation. Biophys J 76: 2329-2345.

Le Novere N, Grutter T, Changeux JP (2002) Models of the extracellular domain of the nicotinic receptors and of ago. Proc Natl Acad Sci U S A 99: 3210-3215.

Lee AG, East JM (2001) What the structure of a calcium pump tells us about its mechanism. Biochem J 356: 665-683.

Lena C, Changeux JP (1993) Allosteric modulations of the nicotinic acetylcholine receptor. Trends Neurosci 16: 181-186.

Leonard S, Adams C, Breese CR, Adler LE, Bickford P, Byerley W, Coon H, Griffith JM, Miller C, Myles-Worsley M, Nagamoto HT, Rollins Y, Stevens KE, Waldo M, Freedman R (1996) Nicotinic receptor function in schizophrenia. Schizophr Bull 22: 431-445.

Levy D, Seigneuret M, Bluzat A, Rigaud JL (1990) Evidence for proton countertransport by the sarcoplasmic reticulum Ca2(+)-ATPase during calcium transport in reconstituted proteoliposomes with low ionic permeability. J Biol Chem 265: 19524-19534.

Lewis CA, Stevens CF (1983) Acetylcholine receptor channel ionic selectivity: ions experience an aqueous environment. Proc Natl Acad Sci U S A 80: 6110-6113.

Lide DR (2001) CRC handbook of chemistry and physics. Boca Raton, Fla., CRC Press.

Lu B, Fu WM, Greengard P, Poo MM (1993) Calcitonin gene-related peptide potentiates synaptic responses at developing neuromuscular junction. Nature 363: 76-79.

Luthy R, Bowie JU, Eisenberg D (1992) Assessment of protein models with three-dimensional profiles. Nature 356: 83-85.

MacLennan DH, Green NM (2000) Structural biology. Pumping ions. Nature 405: 633-634.

MacLennan DH, Rice WJ, Green NM (1997a) The mechanism of Ca2+ transport by sarco(endo)plasmic reticulum Ca2+- ATPases. J Biol Chem 272: 28815-28818.

MacLennan DH, Rice WJ, Odermatt A (1997b) Structure/function analysis of the Ca2+ binding and translocation domain of SERCA1 and the role in Brody disease of the ATP2A1 gene encoding SERCA1. Ann N Y Acad Sci 834: 175-185.

Maelicke A, Schrattenholz A, Storch A, Schroder B, Gutbrod O, Methfessel C, Weber KH, Pereira EE, Alkondon M, Albuquerque EX (1995) Noncompetitive agonism at nicotinic acetylcholine receptors; functional significance for CNS signal transduction. J Recept Signal Transduct Res 15: 333-353.

Makinose M, Hasselbach W (1971) ATP synthesis by the reverse of the sarcoplasmic calcium pump. FEBS Lett 12: 271-272.

Makinose M (1973) Possible functional states of the enzyme of the sarcoplasmic calcium pump. FEBS Lett 37: 143.

Marchand S, Roux B (1998) Molecular dynamics study of calbindin D9k in the apo and singly and doubly calcium-loaded states. Proteins 33: 265-284.

Martin M, Czajkowski C, Karlin A (1996) The contributions of aspartyl residues in the acetylcholine receptor gamma and delta subunits to the binding of agonists and competitive antagonists. J Biol Chem 271: 13497-13503.

Masuda H, de Meis L (1973) Phosphorylation of the sarcoplasmic reticulum membrane by orthophosphate. Inhibition by calcium ions. Biochemistry 12: 4581-4585.

McGehee DS, Heath MJ, Gelber S, Devay P, Role LW (1995) Nicotine enhancement of fast excitatory synaptic transmission in CNS by presynaptic receptors. Science 269: 1692-1696.

McGehee DS, Role LW (1995) Physiological diversity of nicotinic acetylcholine receptors expressed by vertebrate neurons. Annu Rev Physiol 57: 521-546.

McIntosh DB, Woolley DG, Berman MC (1992) 2',3'-O-(2,4,6-trinitrophenyl)-8-azido-AMP and -ATP photolabel Lys-492 at the active site of sarcoplasmic reticulum Ca(2+)-ATPase. J Biol Chem 267: 5301-5309.

McIntosh DB, Woolley DG, Vilsen B, Andersen JP (1996) Mutagenesis of segment 487Phe-Ser-Arg-Asp-Arg-Lys492 of sarcoplasmic reticulum Ca2+-ATPase produces pumps defective in ATP binding. J Biol Chem 271: 25778-25789.

McIntosh DB, Woolley DG, MacLennan DH, Vilsen B, Andersen JP (1999) Interaction of nucleotides with Asp(351) and the conserved phosphorylation loop of sarcoplasmic reticulum Ca(2+)-ATPase. J Biol Chem 274: 25227-25236.

McIntosh DB (2000) Portrait of a P-type pump. Nat Struct Biol 7: 532-535.

Meng EC, Shoichet BK, Kuntz ID (1992) Automated docking with grid-based energy evaluation. J Comp Chem 13: 505-524.

Menguy T, Corre F, Bouneau L, Deschamps S, Moller JV, Champeil P, le Maire M, Falson P (1998) The cytoplasmic loop located between transmembrane segments 6 and 7 controls activation by Ca2+ of sarcoplasmic reticulum Ca2+-ATPase. J Biol Chem 273: 20134-20143.

Menguy T, Corre F, Juul B, Bouneau L, Lafitte D, Derrick PJ, Sharma PS, Falson P, Levine BA, Moller JV, le Maire M (2002) Involvement of the cytoplasmic loop L6-7 in the entry mechanism for transport of Ca2+ through the sarcoplasmic reticulum Ca2+-ATPase. J Biol Chem 277: 13016-13028.

Methot N, Ritchie BD, Blanton MP, Baenziger JE (2001) Structure of the pore-forming transmembrane domain of a ligand-gated ion channel. J Biol Chem 276: 23726-23732.

Middleton RE, Cohen JB (1991) Mapping of the acetylcholine binding site of the nicotinic acetylcholine receptor: [3H]nicotine as an agonist photoaffinity label. Biochemistry 30: 6987-6997.

Miles K, Greengard P, Huganir RL (1989) Calcitonin gene-related peptide regulates phosphorylation of the nicotinic acetylcholine receptor in rat myotubes. Neuron 2: 1517-1524.

Mintz E, Guillain F (1997) Ca2+ transport by the sarcoplasmic reticulum ATPase. Biochim Biophys Acta 1318: 52-70.

Miyazawa A, Fujiyoshi Y, Stowell M, Unwin N (1999) Nicotinic acetylcholine receptor at 4.6 A resolution: transverse tunnels in the channel wall. J Mol Biol 288: 765-786.

Moller JV, Juul B, le Maire M (1996) Structural organization, ion transport, and energy transduction of P- type ATPases. Biochim Biophys Acta 1286: 1-51.

Moore PB, Zhong Q, Husslein T, Klein ML (1998) Simulation of the HIV-1 Vpu transmembrane domain as a pentameric bundle. FEBS Lett 431: 143-148.

Moore SA, Sielecki AR, Chernaia MM, Tarasova NI, James MN (1995) Crystal and molecular structures of human progastricsin at 1.62 A resolution. J Mol Biol 247: 466-485.

Morais-Cabral JH, Zhou Y, MacKinnon R (2001) Energetic optimization of ion conduction rate by the K+ selectivity filter. Nature 414: 37-42.

Mulle C, Benoit P, Pinset C, Roa M, Changeux JP (1988) Calcitonin gene-related peptide enhances the rate of desensitization of the nicotinic acetylcholine receptor in cultured mouse muscle cells. Proc Natl Acad Sci U S A 85: 5728-5732.

Nagle JF, Tristram-Nagle S (2000) Lipid bilayer structure. Curr Opin Struct Biol 10: 474-480.

O'Leary ME, White MM (1992) Mutational analysis of ligand-induced activation of the Torpedo acetylcholine receptor. J Biol Chem 267: 8360-8365.

Odermatt A, Taschner PE, Khanna VK, Busch HF, Karpati G, Jablecki CK, Breuning MH, MacLennan DH (1996) Mutations in the gene-encoding SERCA1, the fast-twitch skeletal muscle sarcoplasmic reticulum Ca2+ ATPase, are associated with Brody disease. Nat Genet 14: 191-194.

Ogawa H, Stokes DL, Sasabe H, Toyoshima C (1998) Structure of the Ca2+ pump of sarcoplasmic reticulum: a view along the lipid bilayer at 9-A resolution. Biophys J 75: 41-52.

Olale F, Gerzanich V, Kuryatov A, Wang F, Lindstrom J (1997) Chronic nicotine exposure differentially affects the function of human alpha3, alpha4, and alpha7 neuronal nicotinic receptor subtypes. J Pharmacol Exp Ther 283: 675-683.

Ortells MO, Lunt GG (1995) Evolutionary history of the ligand-gated ion-channel superfamily of receptors. Trends Neurosci 18: 121-127.

Ortells MO, Barrantes GE, Wood C, Lunt GG, Barrantes FJ (1997) Molecular modelling of the nicotinic acetylcholine receptor transmembrane region in the open state. Protein Eng 10: 511-517.

Osaka H, Sugiyama N, Taylor P (1998) Distinctions in agonist and antagonist specificity conferred by anionic residues of the nicotinic acetylcholine receptor. J Biol Chem 273: 12758-12765.

Otsuka M, Yoshioka K (1993) Neurotransmitter functions of mammalian tachykinins. Physiol Rev 73: 229-308.

Pascuzzo GJ, Akaike A, Maleque MA, Shaw KP, Aronstam RS, Rickett DL, Albuquerque EX (1984) The nature of the interactions of pyridostigmine with the nicotinic acetylcholine receptor-ionic channel complex. I. Agonist, desensitizing, and binding properties. Mol Pharmacol 25: 92-101.

Paterson D, Nordberg A (2000) Neuronal nicotinic receptors in the human brain. Prog Neurobiol 61: 75-111.

Pauling P, Petcher TJ (1973) Neuromuscular blocking agents: structure and activity. Chem Biol Interact 6: 351-365.

Pereira EF, Alkondon M, Tano T, Castro NG, Froes-Ferrao MM, Rozental R, Aronstam RS, Schrattenholz A, Maelicke A, Albuquerque EX (1993) A novel agonist binding site on nicotinic acetylcholine receptors. J Recept Res 13: 413-436.

Perry E, Martin-Ruiz C, Lee M, Griffiths M, Johnson M, Piggott M, Haroutunian V, Buxbaum JD, Nasland J, Davis K, Gotti C, Clementi F, Tzartos S, Cohen O, Soreq H, Jaros E, Perry R, Ballard C, McKeith I, Court J (2000) Nicotinic receptor subtypes in human brain ageing, Alzheimer and Lewy body diseases. Eur J Pharmacol 393: 215-222.

Petithory JR, Jencks WP (1986) Phosphorylation of the calcium adenosinetriphosphatase of sarcoplasmic reticulum: rate-limiting conformational change followed by rapid phosphoryl transfer. Biochemistry 25: 4493-4497.

Pick U, Bassilian S (1981) Modification of the ATP binding site of the Ca2+ -ATPase from sarcoplasmic reticulum by fluorescein isothiocyanate. FEBS Lett 123: 127-130.

Qian C, Li T, Shen TY, Libertine-Garahan L, Eckman J, Biftu T, Ip S (1993) Epibatidine is a nicotinic analgesic. Eur J Pharmacol 250: R13-R14.

Ramachandran GN, Sasisekharan V (1968) Conformation of polypeptides and proteins. Adv Protein Chem 23: 283-438.

Rees J, Reed TA (1997) A set of constructed type spectra for the practical estimation of peptide secondary structure from circular dichroism. Analyt Biochem 254: 36-40.

Reinstein J, Jencks WP (1993) The binding of ATP and Mg2+ to the calcium adenosinetriphosphatase of sarcoplasmic reticulum follows a random mechanism. Biochemistry 32: 6632-6642.

Reitstetter R, Lukas RJ, Gruener R (1999) Dependence of nicotinic acetylcholine receptor recovery from desensitization on the duration of agonist exposure. J Pharmacol Exp Ther 289: 656-660.

Role LW, Berg DK (1996) Nicotinic receptors in the development and modulation of CNS synapses. Neuron 16: 1077-1085.

Ruiz-Perez VL, Carter SA, Healy E, Todd C, Rees JL, Steijlen PM, Carmichael AJ, Lewis HM, Hohl D, Itin P, Vahlquist A, Gobello T, Mazzanti C, Reggazini R, Nagy G, Munro CS, Strachan T (1999) ATP2A2 mutations in Darier's disease: variant cutaneous phenotypes are associated with missense mutations, but neuropsychiatric features are independent of mutation class. Hum Mol Genet 8: 1621-1630.

Rusinko A, Sheridan RP, Nilakatan R, Haraki KS, Bauman N, Venkataraghavan R (1989) Using concord to construct a large database of 3-dimensional coordinates from connection tables. Comput Sci 29: 251-255.

Ryckaert J-P, Berendsen H.J.C., Ciccotti G. (1977) Numerical integration of the cartesian equations of motion of a system with constraints: Molecular Dynamics of n-alkanes. J Comp Phys 23: 327-341.

Sagara Y, Fernandez-Belda F, de Meis L, Inesi G (1992) Characterization of the inhibition of intracellular Ca2+ transport ATPases by thapsigargin. J Biol Chem 267: 12606-12613.

Sagara Y, Inesi G (1991) Inhibition of the sarcoplasmic reticulum Ca2+ transport ATPase by thapsigargin at subnanomolar concentrations. J Biol Chem 266: 13503-13506.

Saitou N, Nei M (1987) The neighbor-joining method: a new method for reconstructing phylogenetic trees. Mol Biol Evol 4: 405-425.

Sakmann B (1992) Elementary steps in synaptic transmission revealed by currents through single ion channels. Biosci Rep 12: 237-262.

Sali A, Blundell TL (1993) Comparative protein modelling by satisfaction of spatial restraints. J Mol Biol 234: 779-815.

Salin-Pascual RJ, Rosas M, Jimenez-Genchi A, Rivera-Meza BL, Delgado-Parra V (1996) Antidepressant effect of transdermal nicotine patches in nonsmoking patients with major depression. J Clin Psychiatry 57: 387-389.

Salomon AR, Marcinowski KJ, Friedland RP, Zagorski MG (1996) Nicotine inhibits amyloid formation by the beta-peptide. Biochemistry 35: 13568-13578.

Sanchez R, Sali A (1997) Evaluation of comparative protein structure modeling by MODELLER-3. Proteins Suppl 1: 50-58.

Sasaki T, Inui M, Kimura Y, Kuzuya T, Tada M (1992) Molecular mechanism of regulation of Ca2+ pump ATPase by phospholamban in cardiac sarcoplasmic reticulum. Effects of synthetic phospholamban peptides on Ca2+ pump ATPase. J Biol Chem 267: 1674-1679.

Schapira M, Abagyan R, Totrov M (2002) Structural model of nicotinic acetylcholine receptor isotypes bound to acetylcholine and nicotine. BMC Struct Biol 2: 1.

Schmitt JD, Sharples CG, Caldwell WS (1999) Molecular recognition in nicotinic acetylcholine receptors: the importance of pi-cation interactions. J Med Chem 42: 3066-3074.

Schrattenholz A, Godovac-Zimmermann J, Schafer HJ, Albuquerque EX, Maelicke A (1993) Photoaffinity labeling of Torpedo acetylcholine receptor by physostigmine. Eur J Biochem 216: 671-677.

Simmerman HK, Jones LR (1998) Phospholamban: protein structure, mechanism of action, and role in cardiac function. Physiol Rev 78: 921-947.

Sine SM (1993) Molecular dissection of subunit interfaces in the acetylcholine receptor: identification of residues that determine curare selectivity. Proc Natl Acad Sci U S A 90: 9436-9440.

Sine SM, Claudio T (1991) Stable expression of the mouse nicotinic acetylcholine receptor in mouse fibroblasts. Comparison of receptors in native and transfected cells. J Biol Chem 266: 13679-13689.

Sine SM, Quiram P, Papanikolaou F, Kreienkamp HJ, Taylor P (1994) Conserved tyrosines in the alpha subunit of the nicotinic acetylcholine receptor stabilize quaternary ammonium groups of agonists and curariform antagonists. J Biol Chem 269: 8808-8816.

Sippl MJ (1993) Recognition of errors in three-dimensional structures of proteins. Proteins 17: 355-362.

Skou JC (1957) The influence of some cations on the adenosine triphosphatase from peripheral nerves. Biochim Biophys Acta 23: 394-401.

Smit AB, Syed NI, Schaap D, van Minnen J, Klumperman J, Kits KS, Lodder H, van der Schors RC, van Elk R, Sorgedrager B, Brejc K, Sixma TK, Geraerts WP (2001) A glia-derived acetylcholine-binding protein that modulates synaptic transmission. Nature 411: 261-268.

Soulie S, Neumann JM, Berthomieu C, Moller JV, le Maire M, Forge V (1999) NMR conformational study of the sixth transmembrane segment of sarcoplasmic reticulum Ca2+-ATPase. Biochemistry 38: 5813-5821.

Stauffer DA, Karlin A (1994) Electrostatic potential of the acetylcholine binding sites in the nicotinic receptor probed by reactions of binding-site cysteines with charged methanethiosulfonates. Biochemistry 33: 6840-6849.

Steinlein OK, Mulley JC, Propping P, Wallace RH, Phillips HA, Sutherland GR, Scheffer IE, Berkovic SF (1995) A missense mutation in the neuronal nicotinic acetylcholine receptor alpha 4 subunit is associated with autosomal dominant nocturnal frontal lobe epilepsy. Nat Genet 11: 201-203.

Stokes DL, Auer M, Zhang P, Kuhlbrandt W (1999) Comparison of H+-ATPase and Ca2+-ATPase suggests that a large conformational change initiates P-type ion pump reaction cycles. Curr Biol 9: 672-679.

Stokes DL, Green NM (2000) Modeling a dehalogenase fold into the 8-A density map for Ca(2+)-ATPase defines a new domain structure. Biophys J 78: 1765-1776.

Sugiyama N, Boyd AE, Taylor P (1996) Anionic residue in the alpha-subunit of the nicotinic acetylcholine receptor contributing to subunit assembly and ligand binding. J Biol Chem 271: 26575-26581.

Suko J, Plank B, Preis P, Kolassa N, Hellmann G, Conca W (1981) Formation of magnesium-phosphoenzyme and magnesium-calcium- phosphoenzyme in the phosphorylation of adenosine triphosphatase by orthophosphate in sarcoplasmic reticulum. Models of a reaction sequence. Eur J Biochem 119: 225-236.

Sullivan DA, Cohen JB (2000) Mapping the agonist binding site of the nicotinic acetylcholine receptor. Orientation requirements for activation by covalent agonist. J Biol Chem 275: 12651-12660.

Sung JJ, Kim SJ, Lee HB, Chung JM, Choi YM, Cha CI, Suh YH, Lee KW (1998) Anticholinesterase induces nicotinic receptor modulation. Muscle Nerve 21: 1135-1144.

Svinning T, Sourum H (1975) Acta Crystallogr B 31: 1581.

Takahama K, Klee MR (1990) Voltage clamp analysis of the kinetics of piperidine-induced chloride current in isolated Aplysia neurons. Naunyn Schmiedebergs Arch Pharmacol 342: 575-581.

Tamamizu S, Guzman GR, Santiago J, Rojas LV, McNamee MG, Lasalde-Dominicci JA (2000) Functional effects of periodic tryptophan substitutions in the alpha M4 transmembrane domain of the Torpedo californica nicotinic acetylcholine receptor. Biochemistry 39: 4666-4673.

Taylor P, Malanz S, Molles BE, Osaka H, Tsigelny I (2000) Subunit interface selective toxins as probes of nicotinic acetylcholine receptor structure. Pflugers Arch 440: R115-R117.

Thompson JD, Gibson TJ, Plewniak F, Jeanmougin F, Higgins DG (1997) The CLUSTAL_X windows interface: flexible strategies for multiple sequence alignment aided by quality analysis tools. Nucleic Acids Res 25: 4876-4882.

Thompson JD, Higgins DG, Gibson TJ (1994) CLUSTAL W: improving the sensitivity of progressive multiple sequence alignment through sequence weighting, position-specific gap penalties and weight matrix choice. Nucleic Acids Res 22: 4673-4680.

Tierney ML, Unwin N (2000) Electron microscopic evidence for the assembly of soluble pentameric extracellular domains of the nicotinic acetylcholine receptor. J Mol Biol 303: 185-196.

Toyofuku T, Kurzydlowski K, Tada M, MacLennan DH (1994) Amino acids Lys-Asp-Asp-Lys-Pro-Val402 in the Ca(2+)-ATPase of cardiac sarcoplasmic reticulum are critical for functional association with phospholamban. J Biol Chem 269: 22929-22932.

Toyoshima C, Nakasako M, Nomura H, Ogawa H (2000) Crystal structure of the calcium pump of sarcoplasmic reticulum at 2.6 A resolution. Nature 405: 647-655.

Toyoshima C, Nomura H (2002) Structural changes in the calcium pump accompanying the dissociation of calcium. Nature 418: 605-611.

Troullier A, Gerwert K, Dupont Y (1996) A time-resolved Fourier transformed infrared difference spectroscopy study of the sarcoplasmic reticulum Ca(2+)-ATPase: kinetics of the high- affinity calcium binding at low temperature. Biophys J 71: 2970-2983.

Tsunoyama K, Gojobori T (1998) Evolution of nicotinic acetylcholine receptor subunits. Mol Biol Evol 15: 518-527.

Unwin N, Toyoshima C, Kubalek E (1988) Arrangement of the acetylcholine receptor subunits in the resting and desensitized states, determined by cryoelectron microscopy of crystallized Torpedo postsynaptic membranes. J Cell Biol 107: 1123-1138.

Unwin N (1993) Nicotinic acetylcholine receptor at 9 A resolution. J Mol Biol 229: 1101-1124.

Unwin N (1995) Acetylcholine receptor channel imaged in the open state. Nature 373: 37-43.

van dB, I, van Kleef RG, Zwart R, Oortgiesen M (1998) Physostigmine and acetylcholine differentially activate nicotinic receptor subpopulations in Locusta migratoria neurons. Brain Res 789: 263-273.

Verlet L (1967) Computer "Experiments" on Classical Fluids. I. Thermodynamical Properties of Lennard-Jones Molecules. Physical Review 159: 98-103.

Vernino S, Amador M, Luetje CW, Patrick J, Dani JA (1992) Calcium modulation and high calcium permeability of neuronal nicotinic acetylcholine receptors. Neuron 8: 127-134.

Villarroel A, Herlitze S, Witzemann V, Koenen M, Sakmann B (1992) Asymmetry of the rat acetylcholine receptor subunits in the narrow region of the pore. Proc R Soc Lond B Biol Sci 249: 317-324.

Vilsen B, Andersen JP (1998) Mutation to the glutamate in the fourth membrane segment of Na+,K+- ATPase and Ca2+-ATPase affects cation binding from both sides of

the membrane and destabilizes the occluded enzyme forms. Biochemistry 37: 10961-10971.

Wang F, Imoto K (1992) Pore size and negative charge as structural determinants of permeability in the Torpedo nicotinic acetylcholine receptor channel. Proc R Soc Lond B Biol Sci 250: 11-17.

Wang HL, Ohno K, Milone M, Brengman JM, Evoli A, Batocchi AP, Middleton LT, Christodoulou K, Engel AG, Sine SM (2000) Fundamental gating mechanism of nicotinic receptor channel revealed by mutation causing a congenital myasthenic syndrome. J Gen Physiol 116: 449-462.

Weinstein H, Mehler EL (1994) Ca(2+)-binding and structural dynamics in the functions of calmodulin. Annu Rev Physiol 56: 213-236.

Wilson G, Karlin A (2001) Acetylcholine receptor channel structure in the resting, open, and desensitized states probed with the substituted-cysteine-accessibility method. Proc Natl Acad Sci U S A 98: 1241-1248.

Wilson GG, Karlin A (1998) The location of the gate in the acetylcholine receptor channel. Neuron 20: 1269-1281.

Wonnacott S, Drasdo A, Sanderson E, Rowell P (1990) Presynaptic nicotinic receptors and the modulation of transmitter release. Ciba Found Symp 152: 87-101.

Wonnacott S (1997) Presynaptic nicotinic ACh receptors. Trends Neurosci 20: 92-98.

Xie Y, Cohen JB (2001) Contributions of Torpedo nicotinic acetylcholine receptor gamma Trp-55 and delta Trp-57 to agonist and competitive antagonist function. J Biol Chem 276: 2417-2426.

Yamaguchi M, Kanazawa T (1984) Protonation of the sarcoplasmic reticulum Ca-ATPase during ATP hydrolysis. J Biol Chem 259: 9526-9531.

Yamaguchi M, Kanazawa T (1985) Coincidence of H+ binding and Ca2+ dissociation in the sarcoplasmic reticulum Ca-ATPase during ATP hydrolysis. J Biol Chem 260: 4896-4900.

Yamamoto H, Imamura Y, Tagaya M, Fukui T, Kawakita M (1989) Ca2(+)-dependent conformational change of the ATP-binding site of Ca2(+)-transporting ATPase of sarcoplasmic reticulum as revealed by an alteration of the target-site specificity of adenosine triphosphopyridoxal. J Biochem (Tokyo) 106: 1121-1125.

Young HS, Xu C, Zhang P, Stokes DL (2001) Locating the thapsigargin-binding site on Ca(2+)-ATPase by cryoelectron microscopy. J Mol Biol 308: 231-240.

Yu M, Zhang L, Rishi AK, Khadeer M, Inesi G, Hussain A (1998) Specific substitutions at amino acid 256 of the sarcoplasmic/endoplasmic reticulum Ca2+ transport ATPase

mediate resistance to thapsigargin in thapsigargin-resistant hamster cells. J Biol Chem 273: 3542-3546.

Yu X, Inesi G (1993) Effects of anions on the Ca2+, H+ and electrical gradients formed by the sarcoplasmic reticulum ATPase in reconstituted proteoliposomes. FEBS Lett 328: 301-304.

Zhang H, Karlin A (1997) Identification of acetylcholine receptor channel-lining residues in the M1 segment of the beta-subunit. Biochemistry 36: 15856-15864.

Zhang P, Toyoshima C, Yonekura K, Green NM, Stokes DL (1998) Structure of the calcium pump from sarcoplasmic reticulum at 8-A resolution. Nature 392: 835-839.

Zhang Z, Lewis D, Strock C, Inesi G, Nakasako M, Nomura H, Toyoshima C (2000) Detailed characterization of the cooperative mechanism of Ca(2+) binding and catalytic activation in the Ca(2+) transport (SERCA) ATPase. Biochemistry 39: 8758-8767.

Zhang Z, Lewis D, Sumbilla C, Inesi G, Toyoshima C (2001) The role of the M6-M7 loop (L67) in stabilization of the phosphorylation and Ca(2+) binding domains of the sarcoplasmic reticulum Ca(2+)-ATPase (SERCA). J Biol Chem 276: 15232-15239.

Zheng Y, Hirschberg B, Yuan J, Wang AP, Hunt DC, Ludmerer SW, Schmatz DM, Cully DF (2002) Identification of two novel Drosophila melanogaster histamine-gated chloride channel subunits expressed in the eye. J Biol Chem 277: 2000-2005.

Zhong Q, Jiang Q, Moore PB, Newns DM, Klein ML (1998b) Molecular dynamics simulation of a synthetic ion channel. Biophys J 74: 3-10.

Zhong W, Gallivan JP, Zhang Y, Li L, Lester HA, Dougherty DA (1998a) From ab initio quantum mechanics to molecular neurobiology: a cation-pi binding site in the nicotinic receptor. Proc Natl Acad Sci U S A 95: 12088-12093.

Zhou Y, Morais-Cabral JH, Kaufman A, MacKinnon R (2001) Chemistry of ion coordination and hydration revealed by a K+ channel- Fab complex at 2.0 A resolution. Nature 414: 43-48.

Zimniak P, Racker E (1978) Electrogenicity of Ca2+ transport catalyzed by the Ca2+-ATPase from sarcoplasmic reticulum. J Biol Chem 253: 4631-4637.